Spatio-Temporal Order of Driven Periodic Systems in Quenched Random Media

Department of Physics, School of Science, Osaka University

Tomoaki Nogawa

December 1, 2009

Abstract

Collective transport phenomena of condensed matters such as charge density waves and flux line lattices are investigated. In the presence of randomness, due to impurities or defects, the periodic properties of such systems are disordered and they show highly nonlinear conductive response to the external drive. Dynamical phase transition from "plastic flow phase" to "moving solid phase", which is expected to occur by increasing the driving force, attracts much attention. This transition occurs between two nonequilibrium steady states and has much outstanding issues such as the very existence of the ordered state, moving solid phase. We numerically investigate the dynamics of these systems based on the driven random-field XY model, which can treat plastic deformations, with paying special attention to the spatio-temporal long range order. There are two kinds of orders, one is for the DC velocity, which is related to the steady plastic deformation, and another is crystalline periodic order.

At first, I discuss the driving force dependence of various physical quantities, which are comparable with the experimental measurements. A lot of characteristic phenomena in the present systems are reproduced in our simulations such as peak effect, delayed switching and broad band noise. I show that plastic deformation plays an important role in these phenomena.

The second subject is to clarify the possibility of the moving solid phase, which is characterized by infinitely large co-moving cluster. We introduce a new method to analyze the transition between plastic flow and moving solid phase using the idea of percolation transition. It is found that such a cluster tears in a finite life time in the presence of randomness and the life time is exponentially increases with the driving force.

Finally, the instantaneous periodic order of the system is argued. This order grows with the driving force. From the analysis of the behavior of dislocations, we found that the effect of random potential in the sliding state is represented by an effective temperature which is proportional to the inverse of the driving force. The long range ordered state which is seen in a clean system is, however, destroyed by weak randomness.

Here, I note the construction of this thesis. In chapter 1, an introduction to our study is made including a review of experimental and theoretical works for the present problem and explanation of the model to analyze. In chapter 2, general feature of our simulation results is overviewed with focusing on the comparison with experiments. In chapter 3 and 4, the possibility of moving solid and spatial periodic orderings are discussed, respectively.

Contents

1 Introduction **4**
- 1.1 Nonlinear Conduction, Depinning . . . 4
- 1.2 Dynamical Solid-Fluid Transition . . . 7
  - 1.2.1 Various Steady States . . . 7
  - 1.2.2 Dynamical Melting . . . 8
  - 1.2.3 Spatial Order in Quenched Disordered Systems . . . 9
  - 1.2.4 Temporal Order . . . 9
- 1.3 Phase Field Model . . . 11
  - 1.3.1 Elastic Manifold Model . . . 11
  - 1.3.2 Driven Random-Field XY Model . . . 12
  - 1.3.3 Review of Previous Works . . . 13
- 1.4 The Scope of the Present Work . . . 14

2 Fundamental Features **16**
- 2.1 Simulation Settings . . . 16
- 2.2 Nonlinear Conduction . . . 17
  - 2.2.1 Plastic Depinning . . . 17
  - 2.2.2 DC Velocity Distribution . . . 19
- 2.3 Spatial Periodicity . . . 22
- 2.4 Hysteresis . . . 23
  - 2.4.1 Switching . . . 24
- 2.5 Conduction Noise . . . 25
- 2.6 Peak Effect . . . 27
- 2.7 Phase Diagram . . . 29
- 2.8 Discussion . . . 30

3 Dynamic Phase Transition between Plastic Flow and Moving Solid **33**
- 3.1 Bond Percolation Analysis . . . 33
- 3.2 Check of Relaxation to the Steady State . . . 34
- 3.3 Solid-Fluid Transition in Finite Time Observation . . . 37
  - 3.3.1 Percolation Probability . . . 37
  - 3.3.2 Finite Size Scaling . . . 39
- 3.4 Observation Time Dependence of the Critical Force . . . 39
  - 3.4.1 Glass Crossover Time . . . 39
  - 3.4.2 Universality of Percolation Transition for Different T . . . 41
- 3.5 Statistics of Co-moving Clusters . . . 41
  - 3.5.1 Fractal Dimensions at the Critical Point . . . 41
  - 3.5.2 Size Distribution . . . 43
- 3.6 Statistics of Phase Slip Frequency on Each Bond . . . 44
- 3.7 Discussion . . . 45

4 Phase Ordering on Moving Frame **47**
4.1 Phase Correlation 47
4.1.1 Correlation Function 47
4.1.2 Phase Displacement 48
4.1.3 Structure Factor 49
4.1.4 The Magnitude of Bragg Peak 51
4.1.5 Comparison with Static and Elastic Models 52
4.1.6 Spatio-Temporal Correlation Function 53
4.2 Topological Defects 55
4.2.1 Dislocation Loops 55
4.2.2 Effective Temperature 57
4.2.3 Power Relaxation 57
4.3 Discussion 58

5 Summary and Discussion **60**

Acknowledgments **62**

Bibliography **62**

Chapter 1

Introduction

Collective transport of condensed matter with random pinning attracts much attention from a view point of solid state physics, nonlinear dynamics and statistical mechanics. There are numerous systems which belong to this class of dynamics, for example directed polymer chains, various domain walls, crack fronts and faults in earthquakes. We are interested particularly in periodic structures such as charge density waves (CDW) [1], spin density waves, flux line lattices (FLL) [2] , colloidal lattices and Wigner crystals. They have many common properties as well as differences due to the dimensionality of space and deformation. It is significant to study them in a systematic way. If these systems are put on perfectly clean environment, they hold long range periodicity. Random pinning will destroy this periodicity and yield many metastable states, then the whole system does not move under smaller driving force than the threshold value and shows highly nonlinear conduction above it. These can be generalized as a frictional dynamics which include maximum static frictional force and dynamic friction.

Recent attractive topic in these systems is a phase transition between two nonequilibrium steady states, "plastic flow phase" and "moving solid phase", which occurs above depinning threshold force [3, 4]. Plastic flow phase and moving solid phase are distinguished by the uniformity of local DC velocity, which is related to the existence of plastic deformation. This transition is triggered by the change of the driving force.

In the theoretical studies of these systems the elastic manifold model is intensively investigated, where periodic structure is expressed as a continuous elastic body whose dynamics is governed by classical mechanics. This picture explains a number of experimentally observed facts such as depinning, mode locking and memory effect of CDW [5, 6, 7]. There are, however, a lot of phenomena where plastic deformation is considered to play an important role. Therefore we adopt an extended model in order to treat plastic flow and perform numerical simulations.

In this chapter I make an introduction to our study. At first the phenomena which interest us are reviewed including both of experimental and theoretical studies. Next I introduce the model to analyze and briefly summarize several previous works based on the same model with the present one. At the last I position the present work in the background.

1.1 Nonlinear Conduction, Depinning

At first I present a brief overview of the nonlinear collective motion in random media taking CDWs as an example. In some quasi one dimensional metals such as $NbSe_3$, which has strong conductive anisotropy, Peierls transition occurs and the charge density is periodically modulated with a half of the Fermi wave length in the low temperature phase [8]. This transiting is characterized by the complex order parameter $\rho e^{i\theta}$. Here, ρ and θ are related

Figure 1.1: (left) Temperature dependence of conductivity of TaS_3 as a function of electric field [10]. (right) Conductivity obtained by the numerical simulation based on Fukuyama-Lee-Rice model [5]. The horizontal axis indicates the electric field normalized by depinning threshold.

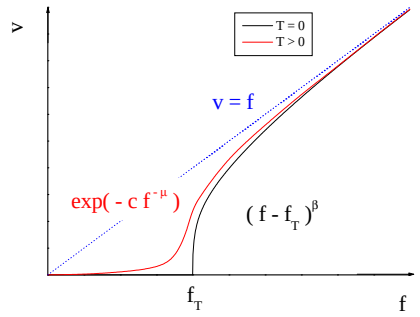

Figure 1.2: Schematic diagram of depinning transition and thermal creep.

to the amplitude and the phase of CDW. There is an energy band gap, called Peierls gap, at the Fermi surface. The material behaves as an insulator and conductivity decreases as temperature becomes lower. However CDW can carry the electric charge even at zero temperature. The current owing to the motion of CDW shows highly nonlinear response to the electric field even for very small field.

The ratio of the period of CDW to the lattice constant of crystal is generally an irrational number then the crystal makes incommensurate periodic potential for the CDW. The system has a translational invariance because the local gain of the potential energy due to translation is canceled by the loss in other place. Thus CDW can freely move. Frölich suggested that this is the mechanism of superconductivity [9]. It turned out to be incorrect because some dissipation mechanisms exist. Much crucial reason is the pinning due to impurities.

depinning

In the presence of random pinning potential there are many metastable pinned states. These states survive at finite but small driving force and vanish at the threshold driving force f_T and depinning happens. The left panel of Figure1.1 shows experimentally measured conductivity $\sigma = I/E$ normalized by the value in the high electric field limit. As temperature decreases, depinning behavior becomes sharper because quasi particles, i.e. excited conduction electrons, are suppressed. CDW can be regarded as a elastic continuum driven by external force, which can deform in order to lower the impurity potential energy. The conductivity obtained by numerical simulations based on the elastic model, so-called Fukuyama-Lee-Rice model, is also shown in Figure1.1 and it reproduces depinning behavior.

D. S. Fisher showed that this depinning has an aspect of a critical phenomena [11]. Correlation length diverges at the driving force f_T. Here correlation length is defined as a velocity-velocity correlation length above the critical force and an avalanche propagation length, which is induced by local perturbation, below the critical force. Additionally velocity obeys to power law $v \propto (f - f_T)^\beta$ in the vicinity of the critical point and it is regarded as a kind of order parameter of continuous phase transition (See Figure 1.2). Unfortunately the critical region of this transition is very narrow and sample size in experiments is too small to observe this critical behavior.

Figure 1.3: Peak effect for the FLL in 2H-$NbSe_2$ [15]. Left figure shows voltage-current character for various magnetic fields. Right figure shows magnetic field dependences of the depinning threshold values, both for electric current and for converted force on vortices. They have peaks at H_p, which is slightly smaller than $H_{c2} \approx 7.0$T.

creep

This depinning transition is rounded at finite temperature because creep motion with thermal activation occurs below f_T. This creep motion is expressed as $v \propto \exp(-Cf^{-\mu}/T)$ [12]. This creep law is very clearly observed in the magnetic domain wall in an ultra-thin film, which driven by external magnetic field. Stretched exponential behavior is observed over twenty decades of velocity [13].

This behavior is understood as follows. We consider the situation that elastic body pinned by random potential moves slowly assisted by thermal activation. It is supposed that the displacement of elastic body, u, grows with distance r as $u \sim r^{\nu}$, which comes from quasi long range order discussed later. The elastic energy $(\nabla u)^2$ of a subsystem with size L is proportional to $L^{d-2+2\nu}$. The energy gain under external force f is given by $fL^{d+\nu}$. Considering the balance between these energies, the size of moving domain is estimated as $f^{-1/(2-\nu)}$ then its energy barrier is expressed as $f^{-(d-2+2\nu)/(2-\nu)} = f^{-\mu}$.

plastic deformation

So far I assume that the pinned and moving states does not coexist in single system. Coexistence of these two states, which yields non-uniform state, should be realized by strong pinning centers which are inhomogeneously distributed in space. These form domains which have various pinning strength and mobilities. At the boundary between the neighboring domains which have different mobilities, strain and stress become larger with time then tearing and slip occurs when the stress reaches the yield stress. When the slip distance reaches one period, i.e. 2π of phase, it can be regarded as the same state as the initial one before tearing. This process, which is characteristic for periodic systems, is called phase slip. In the presence of such tearing, each domain takes depinning independently depending on the local pinning strength. We call this phenomenon plastic depinning. It brings no critical behavior with the divergence of the correlation length as a matter of course. In the steady state phase slips happen recurrently between domains with different velocities.

Plastic deformation has much clear image in the case of lattices made by particle-like compositions such as FLL. Most remarkable phenomenon which manifests the role of plasticity is observed in FLL system. Type II superconductor has a mixed state of Meissner and normal states, which is predicted by Abrikosov at first [14]. Magnetic field in the sample is localized as a vortex whose magnetic flux is quantized by $h/2e$. These have a repulsive interaction and form a two dimensional triangular lattice in the plain which is perpendicular to the magnetic field. When electric current exists, flux line catches Lorentz force. The motion of flux lines results voltage drop, then superconductivity is destroyed. Impurity pinning of FLLs keeps zero resistivity up to depinning threshold current. Then the pinning of vortices has an important meaning to develop superconducting material which bear large electric current.

In the "peak effect" for FLL systems, the threshold force takes the maximum value near the second critical magnetic field H_{c2}, above which the mixed state vanishes, as shown in Figure 1.3. It is believed that FLL melts as increasing magnetic field, then the depinning happens as a local event above the melting point and threshold force takes a peak value at the melting point.

Figure 1.4: Left figure shows the image obtained by Lorentzian microscopy, where plastic flow in a channel (red vortices) is observed in real time [16]. Right figure is the observation of moving FLL by the magnetic decoration method [17]. The left column (RS) shows snapshot of vortices. Central column (FT) is its Fourier transformation and right column (FF) shows real space image after Fourier filtering. The upper row shows smectic flow state in relatively low magnetic field and the lower row shows Bragg glass state in high field.

Figure 1.5: Dynamical phase diagram of anisotropic super conductor 2H-$NbSe_2$ [15].

1.2 Dynamical Solid-Fluid Transition

Above the driving force where plastic depinning occurs, there are both of moving and static regions in one sample. Slightly above the depinning threshold moving regions are distant from each other and move independently with proper local velocity. As the driving force increases, the fraction of moving regions becomes larger and the domains tend to have same DC velocity with neighboring domains in order to prevent plastic deformation. Then the transition between spatially nonuniform and uniform moving states is expected. We call these states plastic flow and moving solid respectively. This transition is intensively investigated in FLL systems, where real time observation of flux line motion is possible by Lorentz microscopy or STM. The images obtained by these methods are shown in Figure 1.4.

1.2.1 Various Steady States

Here I describe several types of moving states and their property. FLL system is taken as an example but the same types of states are found in other systems such as CDW.

Plastic Flow

In the plastic flow phase, local velocity is spatially nonuniform and the system shows fluid like behavior. At the boundary of two regions which have different DC velocities strain and stress grow with time and plastic deformation occurs when stress reaches yield stress. The stress is small just after the slip occurs but it becomes larger again then plastic deformation is steadily happens. In FLL systems moving regions appear as winding channels which run through pinned regions.

Moving Solid

In the moving solid phase, the whole system moves at the same DC velocity, then phase slip does not occur. Some stages of ordering are observed in FLL systems. Anisotropic ordered state is called "smectic flow", in which straight channels align in the direction of drive and the system has spatial periodic order only in the direction perpendicular to the driving force. Each vortex has the same velocity inside channels but the velocity of each channel is not uniform then slips occur between channels.

The system recovers two dimensional periodicity under stronger driving but it is considered that true long range order does not exist in these disordered systems. Moving Bragg glass phase, which has a two dimensional quasi long range order, is believed to exist. We mention this more closely in the later section. The images of both smectic flow and moving Bragg glass are shown in the right panel of Figure 1.4.

Figure 1.6: The result of molecular dynamics simulation for two dimensional FLL systems [18]. Upper row shows trajectory of vortices and bottom row shows its structure factors. The driving forces are 0.5, 2 and 7 from the left column to the left one. These indicate plastic flow, smectic flow and moving solid respectively.

1.2.2 Dynamical Melting

Which type of moving state the system takes depends on many factors such as driving force, pinning strength and temperature. Experimentally obtained phase diagram of FLL system in driving force - magnetic field plane is shown in Figure 1.5. Magnetic field dependence in the case of FLL is complex because it affects on many other parameters through the number density of flux line. I concentrate in a pure mechanical process, zero temperature dynamics with the control of driving force.

Molecular dynamics simulation is a powerful tool to observe the moving state directly. Figure 1.6 shows three moving states. Connected lines in the upper rows show the channels along which vortices move. The structure factors shown in the bottom row indicate their ordering. In the plastic flow state, only single peak at the origin, which indicates mean density of vortices, is observed. Smectic ordered phase has additional two symmetrical peaks on the axis perpendicular to the driving direction. Six fold rotational symmetry peaks which suggest triangular lattice order is seen in moving Bragg glass state.

Basic picture of the melting transition which is observed by decreasing the driving force is as follows. When we are on the inertial system which moves at the same velocity with that of the periodic structure, static random potential $V(\mathbf{r})$ turns to have time dependence as $V(\mathbf{r}+\mathbf{v}t)$. It yields fluctuating random force which has short range correlation in both time and space. This is similar to thermal kicking on local parts of periodic structure, such as single vortex. This force changes more rapidly as the translational velocity increases and the system becomes not able to respond to it. Both of the mean value and amplitude of random force become close to zero as velocity becomes higher. Koshelev and Vinokur calculated spatio-temporal correlation of random pinning forces F_p and found that it behaves like a thermal noise [3]. They define "shaking temperature" from fluctuation dissipation theorem as

$$T_{\rm sh} = \frac{1}{4\eta}\sum_{\alpha}\int d\mathbf{r}dt\Big\langle F_{p\alpha}(\mathbf{0},0)F_{p\alpha}(\mathbf{r},t)\Big\rangle. \tag{1.1}$$

η is dissipation coefficient and α denotes the component, x or y. $T_{\rm sh}$ is found to be proportional to the inverse of the velocity then high velocity regime is related to the low temperature regime. Melting transition should occurs when effective temperature $T_{\rm real}+T_{\rm sh}$ equals to equilibrium melting temperature $T_{\rm m}$.

Although many experimental evidences of both of solid and fluid moving states are reported, whether this melting transition is continuous, discontinuous or crossover is still an unsettled question in spite of extensive studies.

Some CDW samples show hysteresis in current-voltage curves and there are current gaps between bistable states similarly to the first order transition [19]. Some people consider this behavior as a transition between plastic flow and elastic flow, which corresponds to moving solid, phases. Strange switching behavior is observed in the vicinity of the edge where lower current state becomes unstable as shown Figure 1.7 [20, 21]. When a little larger electric field than higher edge value is suddenly imposed, it takes some delay time before current starts. This is called "delayed switching". The delay time has probability distribution. Both of its mean value and deviation seems to diverge as approaching the edge value.

Figure 1.7: Highly nonlinear conductive property of CDW in $K_{0.3}MoO_3$. (Top left) Hysteresis curves in current-voltage character. (Top right) Current switching with delay time. (Bottom) Delay time distribution function. [21].

1.2.3 Spatial Order in Quenched Disordered Systems

The possibility of (quasi) long range order in the systems which have quenched randomness is a long standing problem even in the static case. Imry and Ma stated that long range order is destroyed by infinitesimally weak random-field in the systems below four dimensions [22]. They estimate the typical energy of an elastic domain whose linear size is L. Elastic energy $U_{\rm el} \propto (\nabla \mathbf{u})^2$ is expressed as KL^{d-2}. Here $\mathbf{u}$ is deformation field. Energy gain of the random potential averaged in this elastic domain is proportional to the square root of number of impurities in the domain then $U_{\rm imp} \approx h(cL^d)^{1/2}$. Here c is a impurity concentration. Thus the total energy is written as

$$u(L) \approx KL^{d-2} - hc^{1/2}L^{d/2}. \tag{1.2}$$

This can be regarded as a nucleation energy to make a domain of size L in the flat state. If $d > 4$, $u(L)$ is positive and an increasing function for large L then large size domains are suppressed. For $d < 4$, $u(L)$ turns to decrease and becomes negative at the scale of $L = L_c \approx (K^2/h^2c)^{1/(4-d)}$. Elastic coherence is not held beyond L_c and the system is divided into domains of order L_c. Elastic coherence length L_c is called Larkin length [23] for FLL and Fukuyama-Lee-Rice length for CDW [24, 25]. No long range order exists because L_c is finite for arbitrary small h as far as $d < 4$.

Recently Giarmarchi and Le Doussal suggested the existence of new ordering state in three dimensions [26]. It is named Bragg glass, which has two dimensional quasi long range order and shows Bragg peaks as its evidence. They analyzed the elastic model for periodic systems by Gaussian variational method and functional renormalization group method. They assume the absence of dislocation then treat an elastic manifold. The relative displacement $B(r) = \left\langle (u(r) - u(0))^2 \right\rangle /2$ is logarithmically grows with distance r for large r while it is proportional to r^{4-d} below Larkin length. Then correlation function $C(r) = e^{-B(r)}$ decays as the power function $r^{-\eta}$. The exponent η is an universal value and depends only on the dimension.

They also predicted that this quasi long range order exists even in nonequilibrium steady moving state and named it moving Bragg glass [27]. DC velocity is assumed to be uniform in this state. The transverse glass state, which is equivalent to smectic flow, in the two dimensional system is also claimed. Their main method is functional renormalization group of the action in the Martin-Siggia-Rose formalism [28].

Next, I show the scaling argument of the moving system by Balents and Fisher [4]. There is two time scales, one is a diffusion time $t_\phi = \eta L^2/K$. Another is a refreshing time $t_0 = L/v$ in which random potential below the domain is renewed. Both of which are much larger than microscopic time scale a/v. The net potential energy, averaged over t_ϕ, become small with the factor of $(t_\phi/t_0)^{-1/2} = (K/\eta v)^{1/2}L^{-1/2}$ compared with $h(cL^d)^{1/2}$ in eq.(1.2). It reduces the critical dimensions to three. In three dimensions, the nucleation energy is expressed as $u(L) \sim \left(K - (h^2cK/\eta v)^{1/2}\right)L$. At critical velocity $v_c \sim K/h^2c\eta$, the energy changes its sign. Thus the system obtains quasi long range order in the high velocity regime above v_c.

1.2.4 Temporal Order

The solid-fluid transition mentioned above is notable at the point of temporal regularity. We have a picture as follows. In the plastic flow state, the nonlinearity which corresponds

Figure 1.8: Power spectrum of conduction noise of TaS_3 [10]. Narrow band noise peaks are seen in left figure. The peaks shift to higher frequency as current grows. Right figure shows 1/f behavior of low frequency spectrum.

Figure 1.9: The minimization of narrow band noise peak by the control of the electric field (left) and phase diagram drawn by it (right) for the CDW in TaS_3 [19].

to plastic deformation causes chaotic dynamics. On the contrary, moving lattice phase shows temporally periodic motion which is closely related to the spatial periodicity. These differences are detected by observing fluctuating component of velocity.

Narrow Band Noise

In the moving lattice state, velocity oscillates with characteristic frequency $\omega_{NBN} = 2\pi v/a$. Here a is a lattice constant of a periodic structure. This oscillation results sharp peak in power spectrum and called narrow band noise (NBN). This is experimentally observed in both CDW [10] and FLL systems [29]. The power spectrum of CDW current is shown in Figure1.8. A simple explanation of this phenomena is as follows. Each impurity results a periodic potential for the CDW with a period a. The dynamics of CDW is likened to the motion of a particle on the tilted washboard, which results oscillating motion. Then NBN is also called "washboard noise".

The magnitude of total potential of multiple impurities for rigid crystal is proportional to $(cL^d_{\rm sample})^{1/2}$. The amplitude of washboard noise is proportional to this. In the presence of spatial quasi long range order, in which correlation decays as $r^{-\eta}$, and temporal true long range order, power spectrum of NBN is expressed as $S(\omega) \sim A^{2-\eta/2}\delta(\omega - \omega_{\rm NBN})$. Here, A is a cross section of the sample. The coefficient of the delta function is the order parameter for temporal phase transition. If assuming scaling relation $S(\omega) \sim \epsilon^y \tilde{S}[(\omega - \omega_{\rm NBN})\epsilon^{-z\nu}, A\epsilon^{2\nu}]$, delta peak component vanishes as $\epsilon^{y+\nu(4-\eta+z)}$ at the critical point [4]. Here ϵ is a reduced driving force $|f - f_c|/f_c$, z and η are dynamical and correlation length critical exponents.

Balents and Fisher stated that three dimensional CDW system has a state with spatial quasi long range order and true temporal long range order based on scaling argument mentioned in the previous section and renormalization group argument [4]. They predicted that the amplitude of NBN vanishes at the boundary with the plastic flow phase as shown above. The minimization of the NBN amplitude is observed experimentally for CDW in TaS_3. (See Figure 1.9).

Broad Band Noise

In the plastic flow state, the current noise has broad spectrum then it is called broad band noise (BBN). There would be two reasons for BBN, one is lack of temporal periodicity and another is spatial non-uniformity of $\omega_{\rm NBN}$.

In the presence of finite phase coherence length, the current of a domain with size ξ oscillates with an amplitude of order $(c\xi^d)^{1/2}$. The oscillation amplitude of current through cross section of A, where A/ξ^{d-1} of domains are revealed, is proportional to $(cA\xi)^{1/2}$. The power spectrum of fluctuating current should be given by Lorentzian $(1 + \omega^2\tau^2)^{-1}$ for finite time correlation. Some experiments, however, shows ω^{-1} dependence of the power spectrum, so called 1/f noise, in the low frequency regime at very low temperature as shown in Figure 1.8.

Figure 1.10: Schematic diagram of deformation of two dimensional interface and rectangular lattice. The difference between them is that parameter space and deformation vectors are vertical or parallel.

1.3 Phase Field Model

We perform numerical simulation based on the driven random-field XY model. It is the modified version of the intensively investigated elastic manifold model, such as Fukuyama-Lee-Rice model for CDW [24, 25]. I introduce the elastic model at the beginning of this section and then extend it to treat plastic deformation with considering its physical meanings.

1.3.1 Elastic Manifold Model

In the beginning I consider a domain wall in three dimensional space as shown in Figure 1.10, that is two dimensional plane, as an example. When this plane has no folding, the density of this structure can be described by scalar deformation field $u(\mathbf{r})$ as

$$\rho(\mathbf{r},t) = \rho_{2D}\delta(z - u(\mathbf{r}_\perp)) \quad \text{where} \quad \mathbf{r}_\perp = (x,y). \tag{1.3}$$

The domain wall is supposed to be nearly flat and parallel to xy-plane. In general elastic manifolds are classified by a pair of dimension numbers, d for space $\mathbf{r}$ and N for deformation $\mathbf{u}$ and named $(d+N)$-system in this thesis. In the case of domain walls of D dimensional system, $d = D-1$ and $N = 1$. Polymer chain or single flux line in three dimensions is a (1+2)-system.

The distorted periodic density can be described as

$$\rho(\mathbf{r},t) = \rho_0 + \sum_{\mathbf{q}} \rho_{\mathbf{q}} \cos\Big(\mathbf{q}\cdot(\mathbf{r} - \mathbf{u}(\mathbf{r},t))\Big). \tag{1.4}$$

Here, $\mathbf{q}$'s are reciprocal lattice vectors. Higher harmonic components are ignored as the first order approximation, which are needed for lattice made by particles. $\mathbf{u}(\mathbf{r},t)$ is a deformation field and embedded on the same plain made by lattice constant vectors (See Figure 1.10). CDW is a (3+1)-system and has a strong anisotropy due to crystal structure. This anisotropy is eliminated by rescaling length scale. FLL is a (3+2)-system but a (2+2)-system in thin film superconductor is also well investigated.

In the case that periodic order is only for one direction as one dimensional CDW, $\mathbf{q} = q\hat{\mathbf{x}}$, $\rho(\mathbf{r},t) = \rho_0 \cos\Big(qx - \theta(\mathbf{r},t)\Big)$, scalar phase field $\theta(\mathbf{r},t) = qu_x(\mathbf{r},t)$ is adequate. In the case of two dimensional lattice such as FLL, two component field is needed. There is anisotropy between them due to the direction of driving force even if ignoring that it is triangular lattice. In this thesis we only treat the case of single phase field, which couples to the driving force. This model is most appropriate for CDWs but we expect that essential features of the dynamics of FLL are captured. The observable transport quantity such as electric current for CDWs and voltage drop for FLLs is proportional to the translational velocity $\dot{\theta}(\mathbf{r},t)/q$.

The Hamiltonian of the elastic model is written as

$$H = \int d\mathbf{r}\Big[K(\nabla\theta(\mathbf{r},t))^2 + \rho(\mathbf{r},t)V(\mathbf{r}) - F\theta(\mathbf{r},t)\Big]. \tag{1.5}$$

The first term is an elastic deformation energy and $V(\mathbf{r})$ in the second term is quenched random potential. F is an uniform driving force representing electric field for CDW and electric current for FLL. This Hamiltonian illustrates the domain wall in $d+1$ dimensional space where potential, $\tilde{V}(\mathbf{r},\theta) = \rho(\mathbf{r},\theta)V(\mathbf{r})$, is periodic for θ and random for $\mathbf{r}$. Such

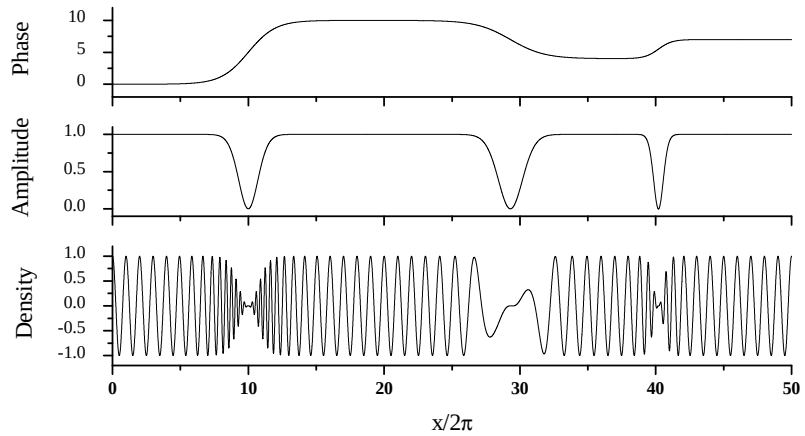

Figure 1.11: Schematic diagram of plastic domains. There are shown the phase, the amplitude and the density. Phases rarely changes in the domain. At the domain boundary, amplitude vanishes, then the energy cost due to phase deformation is suppressed.

periodicity in potential energy changes universality class [27]. The equation of motion for phase is as follows.

$$\eta\dot{\theta}(\mathbf{r},t) = -K\triangle\theta(\mathbf{r},t) - \rho_0 V(\mathbf{r})\sin\Big(\theta(\mathbf{r},t) - qx\Big) + F. \tag{1.6}$$

We ignore the inertial term which is considered to be much smaller than frictional term on the left hand side.

The Hamiltonian of lattice model version is written as

$$H = \frac{J}{2z}\sum_{\langle i,j\rangle}(\theta_i - \theta_j)^2 + \sum_i h_i\cos(\theta_i - \beta_i) - \sum_i f\theta_i. \tag{1.7}$$

Here z is the number of nearest neighbor sites. The effect of impurity potential is supposed to be very short ranged as $V(\mathbf{r}) = \sum_j V_j\delta(\mathbf{r} - \mathbf{r}_j)$ to pin the local phase of impurity site j to $\beta_j = qx_j$. $h_i = \rho_0 V_i$ is finite if i is an impurity site. Due to the randomness of impurity positions, β_i's can be regarded as uniform random numbers between 0 and 2π. So far we consider only the degree of freedom for phase, i.e. amplitude is approximated to be a constant value ρ_0. If considering only the elastic energy of phase, steady plastic flow is never realized. In order to treat plastic deformation precisely, we have to treat the fluctuation of amplitude $\rho(\mathbf{r},t)$ such as soft-spin model [4] however it is tangling to manage two order parameters. Then we adopt the single phase model with nonlinear coupling.

1.3.2 Driven Random-Field XY Model

The most simple way to treat plastic deformation is to replace the harmonic coupling $(\theta_i - \theta_j)^2/2$ in eq.(1.7) with sinusoidal coupling $1 - \cos(\theta_i - \theta_j)$ [30]. They coincide in the limit where phase differences go to zero. In this sinusoidal coupling in a lattice model, i.e. XY spin model, stress-strain relation is given by $\sin(\theta_i - \theta_j)$ while it is given by Hook's low, linear to $\theta_i - \theta_j$, in the elastic model. Sinusoidal coupling makes plastic deformation possible because it has an yield stress and translational invariance of energy for phase with the period of 2π.

Such a nonlinear coupling model does not have continuous limit that lattice constant goes to zero. The lattice points have physical meaning, the indices i's are indicating semi macroscopic domains in which phase coherence is always held. It is illustrated in Figure1.11. At the domain boundary, where stress is particularly concentrated, the amplitude of the

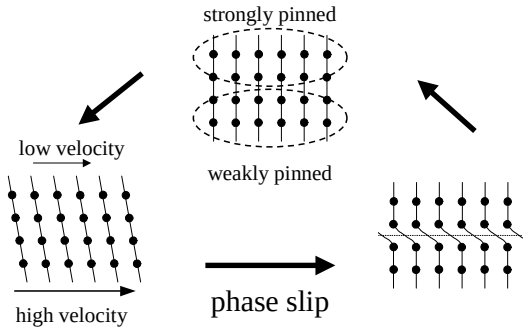

Figure 1.12: Schematic diagram of phase slip cycle between domains which have different mobility. Solid line shows phase equivalent plain, which can be related to the position of particle.

Figure 1.13: (left) velocity-force character. (right) phase diagram in coupling constant-force space.

density sometimes vanishes and the phase can be discontinuous. The domains are formed by the balance between pinning strength and rigidity of periodic structures. Plastic deformation occurs only at the boundary of these domains. In other words, the domains are minimum units which is never dissolved.

One can treat plastic flow state where DC velocity is inhomogeneous by this model (See Figure 1.12). However there is a problem that the current does not satisfy the continuum equation, $\left\langle \mathrm{div}(\dot{\theta}(\mathbf{r},t)\hat{\mathbf{x}}) \right\rangle_{\mathrm{time}} = 0$, when phase slip occurs. It is not a problem in the case of CDW because electrons joining CDW state are transformed to normal electrons, or opposite direction, at the boundary where phase slip occurs.

The overdamped equations of motion for phases of domains are expressed as

$$\dot{\theta}_i = -\frac{J}{z}\sum_j \sin(\theta_i - \theta_j) - \sin(\theta_i - \beta_i) + f. \tag{1.8}$$

We can choose the units of time and space that both of friction coefficient and impurity strength are unity. Then there are only two independent parameters, coupling constant J and driving force f. The reason why we set $h = 1$ instead of usual $J = 1$ is that the disordered phase is confined around the origin of $J - f$ phase space as shown in the next chapter.

I call these domains on the lattice points as "sites" hereafter to avoid confusion.

1.3.3 Review of Previous Works

There are a few studies based on the driven random-field XY model. Here I briefly summarize them.

Mean Field Approximation

Strogatz *et al.* analyzed eq.(1.8) by mean field approximation, in other wards an infinite range interaction model, and found a discontinuous transition by changing external field [30]. There are three regimes, pinned static state below f_{c1}, coherent moving state above f_{c2} and the bistable regime between f_{c1} and f_{c2}, which causes a hysteresis loop in velocity-force curve (See Figure 1.13). Phase coherence order parameter is also calculated and it takes finite value only when velocity is finite. Spatially inhomogeneous motion never appears in mean field treatment. f_{c1} and f_{c2} goes to zero at $J = 1.5$ and 2.0 respectively. Then linear response is realized for large J. They also studied delayed switching [31], that is, it takes some time to starts moving when the driving force is suddenly raised up to slightly

Figure 1.14: (left) delayed switching of phase coherence and velocity. (right) power divergence of delay time.

Figure 1.15: (Left) pinning strength dependence of phase velocity (top) and the maximum Lyapnov exponent (bottom). (Right) pinning strength dependence in the fraction of moving sites with coherent velocity (square) and stopping sites (circle). Filled symbol indicates chaotic states and unfilled one denotes regular motion.

Figure 1.16: The fraction of moving sites and averaged velocity as a function of reduced driving force. Both of them obey to power law near the depinning threshold.

above f_{c2} (See Figure 1.14). The pinned state is unstable then the lowest eigenvalue of the Hessian is negative but its absolute value is small and goes to zero at $f = f_{c2}$. Then it takes a long time to leave away from unstable fixed point and the delay time diverges as $(f - f_{c2})^{-1}$, which is shown Figure 1.14. Such behavior is consistent with experiments of switching sample of CDW mentioned in section 1.2.2.

Temporal Order Transition

Huse performed three dimensional simulation of this model [32]. He calculated Lyapnov exponent and fraction of no-moving site (See Figure 1.15). Spatio-temporal order transition between spatially uniform temporally regular motion and nonuniform chaotic one happens by changing pinning strength [32]. These motions are related to moving solid and plastic flow respectively. It is similar to a first order transition and physical quantity shows hysteresis loop as a function of pinning strength owing to the difference of initial conditions. He implies the possibility that this transition can be understood as a percolation of uniform velocity cluster, which we investigate in chapter 3.

Plastic Depinning

Kawaguchi investigated the plastic depinning of one dimensional system in the strong pinning regime [33, 34]. He found that local depinning has the same critical exponent $\beta = 1/2$, $v \propto (f - f_T)^{\beta}$, as one body model. And the number of moving sites also have power dependence on $n_{\rm mv} \propto (f - f_T)^{\alpha}$. The total current which is approximated as a product of these two quantities proportional to $(f - f_T)^{\beta+\alpha}$ just above f_T.

1.4 The Scope of the Present Work

In the following chapters, I show the results of our numerical simulations based on the driven random-field XY model. In chapter 2, I discuss the driving force dependence of physical quantities. They are compared with the experimental results which are characteristic in the transport of CDW and FLL systems, such as depinning threshold and current noise. Additionally the statistics of local values are investigated in detail because we have an interest in the transition between homogeneous and inhomogeneous moving state. I show that various experimental facts, in which plastic deformation is essential, are semi-quantitatively explained in our simulations.

In chapter 3 and 4, I discuss the spatio-temporal order of the periodic structures in the nonequilibrium steady state. There are two kinds of orderings, one is for phase, which is related to the spatial periodicity, and another is for DC velocity. The states are divided into liquid, glass, Bragg glass and crystal phases by the phase order and into plastic flow

and moving solid phases by the DC velocity order. It is usually considered that the spatio-temporal order of phase and spatial order of DC velocity is established together, i.e. plastic flow state does not have spatial long range order and moving solid is a collective term for moving glasses and crystal. Then phase ordering has been mainly discussed.

In chapter 3, we concentrate into the distinction of dynamical property between plastic flow and moving solid, which has not been discussed closely, and discuss DC velocity ordering independently of phase order. This transition is investigated focusing on the existence of plastic deformation. When macroscopic solid cluster in which plastic deformation does not occur exists, we determine it is the moving solid phase. We propose a new well-defined analysis based on an idea of a bond percolation transition. Spatial long range order can be discussed by the finite size scaling for this transition. The long time behavior is also discussed according to the observation time dependence. Note that if plastic deformation occurs as a temporally local event and the phase configuration returns to the initial one after it, long range order of phase is possible in the plastic flow phase following to the present definition. Our results show that macroscopic plastic deformation is always occurs in infinitely long time in the presence of pinning potential but the system behaves as a moving solid for shorter time observation than the typical life time, which exponentially grows with the driving force.

In chapter 4, phase order in steady state is investigated by analyzing the correlation function and structure factor. We do not find any long range order. Additionally I discuss the driving force dependence of the behavior of topological defects and show that it is characterized by an effective temperature which is proportional to the inverse of the driving force.

Chapter 2

Fundamental Features

We numerically analyze the dynamics of the driven random-field XY model. In this chapter, I show the results which tell us the fundamental feature of this model. These results quantitatively reproduce experimental facts which are beyond the scope of the elastic manifold model. Here, I do not argue the sample size dependence of physical quantities in deep. The behavior in the thermodynamic limit is discussed in the later chapters. The qualitative behavior on almost all aspects is same in one, two and three dimensions. So we show only the result of three dimensional system here.

2.1 Simulation Settings

We numerically solve the equations of motion,

$$\dot{\theta}_i = -\frac{J}{z}\sum_j \sin(\theta_i - \theta_j) - \sin(\theta_i - \beta_i) + f, \tag{2.1}$$

which is introduced in the previous chapter by the forth order Runge-Kutta method. θ_i's are put on regularly on the lattice points of square lattice in two dimensions and simple cubic lattice in three dimensions. Periodic boundary condition is imposed. The linear size of sample L is taken from 4 to 128 in three dimensions. The finite size effect is quite large in these continuous variable systems and it appears as the correlation length overcomes about 10% of L.

$N(= L^d)$ of random number β's are needed for a single d-dimensional sample. These are introduced as follows. We prepare $2\pi m/L^d$ where $m = 1, 2, \ldots, N$ and randomly distribute them on each site in order to hold the global rotational symmetry, $\sum_j e^{i\beta_j} = 0$, even in small samples. As L becomes larger, the result becomes closer to that in the case that an uniform random number is given independently on each site. Almost all quantities to calculate, which are defined later, are averaged values for samples at the final step.

The initial states are given by two opposite ways. One is an uniform state where $\theta_i = 0$ for all i and another is a random state which is obtained by the same way as β's. Uniform shift by a constant in the former case does not yield meaningful change. Physical quantities are calculated after some precursory running for the relaxation to the steady state from the initial state. When same type of calculations are performed for various parameters, f and J, we use the final state for the former parameter as the next initial state to save the calculation time and quantities are calculated after relatively short precursory time. When we repeat such processes with changing parameter monotonically, quantities shows hysteresis between increasing and decreasing cases. It is not only due to the lack of complete relaxation but also to the appearance of metastable states in disordered systems. When parameter changing

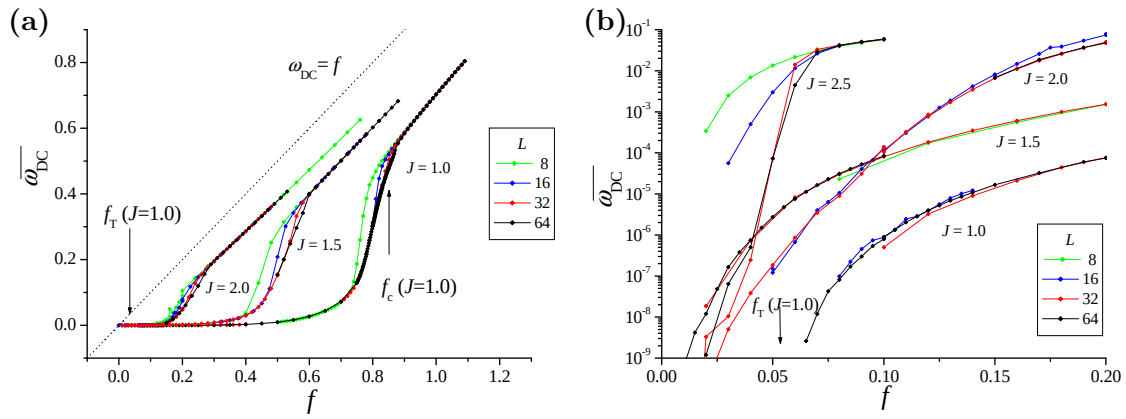

Figure 2.1: DC phase velocity - driving force character in normal scale (a) and semi-logarithmic scale (b).

step is enough small, the hysteretic behavior is similar to that in simulations with sweeping the parameter continuously.

We set the time step for discretized integration as $\Delta t = 2\pi/n_{\rm div}v_0$. Here, $n_{\rm div} = 8$ and $v_0 = J + f$ for $J + f > 1$ or $v_0 = 1$ for $J + f < 1$. The Δt independence of the solution is checked for smaller Δt's if ignoring chaotic sensitivity to the error in the plastic flow regime.

The case of coupling constant $J = 1.0$, relatively weak coupling, is intensively investigated because we are interested in the plastic behavior. I will make discussions with this case in mind when the value of J is not declared.

2.2 Nonlinear Conduction

Most fundamental transport quantity is the phase velocity, which is proportional to the electric current for CDW and the voltage drop for FLL. Spatially averaged DC velocity is calculated as

$$\overline{\omega_{\rm DC}} = \langle \dot{\theta}_i(t) \rangle_{i,t} = \frac{1}{N} \sum_i \frac{\theta_i(T) - \theta_i(0)}{T} \tag{2.2}$$

Here I consider the driving force dependence of the velocity fixing the coupling constant. In Figure 2.1, $\overline{\omega_{\rm DC}} - f$ character curves for various J's are shown. These curves are obtained by force decreasing simulation. Two important features are seen. One is the existence of threshold value $f_T(J)$, below which the whole system is pinned. Another feature is drastic increasing of velocity around $f_c(J)$ which is related to the spatial ordering of DC velocity. With much stronger drive, the behavior of the system become close to the the linear response $\overline{\omega_{\rm DC}} = f - O(f^0)$. There are three regimes divided by f_T and f_c, i.e. "pinned", "plastic flow" and "moving solid" regimes, as shown below. Generally speaking, as J increases, the rapidly growing region of $\overline{\omega_{\rm DC}}$ comes closer to the origin $f = 0$ and $\overline{\omega_{\rm DC}} - f$ characteristics approach to $\overline{\omega_{\rm DC}} = f$.

2.2.1 Plastic Depinning

Here I discuss the depinning behavior. Whether each site is pinned or not is determined by whether $\theta_i(T) - \theta_i(0)$ is larger than 2π or not. Here T is the observation time. Then the resolution of the DC velocity is $2\pi/T$. Under this criterion there is a finite threshold driving force f_T below which all of the sites are pinned. For sufficiently large T, the magnitude of f_T does not depend on T. Only the most weekly pinned region starts to move just on f_T when plastic deformation is allowed while all sites move even just above f_T in the elastic coupling model when seeing in the enough long time scale.

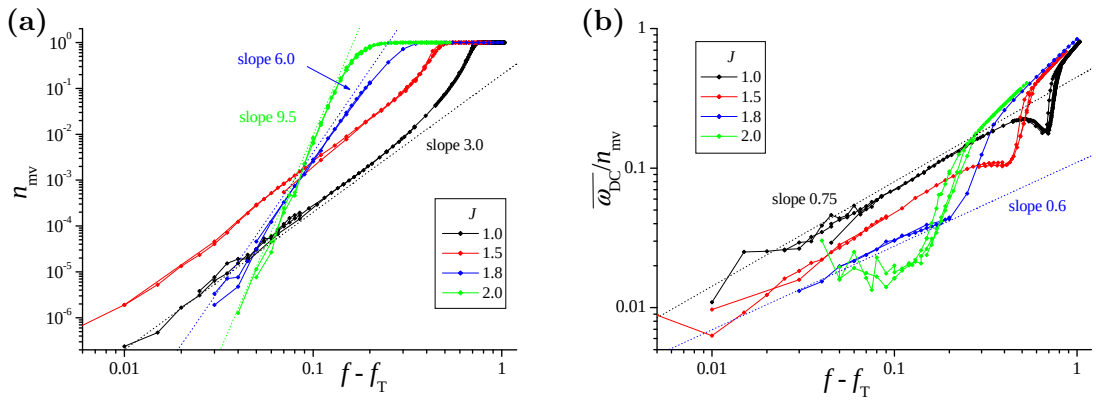

Figure 2.2: (a) The relation between $n_{\rm mv}$ and $f - f_T$. (b) The relation between $f - f_T$ and mean velocity of moving sites $\overline{\omega_{\rm DC}}/n_{\rm mv}$.

If $J = 0$ i.e. no interaction, θ_i on each site shows same time evolution except constant time and phase shifts since pinning strength is uniform. The equation of motion $\dot{\theta} = -\sin\theta + f$ is integrable for one period, $2\pi/\overline{\omega_{\rm DC}}$, then we obtain $\overline{\omega_{\rm DC}} = \sqrt{f^2 - 1}$ for $f > 1$ and $\overline{\omega_{\rm DC}} = 0$ for $f < 1$. Critical exponent $\beta = 1/2$ and $f_T = 1$ in $\overline{\omega_{\rm DC}} \sim (f - f_T)^\beta$. Although every site is depinned at the same threshold when $J = 0$, this is not significant because it comes from the artificial factor that we have set pinning strength uniform. The nonuiformity of local depinning threshold due to the randomness of β appears as far as $J > 0$.

In the vicinity of the depinning point, moving sites are quite rare and all of neighboring sites of a certain site i which starts moving are stopping. When $J \ll 1$, the interaction potential with neighboring sites which keep stopping is regarded as a static potential. Then it yields an effective static pinning force f'_{Ti} as

$$\frac{J}{z}\sum_j \sin(\theta_i - \theta_j) + \sin(\theta_i - \beta_i) = f'_{Ti}\sin(\theta_i - \beta'_i). \tag{2.3}$$

Here $\theta_j = \beta_j + \sin^{-1} f + O(J)$. f'_{Ti} gives a local depinning force. This is minimized when $\beta_j + \sin^{-1} f = \beta_i + \pi$ for all j. Such most weakly pinned site can be found in a large system. Thus pinning force equals $(1 - J)\sin(\theta_i - \beta_i)$ and $f_T = 1 - J$.

The fraction of moving sites $n_{\rm mv}$ becomes larger with the driving force above $f = f_T$. It is expressed as

$$n_{\rm mv} = \int_{2\pi/T}^{\infty} d\omega_{\rm DC} P(\omega_{\rm DC}) = \int_{f_T}^{f} df'_T P(f'_T). \tag{2.4}$$

Here $P(\omega_{\rm DC})$ and $P(f'_T)$ are distribution functions of local DC phase velocity and the local effective depinning force for each site. It increases as

$$n_{\rm mv} \sim (f - f_T)^\alpha \tag{2.5}$$

in the vicinity of f_T as shown in Figure 2.2(a). Then $P(f'_T) \sim (f - f'_T)^{\alpha-1}$. In the case of elastic coupling the DC velocity is always uniform and $n_{\rm mv}$ takes only zero or one. If one supposes that each site is depinned independently and has the same exponent β,

$$\overline{\omega_{\rm DC}} \propto \int_{f_T}^{f} df'_T P(f'_T)(f - f'_T)^\beta \sim \int_{f_T}^{f} df'_T (f - f'_T)^\beta (f'_T - f_T)^{\alpha-1} = \text{const.} \times (f - f_T)^{\alpha+\beta}. \tag{2.6}$$

Here β does not necessarily equal to $1/2$, which is obtained for one body problem, because the neighboring sites should move to some degree as far as they do not advance by 2π. In

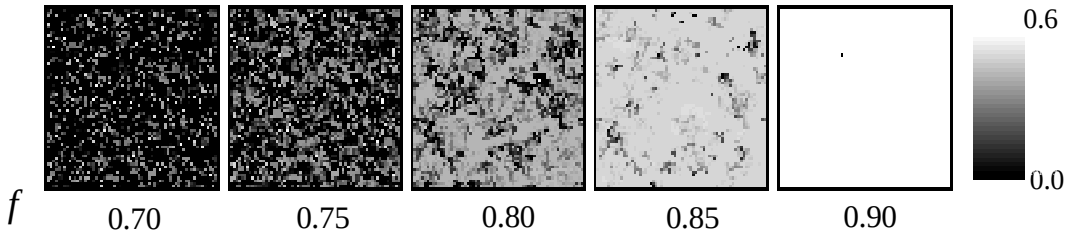

Figure 2.3: The spatial configurations of local DC velocity in single layer of 64^3 sample are shown with gray scale plot.

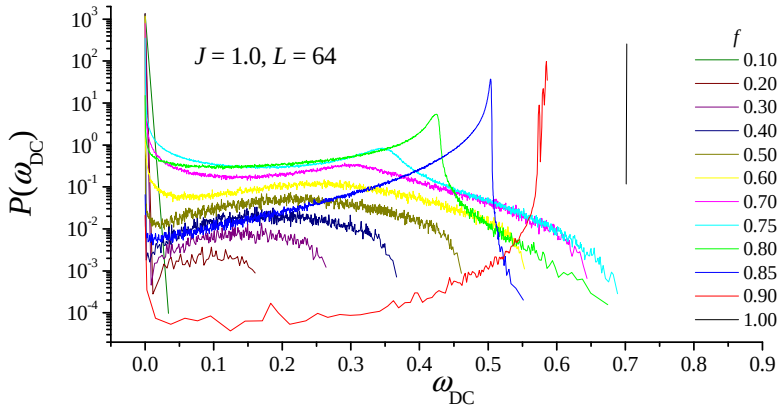

Figure 2.4: Distribution function of $\omega_{\rm DC}$ for various driving forces in semi logarithmic scale.

the case of $J = 1.0$, we obtain $f_T = 0.055$, $\alpha = 3.0$ and $\beta = 0.75$. It is hard to estimate f_T accurately because the exponent α is rather large compared with 1 then the function $n_{\rm mv}(f)$ is flat at $f = f_T$. We calculate f_T and α directly from the curve $n_{\rm mv}(f)$ and estimate β using $\overline{\omega_{\rm DC}}/n_{\rm mv} \sim (f - f_T)^\beta$ as shown in Figure 2.2. Of course, $\overline{\omega_{\rm DC}}$ is well described by the exponent $\alpha + \beta$ obtained above. The exponent α starts to grow with J at $J \approx 1.5$. Then $n_{\rm mv}$ grows rapidly with f and plastic flow regime becomes narrower.

2.2.2 DC Velocity Distribution

The most important difference between the plastic and elastic models is whether spatially nonuniform DC velocity configuration is possible or not. Here I focus on the distribution function of $\omega^i_{\rm DC} =< \dot{\theta}_i >_{\rm time}$.

Before investigating distribution function, I note the spatial configuration of $\omega_{\rm DC}$. When $n_{\rm mv} \ll 1$, moving sites are isolated and form very small clusters, which are typically consist of single site and surrounded by stopping sites. Spatial configurations of $\omega^i_{\rm DC}$ for several f's are shown in Figure 2.3. These small moving cluster behaves as if they were in the static potential. The motions are periodic and each site has the same $\omega_{\rm DC}$ inside each cluster. Such behavior is observed only as far as the radius of a cluster is below two or so. In a larger cluster, the periodicity of the motion is broken. This is because cluster size grows with f faster than the $\omega_{\rm DC}$ coherence length does and overcomes it.

As the driving force increases, more and more sites are depinned. The sizes of moving clusters become larger then come to contact with each other. Such clusters are combined and percolation of a moving cluster over the whole system occurs at $f \approx 0.75$. As a result small islands made by pinned sites are left. Here $n_{\rm mv}$ become $O(1)$ then power low that is observed near the depinning point is broken. At this point most of sites are depinned but each moving site takes various values of velocity then phase slips happen between sites

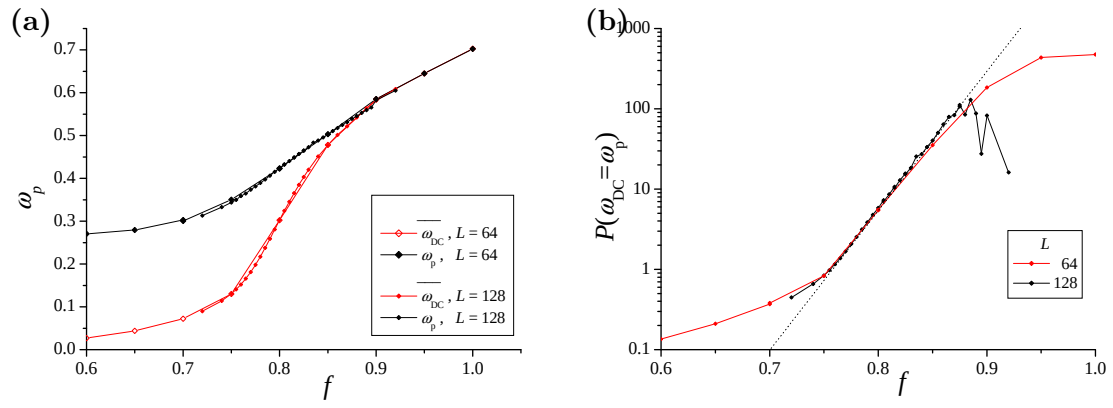

Figure 2.5: (a) The relation between the peak position of $P(\omega_{\rm DC})$ and driving force. Site averaged velocity $\overline{\omega_{\rm DC}}$ is plotted together for the comparison. (b) The relation between the peak hight and the driving force. The dotted line indicates $\exp\Big((f-0.758)/0.025\Big)$.

which have different DC velocity. As the driving force becomes more larger, moving sites come to interact with each other then the velocity becomes uniform at $f \approx 0.90$.

The distribution function of $\omega_{\rm DC}$ is shown in Figure 2.4. In the vicinity of f_T, the shape of distribution function is estimated by some scaling argument as

$$P(\omega_{\rm DC}) = \left(P(f_T')\left|\frac{df_T'}{d\omega_{\rm DC}}\right|\right)_{\omega_{\rm DC}=(f-f_T')^\beta} \sim \omega_{\rm DC}^{(1-\beta)/\beta}\Big(\omega_{\rm max}^{1/\beta}-\omega_{\rm DC}^{1/\beta}\Big)^{\alpha-1}. \qquad (2.7)$$

Here $\omega_{\rm max} \propto (f-f_T)^\beta$. $P(\omega_{\rm DC})$ behaves as $\omega_{\rm DC}^{(1-\beta)/\beta}$ for small $\omega_{\rm DC}$, where $\beta = 0.75$ for $J = 1.0$. The power, however, seems rather larger than $(1-\beta)/\beta = 0.33$ in Figure 2.7(a). $P(\omega_{\rm DC})$ goes to zero at $\omega_{\rm max}$. Strong delta function peak at the origin is also exist. The tail of the peak at the origin turns to be apparent at $f \approx 0.4$. This and another tail of high velocity group make a roughly flat continuous band.

The uniformity of DC velocity

At $f = 0.75$, a peak at $\omega_{\rm DC} = \omega_p(f)$ becomes apparent. This peak corresponds to the narrow band noise peak and $\omega_p(f)$ coincides with the washboard frequency $\omega_{\rm NBN}$ as shown later. This means the creation of large co-moving clusters with a particular velocity which depends on f. In Figure 2.5(a), $\omega_p(f)$ is plotted as a function of f. The linear dependence in the high velocity regime, $f > 0.90$, is smoothly extended to the lower region, where the site averaged velocity $\overline{\omega_{\rm DC}}$ is smaller than ω_p.

The peak hight $P(\omega_p(f))$ is shown in Figure 2.5(b). We found the exponential increase of peak hight as

$$P\Big(\omega_p(f)\Big) \propto \exp(f/f_0). \qquad (2.8)$$

Here $f_0 = 0.025$ for $J = 1.0$. For $f > 0.88$, eq.(2.8) collapses. Here DC velocity in each sample becomes unique in the resolution of $2\pi/T$ and the deviation of $\omega_{\rm DC}$ in each sample becomes smaller than the deviation of ω_p for samples Sample averaged distribution function has multiple peaks with lower hight. This strong uniformity of $\omega_{\rm DC}$ in each sample is, however, considered to be a finite size effect. We do not obtain meaningful values above $f = 0.88$. As far as $f < 0.88$, singular behavior, which implies a phase transition, is not observed.

In Figure 2.6(a), $P(\omega_{\rm DC})$ plotted with $\omega_{\rm DC} - \omega_p(f)$. It is shown that the peak width becomes narrower while the peak hight become taller. In Figure 2.6(b) the $P(\omega_{\rm DC})$ and

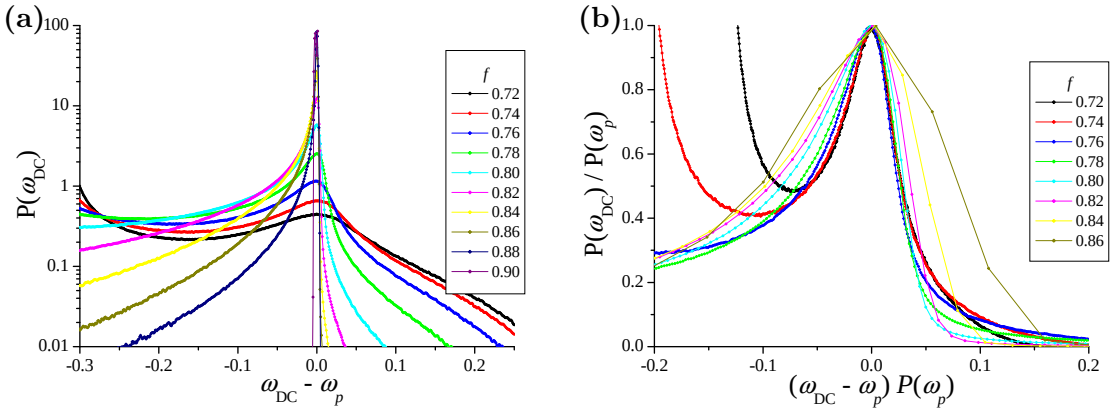

Figure 2.6: (a) $P(\omega_{\rm DC})$ plotted with $\omega_{\rm DC} - \omega_p(f)$. (b) $P(\omega_{\rm DC})$ and $\omega_{\rm DC} - \omega_p(f)$ divided and multiplied by $P(\omega_p(f))$ respectively.

$\omega_{\rm DC} - \omega_p(f)$ are divided and multiplied by $P(\omega_p)$ respectively. Such scaling will yield the convergence if the distribution function is expressed by a homothetic function which does not depend on f. On the other hand if the delta function peak grows with f at $\omega_{\rm DC} = \omega_p$, $P(\omega_p)$ is larger than the peak hight of non-singular part, $\omega \neq \omega_p$, then the scaled width becomes larger. Although Figure 2.6(b) shows that the width grows with f, it is suspicious that the grows is due to the delta function peak. It is likely to be caused by that the sites with very small $\omega_{\rm DC}$ join the peak at ω_p.

The uniformity of $\omega_{\rm DC}$ and the periodicity of time evolution have strong correlation. When $\omega_{\rm DC}$ is distributed widely, phase slips occurs frequently at which interaction is highly nonlinear. In this regime the motion is irregular and chaotic. It becomes gradually periodic with growth of the uniformity of $\omega_{\rm DC}$. The time evolution of the system becomes completely periodic above certain f where all sites, except very rare stopping ones, have exactly same $\omega_{\rm DC}$. But this limit cycle motion comes from the finite size effect as discussed in chapter 3.

Power Law Peaks

The distribution function $P(\omega_{\rm DC})$ has power law shape at two points. One is at $\omega_{\rm DC} = 0$ as shown in Figure 2.7(a).

$$P(\omega_{\rm DC}) \propto \omega_{\rm DC}^{-\gamma_0} \tag{2.9}$$

Such behavior is most apparent at $f \approx 0.75$ where the percolation of moving site just occurs. Here, $\gamma_0 \approx 0.78$. At this point, many stopping or slowly moving sites remain and this peak is contributed by them. They seem stopping for almost all time but intermittently advances by 2π. These motion is quite irregular and there is no typical time scale. The exponent $\gamma_0 = 0.78$ seems not to change with f below $f = 0.75$ although the tail of the growing peak at ω_p makes it unclear. The coefficient decreases rapidly for $f > 0.75$ and exponent seems to be smaller than 0.78.

Another region where power divergence occurs is slightly below the peak position ω_p (See Figure 2.7(b)). This peak is constructed with almost regularly moving sites. Intermittent events are important similar to the peak at $\omega_{\rm DC} \approx 0$. Phase slip occurs irregularly and not frequently between domains with similar $\omega_{\rm DC}$. The distribution is expressed as

$$P(\omega_{\rm DC}) \propto (\omega_p - \omega_{\rm DC})^{-\gamma_1}. \tag{2.10}$$

The exponent γ_1 equals to 1.7. It is larger than 1, thus this peak must be rounded when $\omega_p - \omega_{\rm DC}$ is smaller than certain cut-off value. Otherwise the integrated value of $P(\omega_{\rm DC})$ goes to infinity which should be unity. Such flat region becomes narrower as f increasing. The

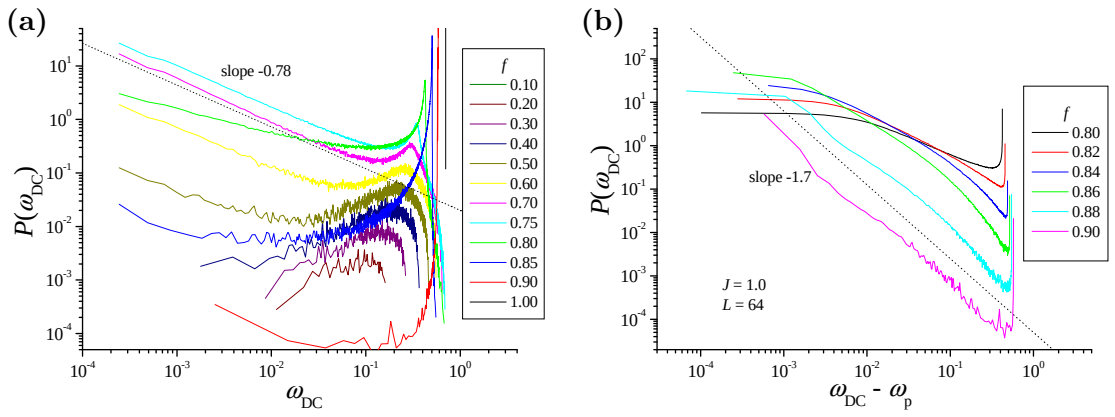

Figure 2.7: The Power low behavior of $P(\omega_{\rm DC})$ around $\omega_{\rm DC} = 0$ (a) and $\omega_{\rm DC} = \omega_p(f)$ (b).

peak continuously becomes sharper rather than delta function peak component $\delta(\omega_{\rm DC} - \omega_p)$, which indicates an infinite co-moving solid cluster, grows. This is closely argued in chapter 3.

The meanings of these power lows behavior are not clear. The case around ω_p may be a kind of self organized criticality. This is also discussed in chapter 3. Power low behavior is not seen on the upper side of ω_p and $P(\omega_{\rm DC})$ seems to decrease exponentially. The origin of such asymmetry is an open question.

2.3 Spatial Periodicity

When the uniformity of DC velocity grows, the phase correlation length also becomes longer. This is related to the periodicity of the moving solid. The degree of periodicity is measured by the ferromagnetic order parameter r, which is written as

$$r = \frac{1}{T}\int_0^T dt \left| \frac{1}{N}\sum_i e^{i\theta_i(t)} \right| \tag{2.11}$$

This shows the instantaneous ordering in space and does not capture temporal order because time averaging is performed after taking absolute value. To argue spatio-temporal ordering, one has to know the velocity of moving frame $\omega_{\rm mf}$ and calculate $\langle e^{i(\theta - \omega_{\rm mf} t)} \rangle$. But $\omega_{\rm mf}$ is difficult both to define and to calculate precisely in spite that the order parameter in long time scale is strongly sensitive to the value of $\omega_{\rm mf}$. The most possible candidate of $\omega_{\rm mf}$ is the peak position of $P(\omega_{\rm DC})$ but it is calculated only to an accuracy of $2\pi/T$, which is insufficient.

The driving force dependence of r is shown in Figure 2.8(a). It rapidly increases at $f \approx 0.8$ and become $O(1)$. This indicates a second order phase transition but strong size, L, dependence is observed. The magnitude of r for fixed f decreases with L and shows no tendency to converge to a finite value. The critical force also shifts to higher value. It suggests that there is not any transition but a crossover. I discuss the phase ordering in more detail in chapter 4.

The phase coherence length ℓ can be roughly estimated from r. When long range order is not established, r equals zero in an infinite size system. In a finite size system, r has a finite value as a fluctuation which is proportional to $N_{\rm domain}^{-1/2}$. Here $N_{\rm domain}$ is a number of phase coherent domains which equals to L^d/ℓ^d. Then $r \sim (L/\ell)^{-d/2}$ or

$$\ell \sim L r^{2/d}. \tag{2.12}$$

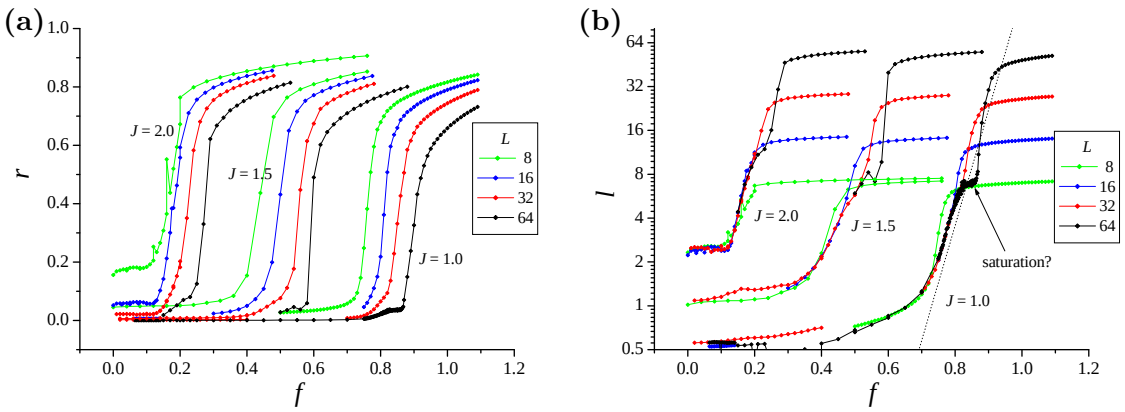

Figure 2.8: (a) The driving force dependence of ferromagnetic order parameter r. (b) Phase coherence length ℓ estimated from r. Dotted line shows $\exp[(f-0.73)/0.045]$.

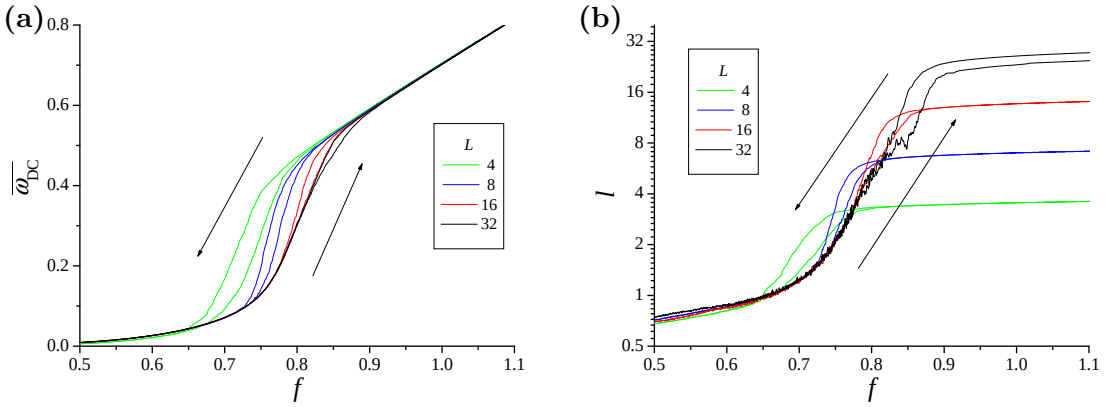

Figure 2.9: Hysteresis loop in $\overline{\omega_{\rm DC}} - f$ curve (a) and $\ell - f$ curve (b). The disagreement of two curves of ℓ in large f region for $L = 32$ is due to the insufficient relaxation in f increasing case. It takes very long time to eliminate unbounded dislocations.

The proportional coefficient should be $O(1)$. When this scaling is performed for various L's, we obtain a conversion to the universal curve as shown in Figure 2.8(b). Curves for each sample size leave away from the universal one when ℓ reaches about 20% of the system size and ℓ rapidly saturates to the sample size. As far as ℓ does not saturate, it seems to grow as an exponential function of f above $f = 0.70$ for $J = 1.0$. There is a faint sign, however, that ℓ saturates to 8.0 in the case $J = 1.0$ and $L = 64$. This is not a finite size effect, which is discussed closely in chapter 4.

2.4 Hysteresis

So far I have shown the results of force decreasing simulations, which start with uniform initial conditions at large f. All quantities show the hysteresis to a varying degree, the system takes more ordered state in the f decreasing case than in the f increasing case at the same f in a certain region. The hysteresis curves of $\overline{\omega_{\rm DC}}$ and ℓ are shown in Figure 2.9. This hysteresis does not vanish even if the sweep rate of f is decreased sufficiently. The area of hysteresis loop $\int df[a_\uparrow(f) - a_\downarrow(f)]$, however, becomes smaller as the system size become larger and its position shift to larger f direction. The hysteresis starts at the same point where the behavior of $\ell \sim Lr^{2/d}$ goes away from the universal curve and f of the starting point increases with L. Then it is expected that hysteresis is caused by the finite size effect and vanishes in the infinite size limit.

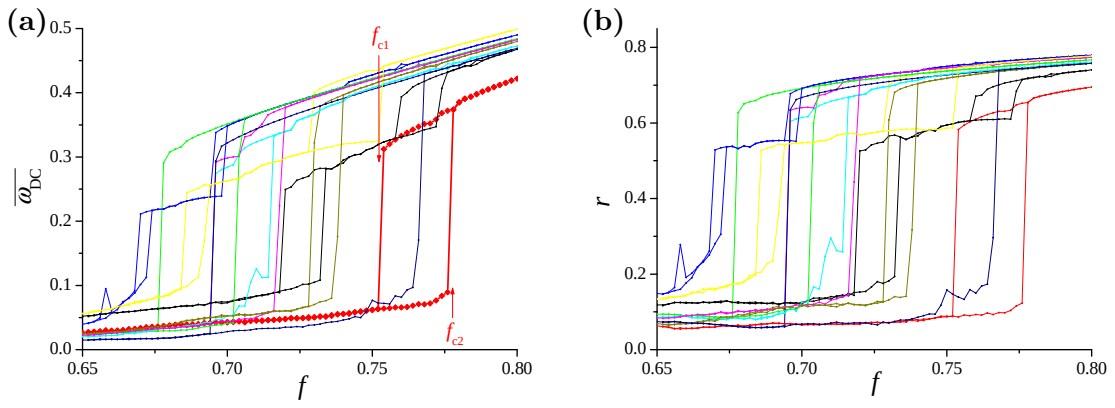

Figure 2.10: Hysteresis loop of $\overline{\omega_{\rm DC}}$ (a) and r (b) with f in the single small samples, $L = 4$. In the figure (a), two threshold values f_{c1} and f_{c2} for the certain sample are pointed.

Figure 2.9 shows data averaged over samples, which are smoothly changing. Single sample results show much larger hysteresis and the behavior of small samples is similar to a first order transition as shown in Figure 2.10. There is two edge values of the driving force, f_{c1} for the transition from order to disorder and $f_{c2}(> f_{c1})$ for the transition in the opposite direction (Some samples show multi step transitions). This discontinuous transition resembles to the case of the infinite range model mentioned in section 1.3.3. The lower branch, both in $\overline{\omega_{\rm DC}}$ and r, indicates pinned regime in that model, on the other hand it is chaotic and disordered plastic flow state in the present model. The Upper branch denotes perfectly periodic and phase coherent moving state.

Small systems have small number of metastable states, only two states exist in the extreme cases. The number becomes larger with system size and the gaps of intensive quantities between neighboring states become narrower. Then such quantity changes more smoothly as an accumulation of small steps of change.

Around the depinning threshold f_T, hysteresis does not appear because no metastability exists at the plastic depinning where each site moves independently. In the case of the elastic model, depinning is a nonlocal event. It can be proved, however, that the configuration which is initially set on behind the another configuration on the driving direction never passes the preceding one [35]. Then unique f_T can be determined.

2.4.1 Switching

Delayed switching mentioned in section 1.2.2 and 1.3.3 is also found in our simulations for very small samples. The switching from plastic flow to coherent flow occurs near and above f_{c2}, where plastic flow is unstable. A very sharp transition in time evolution with time delay τ_d is observed as shown in lower graph of Figure 2.11(a). The simulations start at $t = 0$ with some random phase configurations and f is fixed. Initially non periodic plastic flow is realized. Precursor of switching is hardly observed and the system seems as if it were in the stable steady state before switching. The delay times, which are much larger than the microscopic time scale $2\pi/\overline{\omega_{\rm DC}}$, considerably vary depending on the initial random configurations. We also try the case that the driving force is imposed after relaxation at $f = 0$ but it yields almost same results, averaged delay time, then the time $t = 0$ can be identified as the time at which external driving force is imposed.

We also find the opposite direction switching from coherent flow to plastic flow near and below f_{c1}, where coherent flow is unstable. The switching is shown in the upper graph of Figure 2.11. In this case the initial condition is uniform. The delay times for various initial constant phases fall within the range of $2\pi/\omega_{\rm DC}$ around the averaged value.

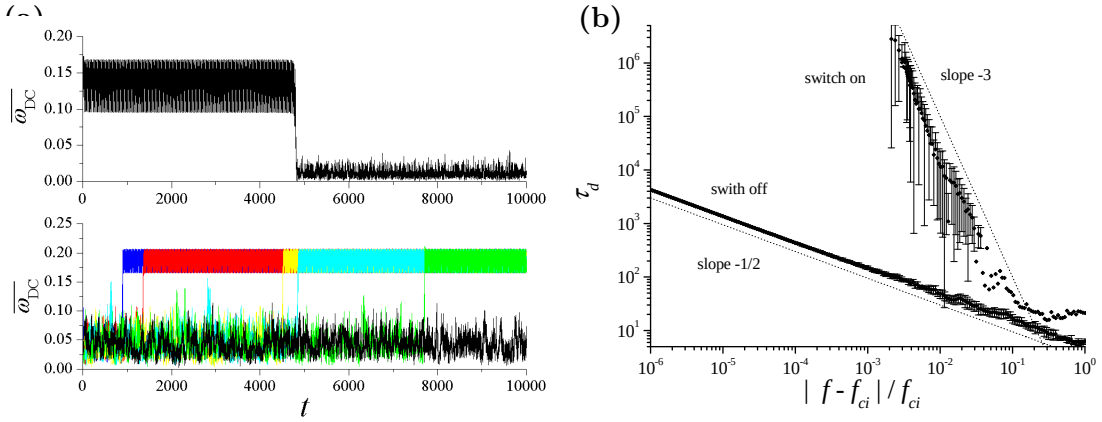

Figure 2.11: (a) Time evolution of $\overline{\omega_{\rm DC}}$ after the driving force is imposed. Upper figure shows switching off at f_{c1} with an uniform initial condition and lower figure shows switching on at f_{c2} with random initial conditions. Each color in lower figure indicates the initial condition. (b) The relation between delay time for switching and reduced driving force. Error bars show the deviation of delay times for different initial conditions. Note that the results, both (a) and (b), are for a single small sample.

The delay time τ_d diverges as

$$\tau_d \propto |f - f_{ci}|^{-z_i}, \quad i = 1, 2 \tag{2.13}$$

when approaching the critical point from below f_{c1} and above f_{c2}. The delay time is plotted as a function of reduced driving force $|f - f_{ci}|/f_{ci}$ in Figure 2.11(b). The critical exponents z_i's are obviously different for f_{c1} and f_{c2} and they seem to be simple numbers, $z_1 = 1/2$ and $z_2 = 3$. These exponents do not depend on samples. The delay time widely varies depending on the random initial condition above f_{c2}. The dispersion of delay time is also diverges at f_{c2} with the same exponent z_2. It means that there are many quasi-metastable plastic flow states which have various degree of instability.

Strogatz *et al.* obtain $z_2 = 1$ by linear stability analysis of static solution with mean field approximation. All of these exponents are clearly different. This reflects the difference among the natures of unstable attractors in these cases, that are limit cycle, chaotic and static ones. (Of course it is more likely mean field treatment have changed the exponent.)

In the experiment of CDW in $K_{0.3}MoO_3$ [21], the exponent is estimated $z_2' = 2.03$. The magnitude of current indicates the switching from pinned state to elastic flow is observed. It is consistent with the result $z_2' = 2$ for the elastic model with inhomogeneous driving force [36]. If it is true, the difference between $z_2' = 2$ and the present result $z_2 = 3$ provides the criterion for the identification of the plastic flow.

2.5 Conduction Noise

Here I discuss about the temporal fluctuation of the current that is proportional to $\dot{\theta}$. The power spectrum of current is defined as follows.

$$S(\omega) = \frac{1}{T} j(\omega) j(-\omega), \quad j(\omega) = \int_0^T dt \frac{1}{N} \sum_i \dot{\theta}_i(t) e^{i\omega t} \tag{2.14}$$

$S(\omega)$ for various f's are shown in Figure 2.12(a).

The sample size dependence of $S(\omega)$ is shown in Figure 2.12(b) where the product of system volume N and $S(k)$ is plotted. $NS(k)$ does not show L dependence except $f = 0.90$. It means that the amplitude of fluctuating part in $\overline{\dot{\theta}(t)} = N^{-1} \sum_i^N \dot{\theta}_i(t)$ is proportional to

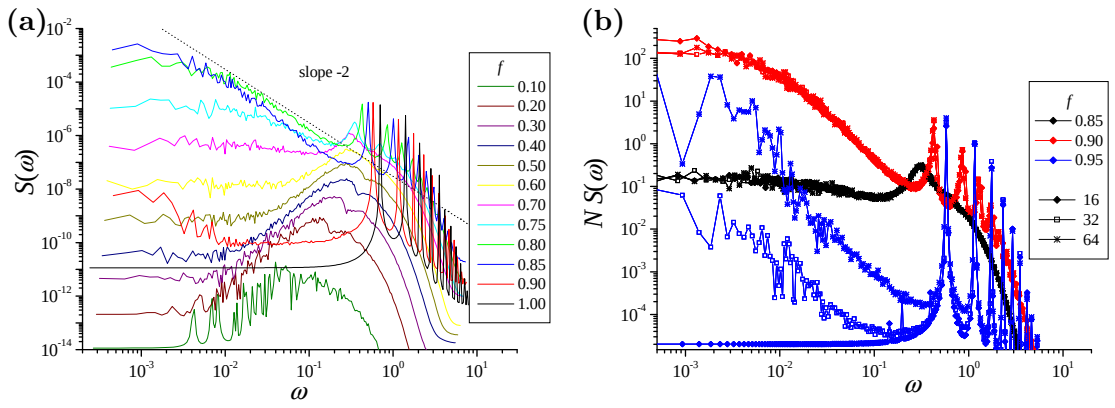

Figure 2.12: Power spectrum of spatially averaged phase velocity. (a) Driving force dependence. (b) Sample size dependence.

$N^{-1/2}$, which comes from the lack of phase coherence of local phase velocity $\dot{\theta}_i(t)$. Note that the phase coherence of oscillation in $\dot{\theta}_i(t)$ and $\theta_i(t)$ itself do not coexist, e.g. if $\theta_i(t) = \overline{\theta(t)}$ for all i, the phase of $\dot{\theta}_i(t) = f - \sin(\overline{\theta(t)} - \beta_i)$ is perfectly random. For $f = 0.95$ smaller sample takes more periodic motion and low frequency component is smaller. This comes from the falling of the system into the limit cycle motion.

When the driving force is small and plastic flow occurs, the power spectrum has a broad band. In the vicinity of the depinning threshold, it has a single peak with a large width. This is constructed by the superposition of delta function peaks with various frequency accompanying harmonics, which is related to the periodic motion of localized moving clusters. The magnitude of $S(\omega)$ decreases as ω goes to zero in this regime.

Low frequency component grows above $f = 0.50$ as the moving cluster becomes larger with the driving force. In this regime, some moving sites make relatively large clusters and periodic motion is not realized in them. The spectrum is flat for small frequency, which means the dynamics loses correlation in long time. The shape of the spectrum for small ω can be expressed by the Lorentzian $S(\omega) \sim (1 + \omega^2\tau^2)^{-1}$ for $t \sim 0.80$. It means that temporal correlation of total current exponentially decays and there is a correlation time $\tau(f)$. It is checked that this does not correspond to the relaxation time to the steady state. This correlation time is expected to correspond to the mean interval between phase slips among moving neighboring domains. Then $\tau(f)$ increases with the driving force as the temporal periodicity holds for longer time and phase slips occur less frequently.

In Figure 2.13(a) the low frequency part of current power spectrum in relatively high velocity regime is shown, which are comparable with the broad band noise in CDW and FLL systems. The spectrum behaves as a power function of frequency. It is shown that as the driving force becomes larger, power low behavior holds down to the smaller frequency and the exponent seems slowly growing up to 2.6. Additionally it takes a crossover to another power low with a lower exponent ~ 1 not to a constant which is expected for finite correlation time. We need, however, more careful and long time investigation to discuss 1/f noise.

In the high frequency region some peaks with constant spacing exist. These indicate the narrow band noise. The peak position with lowest frequency is well matching with that of the distribution function of $\omega_{\rm DC}$ as compared in Figure 2.13(b). Then this fundamental frequency is equivalent to ω_p. Higher frequency components are its harmonics and the peak positions are integral multiple of ω_p. The peak position ω_p becomes larger with f (See Figure 2.5).

The widths of peaks become narrower and the heights grow with f. There is two reasons for this sharpening, the growth of temporal periodicity for each site and the unifromization

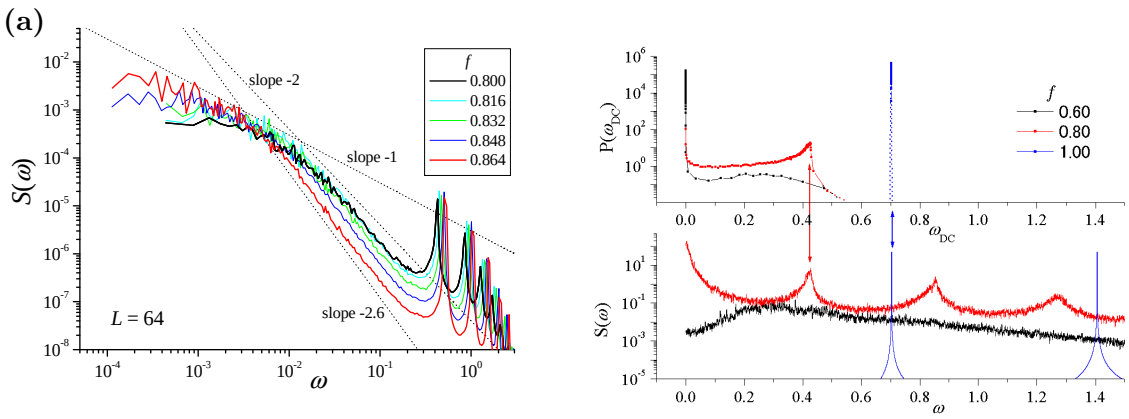

Figure 2.13: (a) Power spectrum of spatially averaged phase velocity. (b) Comparison of positions of peaks in DC velocity distribution function (top) and current power spectrum (bottom). Note that $S(\omega)$ is plotted in an arbitrary unit.

of local DC velocity. The latter is more dominant and the shape of the peak for $S(\omega)$ is well correspond to that of $P(\omega_{\rm DC})$.

The system obtains a perfect periodicity at sufficiently large driving force. In this regime the DC velocity of each site is unique. The only exception is a stopping site, whose phase oscillates around the constant with the same frequency with that of moving sites. Here the phase coherence r becomes $O(1)$ then the uniformity of $\omega_{\rm DC}$ is considered to be a finite size effect. We found that a smaller sample falls into this limit cycle motion at smaller f.

The peak still has a rather large width in this periodic regime (See the spectrum for $f = 1.0$ in Figure 2.12(a)), this is because the observation time T is not an integral multiple of the period $2\pi/\omega_p$. The power spectrum of single frequency oscillation is written as

$$S(\omega_j) \propto \frac{1-\cos[(\omega_j-\omega_p)T]}{1-\cos[(\omega_j-\omega_p)\Delta t]} \quad \text{where} \quad \omega_j = 2\pi j/T \quad \text{and} \quad j = 1, 2, \ldots, T/\Delta t, \qquad (2.15)$$

which results finite width unless $\omega_p T/2\pi$ is an integer.

2.6 Peak Effect

In this section, I discuss the coupling constant dependence of the depinning threshold force and its relation to the peak effect in FLL system. Figure 2.14 shows J dependence of the depinning threshold f_T, which is defined as the value of driving force below which phases of all sites does not advances over 2π within observation time. f_T is calculated for each samples then averaged over samples. It gives a larger value than the f_T of an infinite size system, that is estimated by fitting to $< n_{\rm mv} > \propto (f - f_T)^\alpha$. It is practically impossible to perform it due to very large α for larger J, e.g. $\alpha = 9.5$ for $J = 2.0$. The difference becomes smaller as the sample size become larger.

There is a non trivial peak at $J = J_p \approx 2.2$, which becomes sharper with the system size L. We consider that this should correspond to the peak effect observed in FLL systems due to the melting of vortex lattice. In that case the peak appears at the boundary between pinned solid and pinned liquid by changing magnetic field as shown in Figure 1.5. Unfortunately the relation between magnetic field and the parameters in the present model is not clear. This is because magnetic field affects all of the quantities for continuum description, dissipation coefficient, elastic modulus, the coupling to impurities and driving force, through the number density of flux lines and their changes are not in simple ways near the melting point.

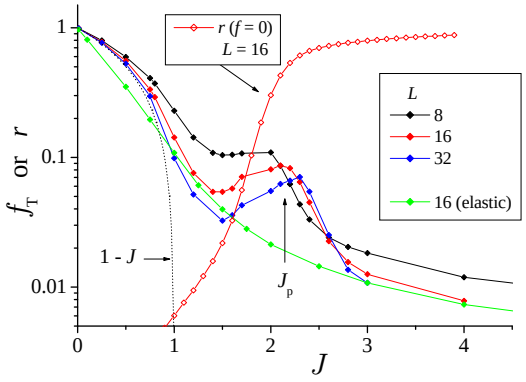

Figure 2.14: Coupling constant dependence of depinning threshold force f_T. The $f_T - J$ curves for the elastic model with $L = 16$ is also shown. Dotted line indicates $f_T = 1 - J$. Ferromagnetic order parameter r at $f = 0$ is also shown together.

We consider, however, that J_p corresponds to the melting point because the phase coherence r of pinned state becomes $O(1)$ above J_p. (The phase coherence r at $f = 0$ is plotted as a function of J in Figure 2.14.) The pinned state below and above J_p is regarded as the pinned liquid (or glass) and the pinned lattice respectively. Then the decrease of J is related to the increase of magnetic field near the melting point at least in the vicinity of J_p.

This peak results reentrant to the pinned state and non-monotonic character of velocity when changing J with fixed small f. In Figure 2.15(a) DC velocities is plotted as functions of the coupling constant for various fixed f's. For $f = 0.05$, $\overline{\omega_{\rm DC}}$ decreases with f above $J = 1.4$ and takes a minimum value at $J = 2.0$ slightly below J_p. We don't find "re-pinning" around J_p which is expected for small f because $\overline{\omega_{\rm DC}}$ is an averaged value over samples and there is a sample which have extremely small f_T. The $\overline{\omega_{\rm DC}} - f$ curve is comparable with the relation between voltage drop and magnetic field with fixed current for super conductors [15]. We can not ask the good correspondence, however, between them in the wide range of J by simple conversion of J to magnetic field because negative (linear) correlation between J and magnetic field can be assumed only in the vicinity of J_p.

Next I discuss the origin of the peak effect. The depinning threshold calculated with the elastic model is also shown in Figure 2.14. It coincides with that of plastic model when $J \gg 1$ where phase differences between neighboring sites are small. The plastic depinning threshold grows faster than the elastic one as J decreases. This is because the phase coherence length of the plastic model is smaller than that of the elastic model and the pinning force per unit volume, $\sim \langle \sin(\theta_i - \beta_i) \rangle$, becomes smaller when it is averaged in the larger phase coherent domain. In another limit of small J, f_T can be described as $1 - J$ as discussed in section 2.2.1. Then f_T goes to zero at $J = 1$ if this expression is extrapolated. If one tries to connect two curves in opposite limits, small $J(\sim 1)$ and large J, around the melting point J_p, non-monotonically changing curve is necessary because a large gap exists between them. The crossover from elastic depinning to plastic one results the peak effect.

The reason why the depinning threshold decreases as leaving away from J_p is understood in different ways as follows. On the upper side of J_p, the effect of random potential is averaged in a large size depinning cluster then net pinning force per volume becomes weak as phase coherence grows. Here the lowering effect on f_T due to the effective pinning potential made by surrounding pinned sites is weak because it appears only on the surface of a cluster. This effect is dominant for small clusters. Then f_T become lower as decreasing J below J_p because the depinning clusters become smaller as J decreases from J_p.

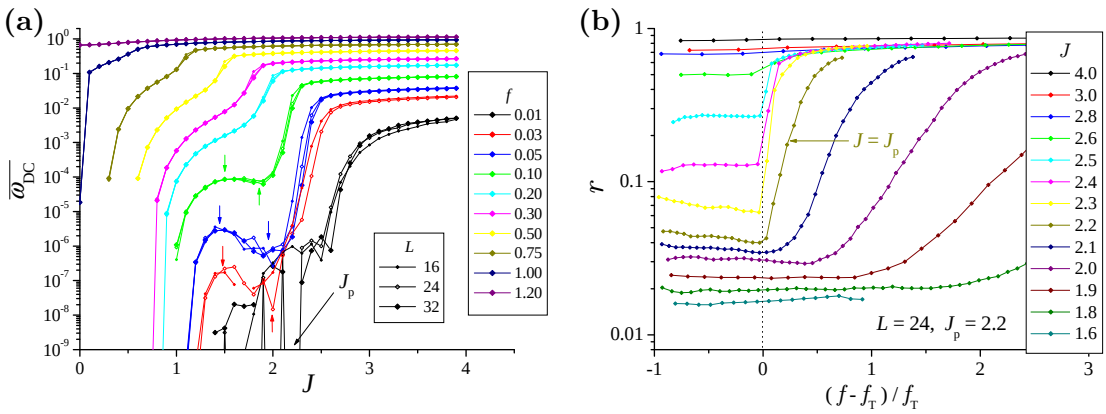

Figure 2.15: (a) Coupling constant dependence of $\overline{\omega_{\rm DC}}$ for various fixed f's. (b) The f dependence of r around the depinning point.

Finally, I consider the difference of phase coherence between the states before and after depinning. The f dependence of phase coherence r around the f_T is shown in Figure 2.15(b). The depinning occurs as a local event below J_p and hardly affects on r while above J_p, the system behaves as an elastic cluster both below and above f_T then r rarely change at f_T also in this regime. Only in the vicinity of J_p, where collective depinning begins to occur, the phase order drastically changes at the depinning point, i.e. the system is rapidly solidified just after depinning.

2.7 Phase Diagram

Here I argue the phase diagram in the J-f plain. There are three kinds of boundary which indicate depinning, phase ordering and DC velocity ordering respectively. These are roughly estimated from the result of finite size samples in the way as explained below and rigorous argument is put off till the following chapters.

Depinning line, which distinguishes pinned and plastic flow states, is drawn by $f_T(J)$ discussed in the previous section. Phase ordering boundary is given by the maximum point of $\partial r/\partial f|_J$. This derivative diverges as approaching the critical point from above and equals to zero below it if the second order phase transition occurs.

DC velocity ordering boundary is most difficult to identify. The velocity of moving frame $\omega_{\rm mf}$ is defined in the ordered state, where macroscopic number of sites moves with this velocity. Then we can adopt

$$q = \left\langle \left| \left\langle e^{i(\theta_i(t)-\phi(t))} \right\rangle_t \right| \right\rangle_i \quad \text{where} \quad \phi(t) = \omega_{\rm mf} t \tag{2.16}$$

as the order parameter. This does not capture spatial order of phase but only temporal one because absolute value is taken before site averaging. $\left\langle e^{i(\theta_i(t)-\phi(t))} \right\rangle_t$ does not equal to zero only when $\omega^i_{\rm DC} = \omega_{\rm mf}$. q has a similar behavior to the component of current power spectrum at $\omega = \omega_{\rm mf}$. The difference is order of i-summation and Fourier integral. Then q is quite sensitive to the value of $\omega_{\rm mf}$ when the narrow band noise peak is very sharp. If one wants to capture the delta function component which means temporal order, exact $\omega_{\rm mf}$ is needed. Here we approximate the phase of moving frame $\phi(t)$ as $r(t)e^{i\phi(t)} = \left\langle e^{i\theta(t)_i} \right\rangle_i$. In this way, $\dot{\phi}(t)$ does not always equal to $\omega_{\rm mf}$ but fluctuates in some degree. $\phi(t)$ sometimes takes discontinuous jump where amplitude $r(t)$ is very small. It works well when $r(t)$ is sufficiently large and the system size is large where the fluctuation of $\dot{\phi}(t)$ is small. The f dependence of q is shown in Figure 2.16. It has a value of $O(1)$ in the high velocity ordered

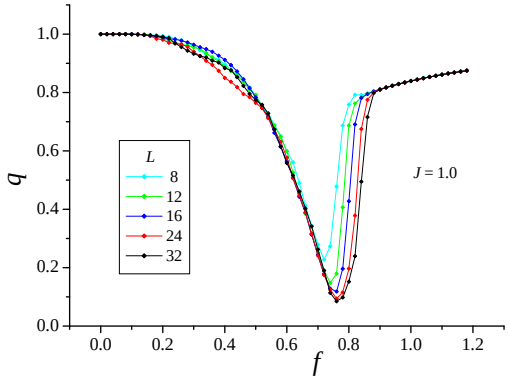

Figure 2.16: The f dependence of the order parameter q for DC velocity ordering.

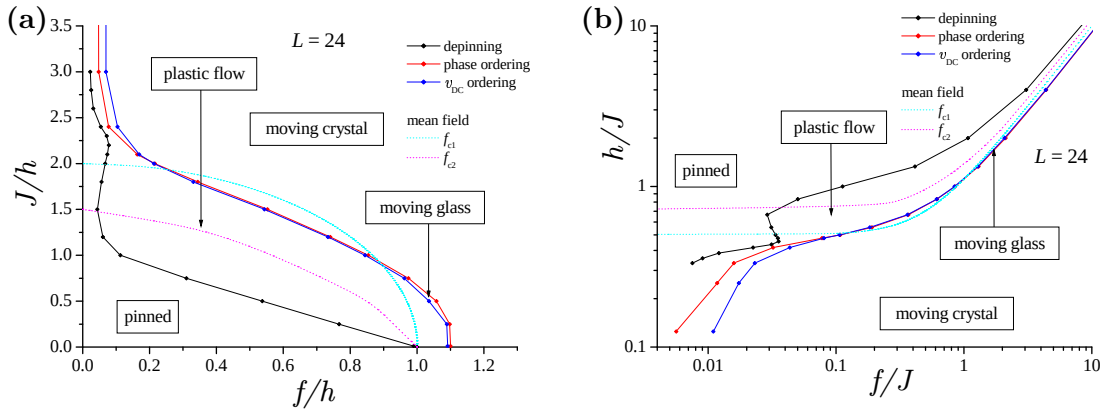

Figure 2.17: The phase diagram for the driven random-field XY model. (a) J-f plane. (b) h-f plane.

region, which indicates moving solid order. q also takes a large value in small f region. But this does not indicate moving solid order because $\phi(t)$ is static governed by majority pinned sites and they contribute to q in this regime. We draw DC velocity ordering boundary in the same way as phase ordering, by the maximum points of $\partial q/\partial f|_J$.

The obtained phase diagram is shown in Figure 2.17(a). The boundary of DC velocity ordering and phase ordering seems to be almost same. The difference grows, however, with the simulation sample size and phase ordering boundary shifts faster to the high f side than DC velocity ordering boundary. In the region between these boundaries, DC velocity is ordered but phase is disordered. Therefore this region is identified as a moving glass phase. The upper side of phase ordering boundary is the moving crystal phase. Roughly speaking, the moving state changes in the order of pinned state, plastic flow, moving glass, moving solid as increasing f or J. Reminding both J and f is scaled by pinning strength h, the phase diagram in h-f plain, scaled by J, is easily obtained. It is also shown in Figure 2.17(b).

2.8 Discussion

In this chapter, I showed that the driven random-field XY model successively describes the many experimental results for CDW and FLL systems beyond the elastic model, e.g. local depinning, plastic flow, hysteresis, delayed switching, broad band noises and peak effect. In these phenomena plastic deformation plays an important role.

At first, I focused on the boundary between pinned and plastic flow states where plastic depinning occurs. We obtain the same formula $v \propto (f - f_T)^{\alpha+\beta}$ as the depinning transition in the elastic model. However this is not a cooperative phenomenon in a long scale. The local depinning is described by a single degree of freedom (and a few neighbors at most) and the exponent β is determined from its dynamics. The exponent α, which reflects the distribution of local depinning thresholds, depends on the distribution of local effective pinning force which can be calculated by analyzing randomly provided local configuration of β's.

We also investigate the coupling constant dependence of the depinning and found a peak of f_T as a result of crossover between ordered and disordered states in the pinned regime. This mechanism discussed here is considered to be applied to the peak effect of superconductors.

In addition to the depinning behaviors, We investigate the ordering of both phase and DC velocity in steady moving states by analyzing order parameter of phase coherence and distribution function of DC velocity. We found the growth of the peak in it which indicates the uniformity of DC velocities. But it is hard to clarify whether the delta function peak exists or not because remaining of nearly stopping sites, whose dynamics is qualitatively different from the sites in peak, disturbs quantitative argument. In the next chapter I introduce better analysis in which the spatial configuration of DC velocities is also taken into account.

Additionally the temporal periodicity of the motion is investigated by the power spectrum of the velocity. We found not only narrow band noise, which is also but also observed in elastic model, but also broad band noise. They represent periodic and chaotic motion respectively. The uniformity of DC velocity and temporal periodicity have strong correlation.

First order like transition and hysteresis are observed clearly in the small samples. The system with $N < 4^3$ shows very sharp discontinuous transition and hysteresis. At the edges of bistable region, delayed switching is observed. Although first order transition like hysteresis and power divergence of delay time are observed, this is not a phase transition in thermodynamic meaning but a bifurcation in the system with small degrees of freedom. Such switching events should also happen locally in the large systems, but the wide distribution of local f_c's and small gaps smear them away. Smooth and non history independent driving force dependence for physical quantities are implied in the large size limit.

The features seen in small samples, however, agree with some experimental results of CDWs quite well, which are mentioned in 1.2.2. In our simulations each degree of freedom is regarded as the semi macroscopic domain in which plastic deformation never occurs. The experimental situations are not necessarily related to the thermodynamic limit $L \to \infty$. It is reasonable to suggest that real samples should have only a few such domains whose sizes are the same order as the sample size. We hope that these are clarified in the experiments. If one requires more quantitative speculation, the model parameters involving the size of the units, elastic domain, and interaction between them should be calculated with microscopic picture, which is also a challenging problem.

Finally I showed the phase diagram of the driven random-field XY model. There are four dynamical regimes; pinned, plastic flow, moving glass and moving solid regimes in order from small to large driving force f. There is a tendency, however, that phase boundaries both of DC velocity and phase orderings shift to the high driving force direction as the system size increases and it would not converge. It is implied that they are not phase transitions but crossovers. In addition to the finite size effect we have to pay attention to the finiteness of observation time which makes the temporal order overestimated. In short time observation one has low resolution of DC velocity although we have to analyze some delta function peaks in DC velocity distribution function or current power spectrum to

discuss temporal long range order. Thus there remains the theoretical interest in whether the ordered state such as moving crystal or moving glass holds or not in infinitely long scale of space and time. This is the theme of the rest of this thesis.

Chapter 3

Dynamic Phase Transition between Plastic Flow and Moving Solid

In this chapter, I argue the possibility of the moving solid phase. The moving solid phase is characterized by the cluster which extends to the system size and its constituents have the same DC velocity in contrast to the plastic flow regime. Here, I concentrate only in the DC velocity ordering and do not care about the phase ordering, i.e. liquid, crystal and (Bragg) glass are not distinguished, which is discussed in the next chapter.

As shown in the previous chapter, the DC velocity on each site has closer value as the driving force becomes larger. Finite size system has a finite fraction of sites with the exactly same DC velocity simultaneously with the acquisition of perfect temporal periodicity. Here I try to clarify the temporal behavior of the spatially infinite system.

3.1 Bond Percolation Analysis

At first, I explain how to identify plastic flow and moving solid. One view point to distinguish these two phases is the uniformity of the time averaged sliding velocity. It is characterized by the single delta function peak in the distribution function of $\omega_{\rm DC}$ but this is difficult to deal with as mentioned in the previous chapter. To make matter worse, the distribution function lacks the information of spatial configuration about sites with the same velocity.

The spatial correlation function of local DC velocity, $\langle(\omega^i_{\rm DC} - \langle\omega_{\rm DC}\rangle)(\omega^j_{\rm DC} - \langle\omega_{\rm DC}\rangle)\rangle$, is also a candidate which characterizes the moving solid phase. This correlation function is, however, governed by a few pinned sites although we have an interest in the very small difference in DC velocities between moving sites. In the relatively large f regime where solidification transition is argued, the number of pinned sites is very small and each of them is isolated but they contribute to the correlation function so much because of the large difference of the velocity from moving sites. This irrelevant factor can not be eliminated in a straight forward way. We need better method to treat the spatial correlation of $\omega_{\rm DC}$ precisely.

Here we focus on the phase slip process to discuss the spatial correlation of the motion. This is closely related to the uniformity of DC velocity. We characterize the moving solid phase by an infinitely large cluster which is made from the sites connected by bonds on which phase slip does not occurs. In contrast, only finite size clusters exist in the plastic flow phase.

Note that the dynamical transition discussed here is not identical to the transition between liquid and crystal (or Bragg glass) on the moving frame, i.e. the phase order is irrelevant. Steadily occurring plastic deformation, in which accumulation of stress and yield

(a) 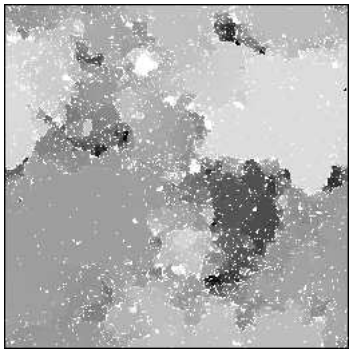 **(b)** 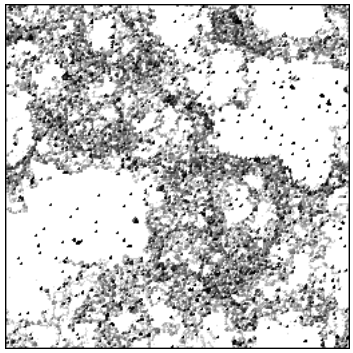

Figure 3.1: Spatial configuration of DC velocities on site (a) and Δv_{DC} on bond (b) in two dimensional system. The DC velocities divided by $2\pi/T$ from 2730 to 2820 are plotted with gray scale from white to black. $\log \Delta v_{DC}$ changes from 0 to log(400) in logarithmic scale with the unit $2\pi/T$. Connected bonds are plotted with white color. This is the result of two dimensional system with $L = 256$, $T \approx 27000$, and $f = 1.0$. Critical force for this T is about 1.06.

are repeated alternately, are the matter. Corresponding transition to the present one is not defined in the static regime.

The concrete method is as follows. Phase slip is a process in which phase difference between neighboring sites increases or decreases by 2π. It results no change in the coupling energy. In order to clarify the phase slip process, we calculate DC velocity $v^i_{DC} = \langle \dot{\theta}_i(t) \rangle_T$ and its difference $\Delta v^{i,j}_{DC} = v^i_{DC} - v^j_{DC}$ on each bond between neighboring sites i and j. Here $\langle \ldots \rangle_T$ denotes time averaging for the observation time T. The resolution of DC velocity is given by $2\pi/T$. When $|\Delta v^{i,j}_{DC}|$ is larger than this resolution, the phase difference grows over 2π, therefore some phase slips have happened and we determine that this bond is "disconnected". Otherwise if $|\Delta v_{DC}| < 2\pi/T$, the bond is "connected" and two sites belong to the same cluster. When both of pair sites are pinned, i.e. $v^i_{DC}, v^j_{DC} < 2\pi/T$, Δv_{DC} is less than $2\pi/T$ but we regard such a bond as disconnected. It is because such bonds make non-moving solid clusters. We analyze the bond percolation transition by controlling the driving force. Percolating phase is then the moving solid phase. Typical configuration of local v_{DC} and Δv_{DC} in a two dimensional system is shown in Fig.3.1. It is slightly below the critical point and shows fractal domain structure, where phase slip bonds play a role of domain boundaries.

We divide the system into subsystems, whose size L is smaller than the real sample size $L_{\max}$. Then we determine that percolation occurs if a certain cluster reaches on both of two opposite edges in two dimensions or plains in three dimensions of each subsystems. The statics on them yields percolation probability $P(f, L, T)$. The sample numbers used here are 32,16,16,4 for $L_{\max}$=16,32,64,128 respectively. The numbers of subsystems are given by multiplying $(L_{\max}/L)^3$. We don't use the data for $L = L_{\max}$ because of the small number of samples.

3.2 Check of Relaxation to the Steady State

In this section, I clarify the reliability of the present numerical results. There are two points to check. One is whether the relaxation to the steady state is sufficiently achieved in the precursor running. Another is the effect of irrelevant length scale to the percolation transition, the phase coherence length.

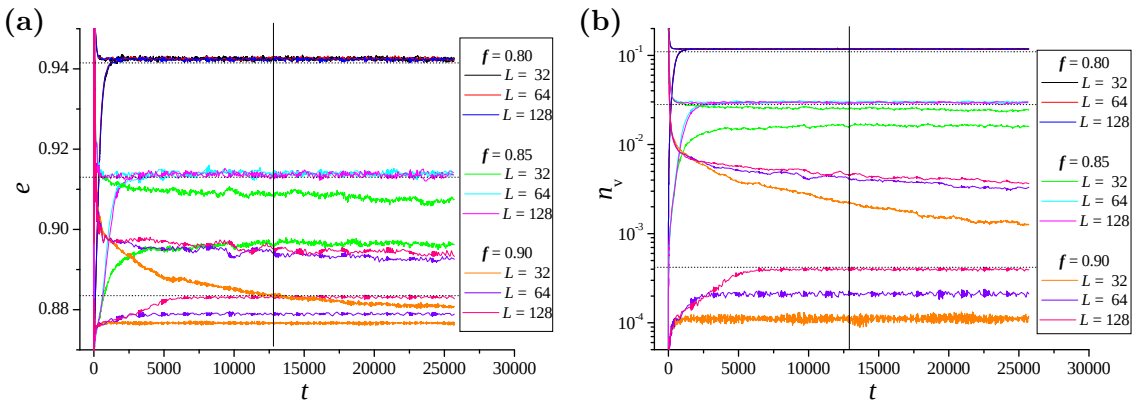

Figure 3.2: The relaxation to the steady state of total energy(a) and vortex density(b). The data for various f, $L_{\max}$ and initial conditions (random and uniform) are shown. The curves for different initial conditions are drawn with the same color but they are distinguished by the fact that the value for the random initial condition is always larger when t is very small for both energy and vortex density. Vertical solid line indicates the typical precursor simulation time. The sample number is 128, 16, 2 for $L = 32, 64, 128$ then the total number of sites are same. Note that the data points are skipped in not constant time spacing.

Total energy

The relaxation of total energy, the summation of interaction energy and random potential energy, per site e is shown in Figure 3.2(a). I show the data for f=0.80, 0.85 and 0.90 for system sizes $L_{\max}$=32, 64 and 128. The simulations start with random and uniform initial conditions at $t = 0$. The plot range of time is twice of that for the precursor running.

For f=0.80, all of the data rapidly converges to the same constant value $e = 0.942$ at $t = 2000$ then we obtain the steady state which does not depend on both $L_{\max}$ and initial conditions.

For f=0.85, the energies for $L_{\max}$=64 and 128 converge to e=0.912 at $t = 5000$ but the data for $L_{\max}$=32 does not. The system is in the region of hysteresis, where the phase coherence length ℓ is comparable to $L_{\max}$ as discussed in section 2.4. The whole system takes periodic motion for uniform initial condition and irregular events such as phase slips are highly suppressed then moving solid state is realized below true f_c. This is more crucial problem than relaxation. We can analyze the $\omega_{\rm DC}$ ordering appropriately when $L_{\max}$ is much larger than the phase coherence length.

For f=0.90, the data for all $L_{\max}$ does not converge. The uniform initial condition, which yields the initial state with lower energy, seems to give saturation, e.g. e=0.882 above $t = 10000$ for $L_{\max}$=128. The steady states are, however, depend on the $L_{\max}$. This is because the phase coherence length saturates $L_{\max}$ and the system falls into the limit cycle motion. We check that some samples with $L = 32$ show perfectly periodic motion here. Although such saturation occurs, steady states are achieved when the uniform initial conditions are employed. The property of percolation transition systematically changes with $L_{\max}$, e.g. the critical force saturate to a finite value with T in order from smaller samples.

Vortex density

In Figure 3.2(b), the relaxation of vortex density n_v, which will be defined in section 4.2.1 is shown. Here I show it only to confirm that the steady states for different initial conditions have same degree of phase order. (There was a possibility that even if total energy is the

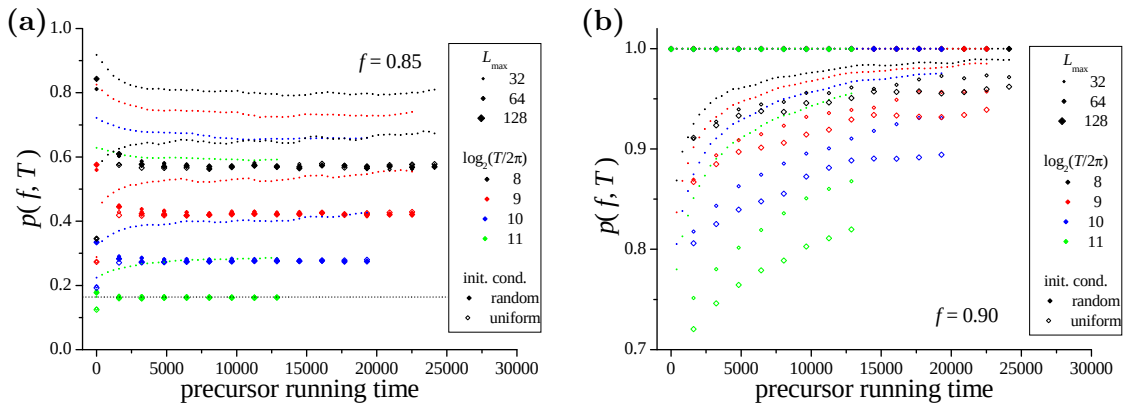

Figure 3.3: Precursor running time dependence of the fraction of connected bonds. The data for various $L_{\max}$, T and initial conditions (random and uniform) are shown.

same, the ratio of interaction energy to the random potential energy is different because of the difference of phase configuration. This actually occurs in the quenching without driving force.) For very small t, n_v is large for random initial conditions and small for uniform ones. The conversion occurs in the same way with e and steady states for different initial conditions have same value of n_v then phase configuration is considered to be qualitatively same.

Fraction of Connected Bond

In Figure 3.3, the fraction of the connected bonds $p(f,T)$ is plotted as a function of the precursor running time. The convergence to the steady state is obtained in the same time scale with that of total energy. Uniform and Random initial conditions yield the states similar to moving solid with small p and plastic flow with large p respectively for short precursor running. For $f = 0.85$, $p(f,T)$ with $L_{\max} > 64$ converges to the same value for $t > 5000$ for all subsystem size $L_{\max}$ and observation time T. For $f = 0.90$, $p(f,T)$ for random initial condition does not show the convergence to the value of steady state in the plot range of t. On the other hand $p(f,T)$ for uniform one keeps 1 independently of both $L_{\max}$ and T because phase slip does not occurs in the limit cycle motion where ω_{DC} is uniform.

Percolation Probability

In Figure 3.4(a), the percolation probability $P(f, L = 8, T)$ for $f = 0.85$ is plotted as a function of the precursor running time. The values of the steady state for $L_{\max} \geq 64$ do not depend on T, $L_{\max}$ and an initial condition as well as the other quantities. There is no tendency that the relaxation of $P(f, L, T)$ with larger T is much slower than that with smaller T. We also check the subsystem size, L, independence of the relaxation in Figure 3.4(b).

The Limit of Calculation

Finally I show the limit of f below which our simulation captures appropriate steady states. In Figure 3.5(a) total energies are plotted with respect to t for $f = 0.875$ and 0.885. Note that the data for individual samples are shown together there. For $f = 0.875$ the data of all samples for both of initial conditions converge to $e = 0.902$. For $f = 0.885$ random initial condition yields the steady state with unique energy for $f = 0.885$. In contrast two samples with uniform initial conditions converge to the same energy state but another two samples,

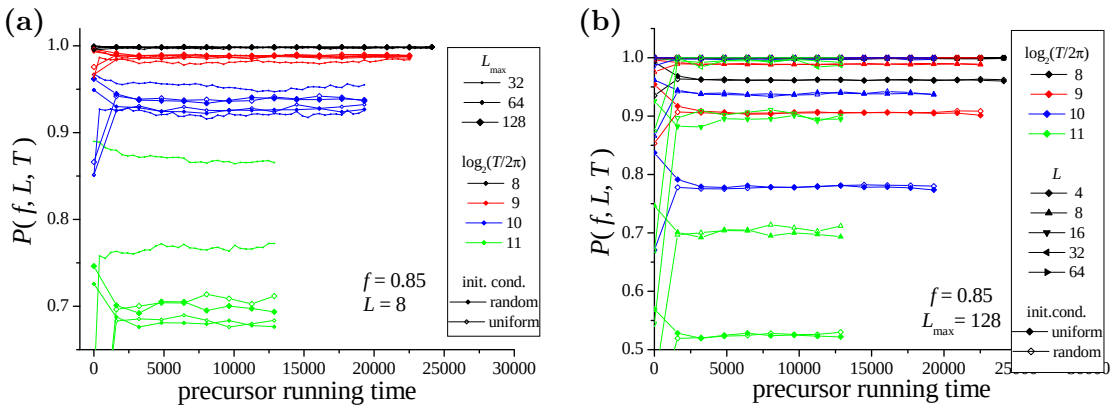

Figure 3.4: Precursor running time dependence of the percolation probability for $f = 0.85$. (a) The data for various $L_{\max}$, T and initial conditions (random and uniform) are shown. Subsystem size is fixed to 8. (b) The data for various T, L and initial conditions (random and uniform) are shown. $L_{\max}$ is fixed to 128.

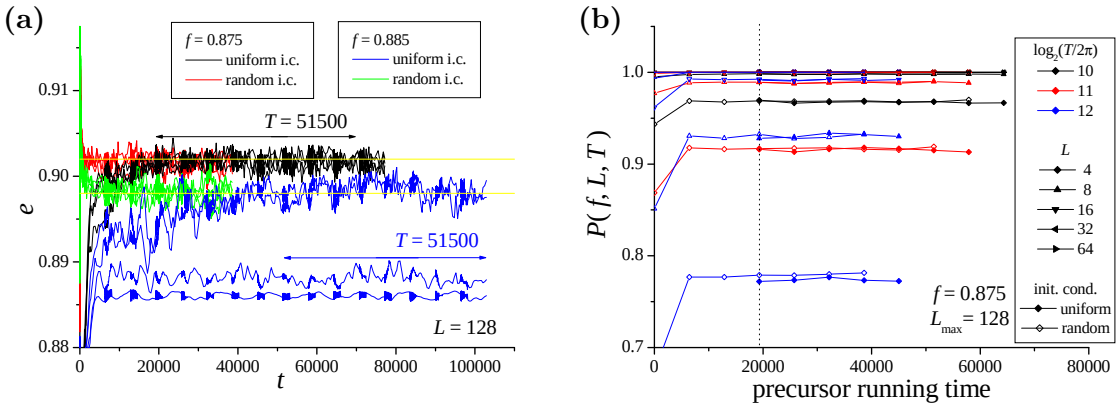

Figure 3.5: (a) The relaxation of total energy at $f = 0.875$ starting from random and initial conditions. The results for four samples with $L = 128$ are shown for each f and initial conditions. (b) Precursor running time dependence of percolation probability at $f = 0.875$ for various observation times and subsystem sizes.

which show small fluctuations, have different smaller energies. The latter's are falling into limit cycle motions. Thus the data for $f \leq 0.875$ are considered not to be affected by the finite size. The precursor running time dependence of percolation probability for $f = 0.875$ is shown in Figure 3.5(b). We use the data above $t = 20000$ for $f = 0.875$.

3.3 Solid-Fluid Transition in Finite Time Observation

In the previous section I show that percolation probabilities in steady states are obtained for uniform initial conditions. Next, I analyze the percolation transition in three dimensions in the case of $J = 1.0$. First, we consider the limit of large L at fixed T based on finite size scaling and then the large T limit.

3.3.1 Percolation Probability

Connected bond density $p(f, T)$ is plotted as a function of the driving force in Figure 3.6(a). $p(f, T)$ exponentially grows with f and saturate to 1 then the transition from plastic flow to moving solid is expected to occur on the way. It decreases roughly logarithmically with

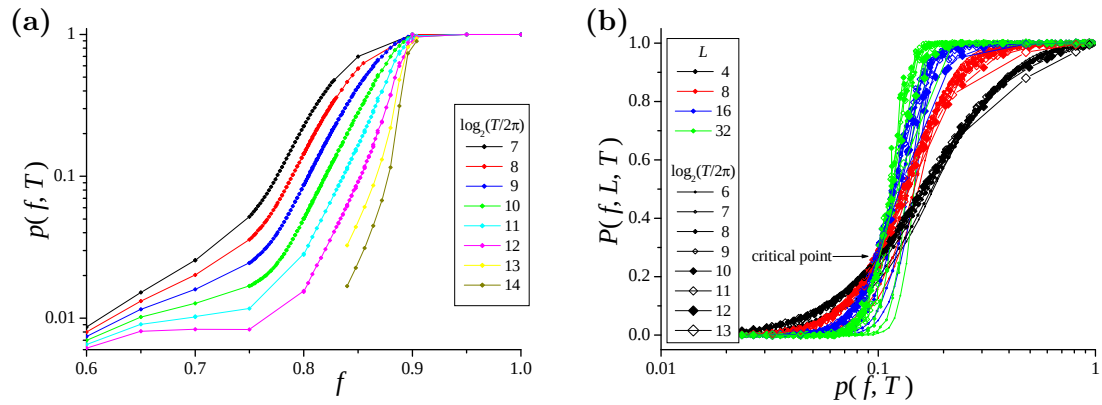

Figure 3.6: (a) The relation between fraction of connected bonds and the driving force. Each colored curves indicate the different observation time. (b) The relation between percolation probability and connected bond density. The results for different subsystem size and observation time are plotted in the same figure. Note that p is plotted in logarithmic scale. Here $L_{\max} = 64$.

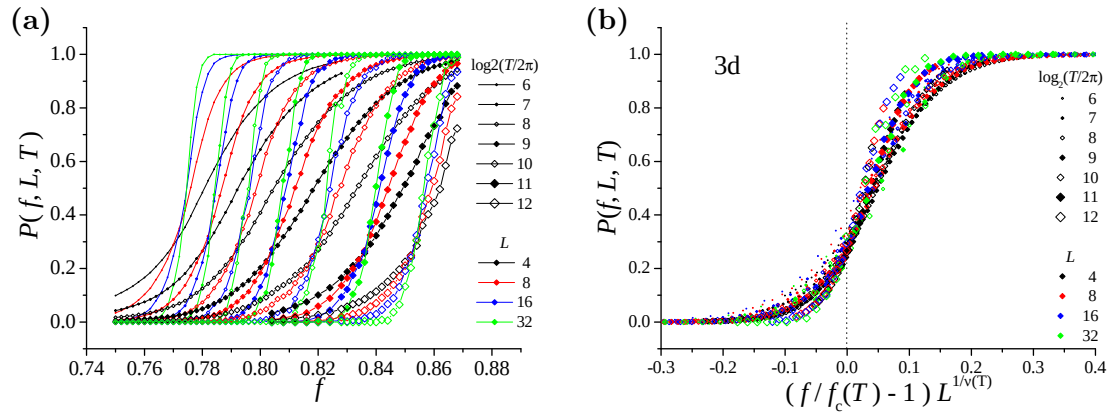

Figure 3.7: The raw data of percolation probabilities for various size and observation time (a) and result of finite size scaling (b). This is the result of three dimensional samples with $L_{\max} = 64$ and maximum observation time $T \approx 26000$.

the observation time T at fixed f. This is because the bond on which phase slips occur less frequently is counted as a disconnected one for the longer time observation. This implies that the critical driving force for the percolation transition depends on the observation time and becomes larger with T. Although all curves seem to converge to 1 at $f \approx 0.89$, this is due to the finite size effect as discussed in the previous section.

Percolation probability $P(f, L, T)$ is plotted as a function of f in the Figure 3.7(a). $P(f, L, T)$ grows with f. Its shape becomes closer to a step function as L becomes larger. There is a certain f for each T, below and above which L dependence is opposite and the value just on it does not depend on L. This is the critical point of the percolation transition.

In Figure 3.6(b) $P(f, L, T)$ is plotted as a function of $p(f, T)$. Much weaker T dependence is seen in comparison with the plot with f then $P(f, L, T)$ seems to be a function of only $p(f, T)$. There seems to be an unique crossing point, $p \sim 0.1$ and $P \sim 0.25$, for curves with different L, which rarely depends on T. The curves for very small T yields a little smaller $P(f, L, T)$ for the same value of $p(f, T)$. This is because they are related to smaller f, at which remaining pinned sites prevent the percolation.

Whether percolation occurs or not is determined not only by the magnitude of the connected bond density $p(f, T)$ but the spatial correlation of bonds is also important. Both

of connected and disconnected bonds have attractive correlation as seen in Figure 3.1(b) and roundish domains and their boundary are formed. Then critical value, $p_c(T) = p(f_c, T) \approx 0.10$, is smaller than the critical probability for the purely stochastic percolation transition, in which p_c is about 0.249 for three dimensional simple cubic lattice, due to the attractive nature of connected bonds.

3.3.2 Finite Size Scaling

Finite size scaling can be performed in the same way as stochastic percolations [37]. The curves for different L's converge to the universal one as the driving force is scaled as

$$x = \frac{f - f_c}{f_c} L^{1/\nu} \tag{3.1}$$

with the suitable choice of the critical force f_c and the critical exponent ν. Here, ν is the critical exponent which characterize the divergence of DC velocity coherence length as $\sim (f - f_c)^{-\nu}$. We use

$$g(x) = \frac{1}{2} + \frac{1}{2} \tanh\left(\frac{x - x_1}{x_0}\right) \tag{3.2}$$

as a scaling function and it works quite well. x_0 and x_1 are fitting parameter and allowed to have T dependence.

Quite good conversion is obtained for each T as shown in Figure 3.7(b). Therefore $f_c(T)$'s and $\nu(T)$'s are obtained for each T. For example, $f_c = 0.84$ and $\nu = 1.3$ in the case of $J = 1.0$ and $T \approx 13000$. A little T dependence is found in Figure 3.7(b). We consider, however, that the T dependence vanishes for sufficiently large T except in the value of f_c , which is discussed in section 3.4.2.

3.4 Observation Time Dependence of the Critical Force

3.4.1 Glass Crossover Time

T dependence of f_c for several $L_{\max}$'s are shown is shown in Figure 3.8(a). That is expressed as

$$f_c(T) = f_0 \log(T/t_1), \tag{3.3}$$

for large T. Here, t_1 and f_0 are constants. $f_0 = 0.025$ coincides well with the constant which characterize the growth of the peak hight in the distribution function of $\omega_{\rm DC}$ (See Figure 2.5(b)). We consider the reason for the disagreement between the present data and eq.(3.3) for smaller f and smaller $L_{\max}$ as follows.

For $T < 3000$, f_c's for smaller T is a little larger than that expected from eq.(3.3). We consider the reason for this at first. The dynamics of sites in samples are roughly classified into two groups. One is represented by the power peak of the distribution function of $\omega_{\rm DC}$ at the origin (see section 2.2.2) and another is represented by the power peak at ω_p. The sites which belong to the percolating cluster are in the latter group and ω_p is 0.35∼0.55 for $f = 0.75 \sim 0.875$. The sites of former group do not affect the percolation in large L subsystems when they are rare and isolated. For smaller f, however, these are not rare, e.g the fractions of sites with $\omega_{\rm DC} < 0.050$ are 0.51, 0.090 and 0.00054 for f=0.75, 0.80 and 0.85 respectively. The percolation probability becomes larger in such case of lattice with "defects". These sites decrease rapidly with f and have less effect on f_c for higher T.

The another problem is that there remains another kind of size dependence at large f although finite size scaling has been already performed. For small $L_{\max}$, f_c shows saturating behavior to a finite value above certain T, which becomes larger with $L_{\max}$. This is caused

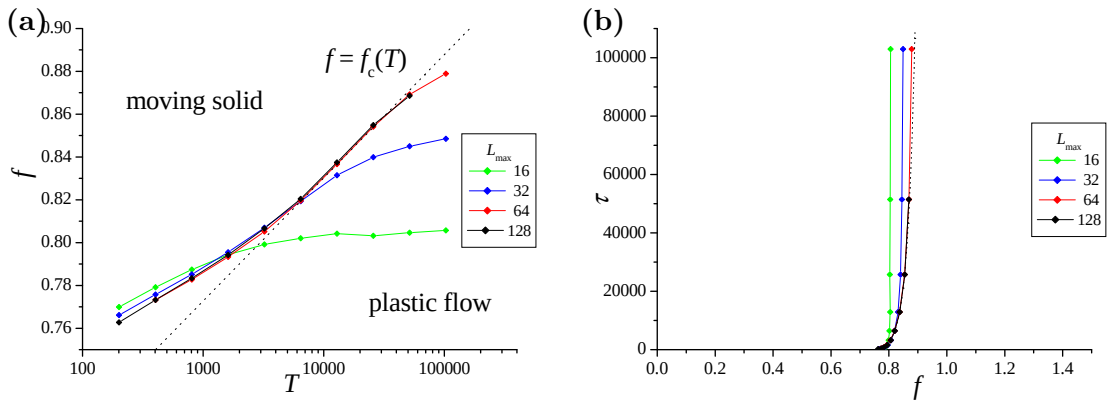

Figure 3.8: (a) The observation time dependence of the critical force. The curve is regarded as the phase boundary in $f - t$ plain which distinguish between plastic flow and moving glass. Note that horizontal axis is in a logarithmic scale. The solid line indicates $f = 0.025 \ln T + 0.60$. The sample number used here is 32,16,8,4 for $L_{\max}$=16,32,64,128. The number of subsystems is $(L_{\max}/L)^3$. (b) Glass crossover time τ as a function of the driving force in a normal scale.

by the falling of the system into the limit cycle motion when the phase coherence length becomes the same order with $L_{\max}$ as discussed in section 3.2.

For $T \leq 51500$, the results for $L = 64$ and $L = 128$ hardly differ and they shows reliable $f_c < 0.870$. (We have shown that limit cycle motion does not appears for $L = 128$ below $f = 0.875$ in section 3.2. f_c is sensitive only to the data in the vicinity of the crossing point of $P(f, L, T)$ while the critical exponent ν is affected by the data for $f > 0.875$) Eq.(3.3) is expected to hold till the infinite T. It means that f_c diverges logarithmically as T goes to infinity and the moving solid *phase* which is defined in the long time limit does not exist as far as in the present definition. According to the preliminary research this behavior does not change for the system with stronger coupling.

In another point of view, Eq.(3.3) is regarded as the phase boundary in a force-time plane between the plastic flow and the moving solid regimes (See Figure 3.8(a)), which is moving glass rather than moving crystal or Bragg glass as shown in chapter 4. Considering the observation with fixed f, the glass crossover time $\tau(f)$ can be obtained from eq.(3.3) as

$$\tau(f) = t_1 \exp(f/f_0). \tag{3.4}$$

The system behaves as if it were in the moving glass phase with the shorter observation time than $\tau(f)$. Beyond this time, cracks of plastic deformation, they are the sheets of phase slip bonds, propagate to macroscopic scale and fluid-like property is revealed.

In a finite size system, $\tau(f)$ diverges above certain f, where the system falls into the limit cycle, which is related to the saturation of $f_c(T)$. In Figure 3.8(b), τ is plotted as a function of the driving force. The extrapolated exponential curve for $L_{\max} \to \infty$, which is drawn by a dotted line, shows so rapid rising that τ seems to diverge at a certain f and the phase transition exists. However this is hard to insist when watching the plot of τ in a logarithmic scale, which is obtained by the exchange of horizontal and vertical axises of Figure 3.8(a). Contrary the curve for $L_{\max} = 128$ bends with a tendency for saturation of $\tau(f)$ and rather suggests the exponential divergence at $f = \infty$. The additional fact that implies the absence of the phase transition is that τ seems to diverge even in finite size systems. This is in contrast to the case of usual phase transitions where the characteristic time scale saturates to a finite value, which increases with the system size.

The exponential growth in eq.(3.4) can be translated as a thermal activation process,

$$\tau \propto \exp\left(\frac{V}{k_B T_{\rm eff}}\right), \quad T_{\rm eff} = \frac{V}{k_B}\frac{f_0}{f} \tag{3.5}$$

when an effective temperature $T_{\rm eff}$ which is proportional to $f^{-1} \approx v_{DC}^{-1}$ is introduced. Here V means the typical energy barrier between metastable states. This is consistent with the idea of "shaking temperature" proposed by Koshelev and Vinokur [3]. We also found that the excitation of dislocations is also governed by this temperature, which is shown in the next chapter. $T_{\rm eff}$ should not depend on the potential barrier V then $f_0 \propto V^{-1}$.

3.4.2 Universality of Percolation Transition for Different T

So far, it is shown that percolation transition of an elastic moving cluster really happens even if it is defined in the finite time observation. We can obtain some information of the spatial pattern of DC velocity from the analysis of percolation transition. The property at f is investigated by the percolation transition with the observation time $T = \tau(f)$, which yields $f_c = f$. We discuss the self-similarity of DC velocity configuration for different f based on the universality of these transitions for different T. These appears in the critical exponent ν, the connected bond density $p_c(T) = p(f_c, T)$ and percolation probability $P_c(T) = P(f_c, L, T)$ at the critical point.

The T dependence of the critical exponent ν^{-1} is shown in Figure 3.9(a). For small T, ν^{-1} is constant, ≈ 0.8 for $L = 64, 128$ but it goes to zero as T increases and universality seems not to exist. This decreasing is, however, finite size effect which corresponds to the phase ordering as discussed above and ν is expected to have an universal value. In the limit cycle motion, the dynamics of all sites are regular with the period $2\pi/\omega_p$ then phase slip does not occur except between stopping and moving sites. When the phase coherence length saturate to $L_{\rm max}$, percolation probability is forced to rise and go to 1 in the same way for all L's. $\nu^{-1} = 0$ means the curves for various L's are convergent without any scaling. ν tends to keep constant value up to higher T for larger $L_{\rm max}$ and is expected to have a unique value independent of T in the large size limit. ν is roughly estimated to be 1.3 (0.88 for stochastic percolation). The T dependences of connected bond density and percolation probability at $f_c(T)$ are shown in Figure 3.9(b). We roughly estimate that $p_c = 0.10$ and $P_c = 0.28$. It may be difficult to insist the universality of percolation transitions in the present results. Other much more clear evidences of the universality, however, are seen in the cluster statistics, which is discussed in the next section.

The universality of the critical point for T is related to the self similarity of $\omega_{\rm DC}$ structure for various f's. DC velocity has a scaleless spatial pattern which does not depend on f if one chooses proper time scale $\tau(f)$. This may be a kind of self-organized criticality, the system is in the critical state without tuning the parameter to the special value, i.e. critical point. Finite time observation means the course-graining of $\omega_{\rm DC}$ and $\Delta\omega_{\rm DC}$ by $2\pi/T$. Note that space is not rescaled as usual critical phenomena.

3.5 Statistics of Co-moving Clusters

Next, I argue the fractal dimension of clusters and the size distribution of them.

3.5.1 Fractal Dimensions at the Critical Point

At first we investigate the dimension of the clusters, both non-percolating ones and percolating ones at the critical point. The volume of the cluster s is identified with the number

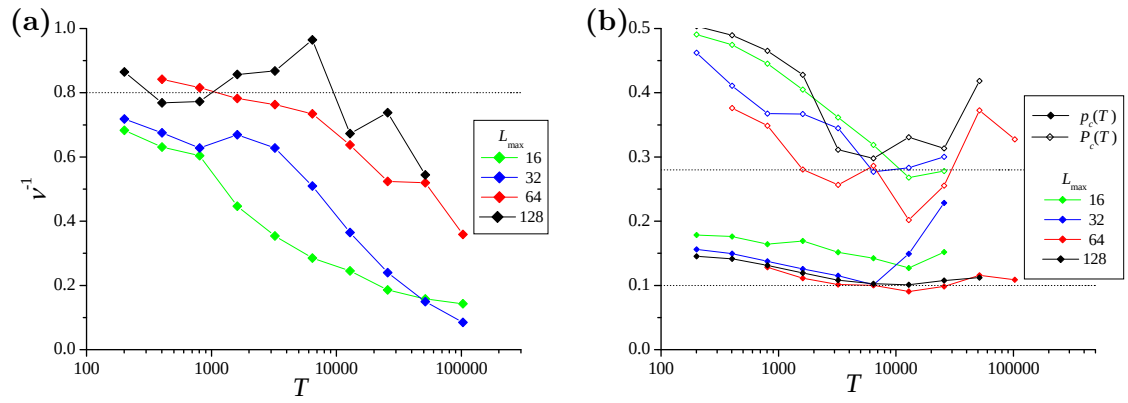

Figure 3.9: The observation time and system size $L_{\max}$ dependence of the critical exponent ν^{-1} (a) and percolation probability and the connected bond density at the critical point (b).

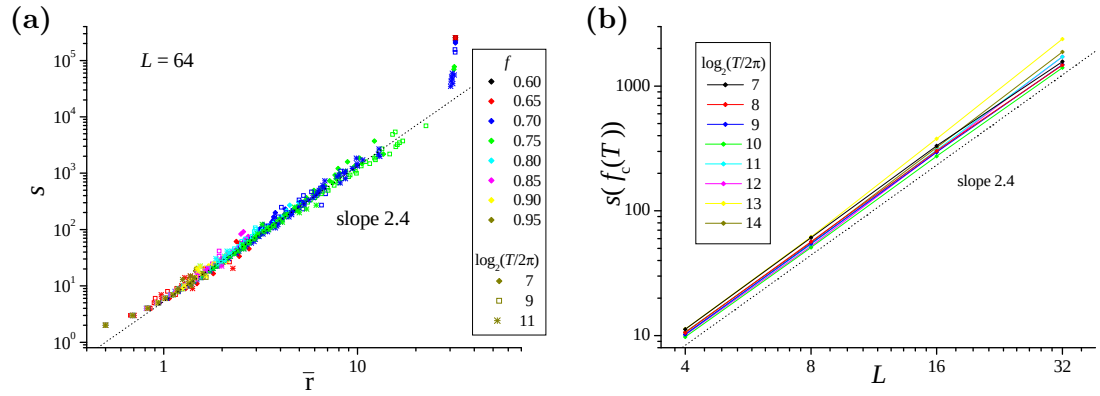

Figure 3.10: (a) The relation between the volume and the mean radius of the co-moving cluster. The result for various driving forces and observation times are plotted together. (b) The system size dependence of the size of the maximum cluster in each subsystem. Here $L_{\max} = 64$.

of contained sites. The radius can be estimated by the root mean square of the distance from the center of mass as

$$\bar{r} = \left\langle \sqrt{\frac{1}{s}\sum_i \left(\mathbf{r}_i - \frac{1}{s}\sum_j \mathbf{r}_j\right)^2} \right\rangle_s . \tag{3.6}$$

Here $\langle \ldots \rangle_s$ means average for clusters with the same sizes, which can have various radius depending on their shapes. The relation between this radius and the volume of cluster s are shown in Figure 3.10(a). We find that s is not proportional to $\bar{r}^3$ but to $\bar{r}^{2.4}$ in three dimensions except for very small clusters and ones which saturate to the system size. The fractal dimension of the cluster, D, equals 2.4 and does not depend on T. This holds in all region of f except the percolating cluster above f_c, which has the same dimension with the space.

The percolating cluster at the critical point is also fractal. This is estimated by box counting for the maximum clusters in subsystems $s_{\max}$. $s_{\max}$ in the sample of size L is plotted as a function of f in Figure 3.11 where the scaling result is also shown. It shows divergent behavior at the critical point although the finite sample size suppresses this divergence. The L dependence of $s_{\max}$ at $f = f_c$ for various T is shown in Figure

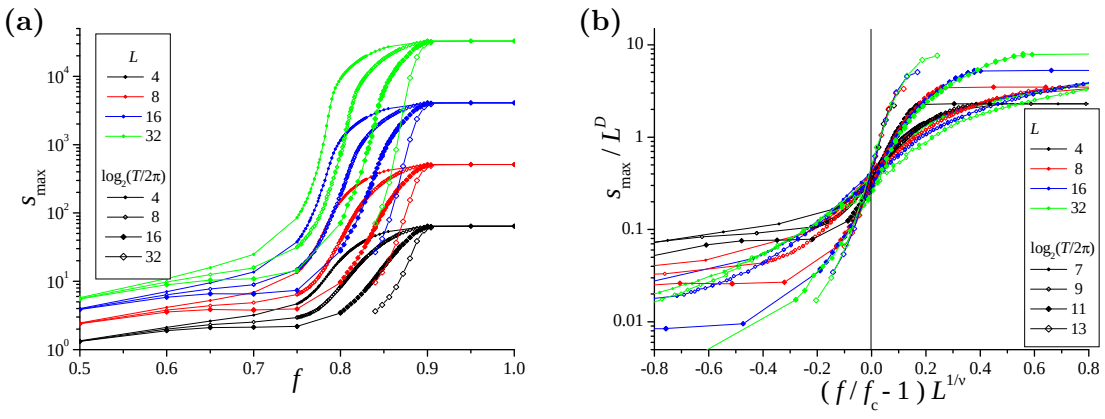

Figure 3.11: The relation between the maximum cluster size and the driving force. The results both before (a) and after scaling (b) are shown.

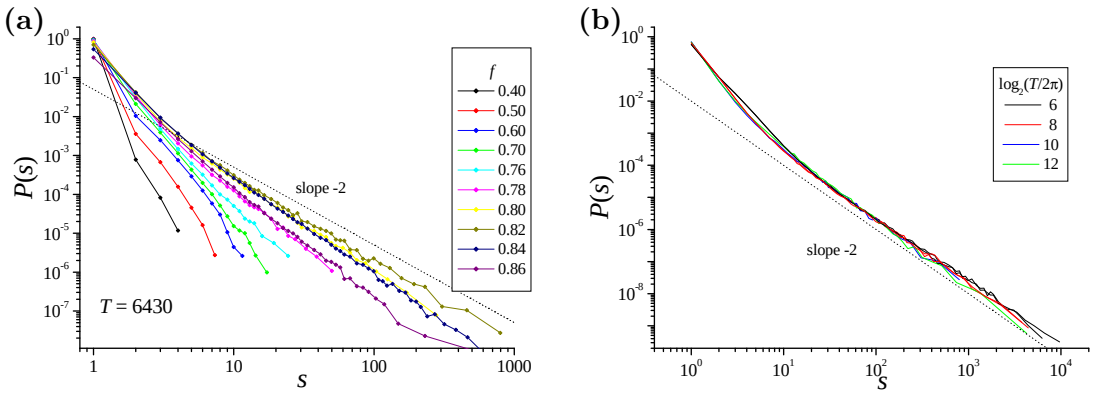

Figure 3.12: (a) The distribution function of the size of the co-moving cluster. The cut-off is so sharp that each curves seem to end discontinuously with the present resolution in a logarithmic plot. (b) The distribution function at the critical point for different T.

3.10(b). We obtain

$$s_{\max}(f = f_c) \propto L^D. \tag{3.7}$$

The T dependence is not rarely seen both in $D = 2.4$ and coefficient. The percolating cluster at $f_c(T)$ can not be distinguished from its shape. This indicates the universality among the percolation transitions for different observation times and then supports the existence of the self-similar configuration of DC velocity for different f. The fractal dimension of percolating cluster at the critical point coincides with that of non-percolating clusters.

3.5.2 Size Distribution

The distribution functions of cluster size $P(s)$ for various f's are shown in Figure 3.12(a). The normalization condition is $\sum_s sP(s) = 1$. It has a power low shape $P(s) \propto s^{-\tau}$ at the critical point f_c. The exponent τ is about 2.0. For $f < f_c$ there is a cut-off of s, i.e. a cluster larger than it does not exist. This cut-off diverges at f_c but is finite again above f_c when ignoring the percolating cluster. The cut-off, which gives the correlation length, is much sharper than that expected from the exponential decay. Each curves seem to have different exponents from 2 for f_c, which become larger as leaving away from f_c, rather than the slope is rounded by cut-off function.

In Figure 3.12(b), $P(s)$'s at the critical point f_c for different observation time are shown. There is little difference beyond the error in both the exponent and coefficient, which

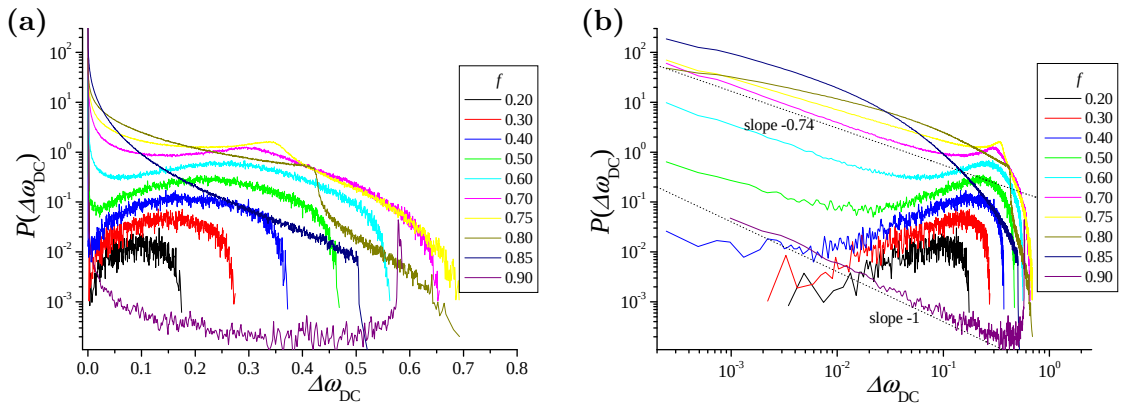

Figure 3.13: The distribution function of $\Delta\omega_{\rm DC}$ in semi (a) and double (b) logarithmic scale.

strongly suggests that the DC velocity has an universal spatial structure independent of T.

3.6 Statistics of Phase Slip Frequency on Each Bond

Next, I focus on the DC velocity difference $\Delta\omega_{\rm DC}$. So far, we have analyzed the percolation transition using the connected bonds on which no phase slip occurs. Whether phase slip occurs or not is determined by $\Delta\omega_{\rm DC}$ then only the initial and final states are taken into account. This is justified by the fact that each bond has a favorable direction, i.e. $\Delta\omega^{i,j}_{\rm DC}$ on each bond is steadily positive or negative independently of when and how long it is observed. Furthermore it is expected that phase slip rate $\Delta\omega^{i,j}_{\rm DC}$ converges to a certain value as the observation time goes to infinity. The spatial DC velocity pattern is static in sufficiently large length and long time scales because it is governed by the quenched random potential, not fluctuating noise. If the sign of $\Delta\omega_{\rm DC}$ depended on when it is observed, the distribution function would take a Gaussian form but such form is not seen.

$\Delta\omega_{\rm DC}$ on each bond indicates how frequently phase slips occur. The distribution function of the DC velocity difference $P(\Delta\omega_{\rm DC})$ is plotted in Figure 3.13. Even if the observation time becomes longer, the shape of the distribution function does not change. The curve is only smoothly extended to the lower $\Delta\omega_{\rm DC}$ region. The bonds contributing to this region was counted as connected bonds in shorter time observation. Then the connected bond density is obeys to a differential equation,

$$\frac{dp(f,T)}{dT} = P(\Delta\omega_{\rm DC} = \frac{2\pi}{T})\frac{d}{dT}\frac{2\pi}{T} = -\frac{2\pi}{T^2}P(\Delta\omega_{\rm DC} = \frac{2\pi}{T}). \tag{3.8}$$

The peak in $P(\omega_{\rm DC})$ at $\omega_{\rm DC} = 0$ and $\omega_{\rm DC} = \omega_{\rm p}$ discussed in section 2.2.2 is useful to understand the behavior of $P(\Delta\omega_{\rm DC})$. Large $\Delta\omega_{\rm DC}$ part is contributed by the bonds between a nearly stopping site and an almost periodically moving site while the small $\Delta\omega_{\rm DC}$ part comes from the bonds between sites which have nearly same velocity. When f is small, the $|\Delta\omega_{\rm DC}|$ is same with the $\omega_{\rm DC}$ itself of the one site because the velocities of neighboring sites are almost always zero. Then $P(\Delta\omega_{\rm DC})$ is similar to $P(\omega_{\rm DC})$ when the fraction of moving sites is small.

The peak at the origin is governed by the bond between the sites with nearly same velocities. Two types of power divergence with exponents, ζ_0 and ζ_1, are observed for relatively lower and higher f (See Figure 3.13(b)).

$$P(\Delta\omega_{\rm DC}) = (\Delta\omega_{\rm DC})^{-\zeta_i}, \quad i = 0, 1 \tag{3.9}$$

They correspond to the divergence of $P(\omega_{\rm DC})$ at ω_0 and ω_p which are discussed in the section 2.2.2. The exponent for lower f, $\zeta_0 \approx 0.74$ is almost equivalent to $\gamma_0 \approx 0.78$. This implies that the bond which contribute to this power law part is connected to the stopping site. As the driving force increases, the number of pinned or small velocity sites decrease and the peak with exponent ζ_0 fades away.

On the other hand bonds between sites with similar velocities whose motions are nearly periodic make the peak with the exponent ζ_1, which should be related to $\gamma_1 \approx 1.7$ in anyway. ζ_1 equals about 1.0. $\zeta_1 = 1$ is a critical value because at which logarithmic decay of $p(f,T)$

$$p(f,T) = \text{const.} - \log T. \tag{3.10}$$

is derived from eq. (3.8). When ζ_1 is larger than 1, $p(f,T) \sim -T^{\zeta_1 - 1}$.

3.7 Discussion

In this chapter I have discussed the possibility of the moving solid phase by defining it as the phase which has a macroscopic cluster moving with the same DC velocity. To analyze this numerically, percolation transition of bonds which never take any phase slip is investigated. We pay attention to the effect of both finite size and the finite observation time. Clear percolation transition is obtained at finite time observation. The critical force logarithmically diverges with the observation time. Then the moving solid phase is concluded not to exist for the infinite time observation.

The condition for the connected bond, that no phase slip occurs eternally, may seem too strict. For example all bonds necessarily takes phase slips if thermal fluctuation exists. It is important, however, to note that there is not the local symmetry, $\langle \Delta\omega_{{\rm DC},i} \rangle = 0$ at the beginning. The local stress monotonically increases and the bond steadily takes a phase slip on the same direction no matter how rarely it occurs. The phase transition discussed here may be rounded at the finite temperature even in the finite time observation.

We focused on the macroscopic plastic deformation and attempt to distinguish between plastic flow and moving solid. This stance is different from the conventional interest in the liquid-crystal(Bragg glass) transition in principle though it seems natural that these transitions occurs at the same time. The absence of the moving solid phase discussed here is not immediately related to the absence of the periodic long range order. When the propagation of plastic deformation along the domain boundary is temporally localized, the spatial phase order in long span can exist in the plastic flow phase. On the other hand we see that the saturation of phase correlation length to the system size results the limit cycle motion and plastic deformation is suppressed. Then if the transition from liquid to crystal or Bragg glass occurs in moving state, the present transition would happen at the same time.

From the observation time dependence of the critical driving force, glass crossover time can be defined clearly, the system behaves like a moving glass in shorter time scale than this, beyond which macroscopic plastic deformation occurs. This crossover time increases exponentially with the driving force. Its characteristic scale of a driving force, $f_0 \approx 0.025$, is very small compared with the scale such as pinning strength ~ 1 and the driving force, ~ 0.75, at which the number of depinned sites becomes $O(N)$. Therefore it grows very rapidly in narrow region of f and would overcome the macroscopic time scale at not so large f. This is a possible reason why moving solid phase is observed in experiments. The situation might be similar to the case of structure glasses, whose viscosity grows quite large and show slow dynamics. Then it is hard to distinguish whether the equilibrium phase transition exists or not.

Even though a certain connected cluster has a finite life time, however, there are always some percolating networks in a short time scale which are not permanent but dynamically

change their shapes. (Unfortunately we can not define the instantaneous solidification order clearly because phase slip is temporally discrete event and DC velocity ordering is discussed in long time scheme.) It is interesting to investigate the mechanical property mediated by this percolating network, such as shear modulus and yield stress. The response to the AC external field especially significant which may capture the glass crossover time. It is expected that the system shows elastic response to the shear with high frequency modulation and rheological property to that with low frequency.

I showed some evidences which implies that the spatial configuration of DC velocity has the universal structure if one makes a course-graining and ignoring small fluctuation below proper threshold, which depends on f. This means that the self-similar pattern is obtained even though the space is not scaled but only field variable is done. The physical meaning of this is an open question.

Chapter 4

Phase Ordering on Moving Frame

In the previous chapter, I showed that the moving solid phase, where DC velocity is spatially homogeneous, becomes unstable in a finite life time. Although the absence of moving solid order does not directly correspond to liquid like state, permanent phase ordering on the moving frame is also expected not to exist.

In this chapter, I discuss the phase ordering, which is related to the periodicity of the moving structures. We mainly focus on the instantaneous order. We attempt to capture temporal order with a spatio-temporal correlation function and argue the relation to the life time of the moving solid phase $\tau(f)$ which is discussed in the previous chapter. In the last part of this chapter, dislocations, which take a important role on the disorder, is investigated closely.

4.1 Phase Correlation

I have shown that the ferromagnetic order parameter r grows with the driving force but decreases with the system size in section 2.3, which indicates that there is not the phase with true long range order. To obtain more information about this problem, we investigate the spatial correlation function and some quantities of similar kind.

As shown in section 3.2, we obtain initial condition independent steady states below $f \approx 0.88$ for $L = 128$. The phase coherence length saturates to the system size above it and we only obtain the steady state, which shows periodic motion, for uniform initial condition. Note that I only show the results with the uniform initial conditions in this chapter.

4.1.1 Correlation Function

At first I consider the phase correlation function which reflects the 2π invariance of the phase.

$$C(r) = \left\langle \cos(\theta_{i+r} - \theta_i) \right\rangle \tag{4.1}$$

Here $\langle \ldots \rangle$ means the averaging for time, random samples and the starting point i. We treat only the correlation on the direction of (1,0,0) and symmetric ones with it. $C(r)$ is also averaged for such directions. When the distance r is sufficiently large, anisotropy due to the cubic lattice is not so significant.

This correlation function exponentially decays with r and goes to zero when any long range order does not exist. In the presence of true long range order, it exponentially decreases to a finite value. In the quasi long range ordered phase such as Bragg glass, $C(r)$ goes to zero at $r = \infty$ but slowly decays as a power function $r^{-\eta}$. Bragg glass phase in equilibrium is considered to have an universal exponent η for power decay which only

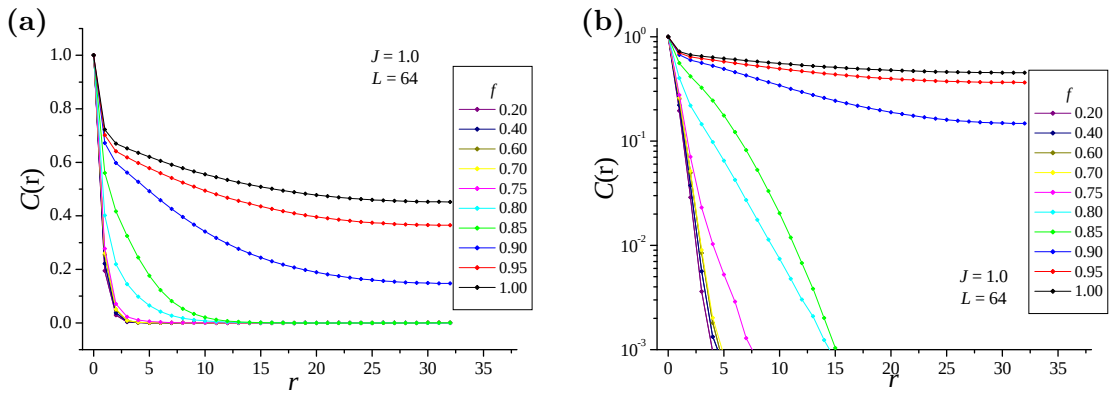

Figure 4.1: Correlation function of phase in normal scale (a) and semi-logarithmic scale (b).

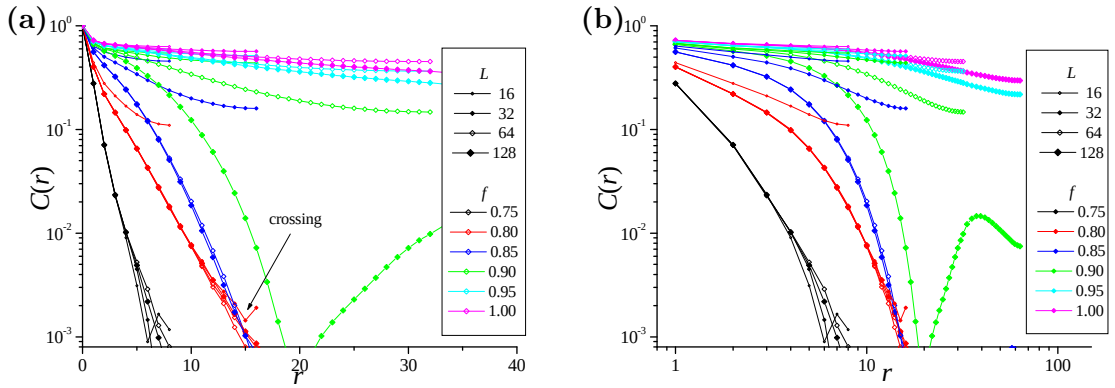

Figure 4.2: The correlation function for various sample size is shown in semi-logarithmic (a) and double-logarithmic scales.

depends on dimensionality [38] in contrast to the ordered phase of the pure two dimensional XY model [39], where exponent depends on temperature.

The f dependence of the correlation function is shown in Figure 4.1. As f increases, the correlation holds for longer distance. At $f \approx 0.90$, the correlation length saturates to the system size and then the periodic boundary condition strongly affects on $C(r)$.

The sample size L dependence is shown in Figure 4.2. Strong size dependence is observed for almost all region of r above $f = 0.90$, where the phase coherence length is larger than the linear system size and the dynamics becomes periodic. As discussed in section 3.2 initial condition independent steady state is obtained below $f = 0.875$ for $L = 128$. As far as the finite size effect does not appears, $C(r)$ looks an exponential function rather than a power function.

4.1.2 Phase Displacement

Next we consider the displacement function

$$B(r) = \frac{1}{2}\Big\langle |\theta_{i+r} - \theta_i|^2 \Big\rangle. \tag{4.2}$$

This is directly related to the correlation function for the elastic manifold as

$$C_{\rm el}(r) = \Big\langle \Big(\theta_i - \langle\theta\rangle\Big)\Big(\theta_{i+r} - \langle\theta\rangle\Big)\Big\rangle = 2\Big[\Big\langle |\theta_i - \langle\theta\rangle|^2 \Big\rangle - \frac{1}{2}\Big\langle |\theta_{i+r} - \theta_i|^2 \Big\rangle\Big]. \tag{4.3}$$

In the present model, in which the mod 2π invariance of phase exists, the direct difference of θ does not have meaning. Then we define the phase difference between the phases of sites apart by a distance r as

$$\theta_{i+r} - \theta_i = \sum_{j=i}^{i+r-1} \Delta\theta_j \quad \text{where} \quad \Delta\theta_i = \theta_{i+1} - \theta_i \in (-\pi, \pi). \tag{4.4}$$

This coincides with the direct phase difference when no phase slip occurs and the absolute coordinate of phase can be defined. In Figure 4.3(a), displacement function for various f's are shown. When f is small and phase correlation is weak, $B(r)$ linearly grows with r like a random walk. This means that $\Delta\theta_i$ loses the correlation in a very short range. The correlation length of phase is estimated from the distance where $B(r)$ excess over the π^2.

As f becomes larger, the coefficient of linear growth becomes smaller due to the growth of short range order. The behavior changes at $f \approx 0.85$. Above which, the growth rate becomes larger around $r = 10$ than linear one. As a result, the crossing of curves for different f's occurs as shown in the Figure 4.3(a). Same kind of crossing also exists in the case of $C(r)$ in Figure 4.2(a). This seems strange because the phase coherence is considered to grow monotonically with f.

The origin of this decline of phase order with f is considered to be in the crossover between plastic flow and moving solid as explained below. The phase difference on bond is restricted between $-\pi$ and π then most disordered configuration is $\Delta\theta = \pm\pi$. This state is unstable because at which the interaction potential, $-\cos\Delta\theta$, takes a maximum value. Of course, such configuration can be stabilized by the balance with the pinning potential in a static state. In the moving state, contrastingly, temporal fluctuation of phase and phase slip are induced by the fluctuation of pinning potential, $-\cos(\theta(t) - \beta)$, and $\Delta\theta$ spends the time on smaller value rather than keeps the value near $\pm\pi$. Phase difference is suppressed in this mechanism.

Such effect becomes smaller as the phase slips are suppressed. Tentative growth of disorder with f is observed if the reduction of such fluctuation is faster than growth of net phase correlation. For much larger f, the phase order grows as the phase difference, which does not fluctuate so much, becomes smaller. This explanation is consistent with the fact that such tentative order decreasing is not observed both in the non driven model, in which order grows with the coupling constant, and in the elastic model.

Saturation of $B(r)$ due to the periodic boundary condition becomes apparent above $f \approx 0.87$, which is rarely found below $f = 0.87$. (The saturation is remarkable in the fact $dB(r)/dr$ equals zero at $r = L/2$.) The system size dependence of $B(r)$ is shown in Figure 4.3(b). Size independent behavior can be observed only in the linearly growing regime. At $f = 0.92$, the size effect is not negligible even at $r \approx 3$. In the large f regime, the growth of $B(r)$ show the trend to become faster as L becomes larger. The curve for $L = \infty$ is expected to grow faster than a linear one. The present result implies that the logarithmic growth, which characterizes the quasi long range order, does not exist since logarithmic growth is slower than the linear one. If quasi long range order really exists, much longer range of r in more several decades is needed to observe it

4.1.3 Structure Factor

$C(r)$ and $B(r)$ is considerably affected by the finite size above $f \approx 0.90$ as shown in Figure 4.2(b) and 4.3(b). It is better to see the phase correlation in the momentum space. Then we investigate the structure factor

$$S(\mathbf{k}) = \frac{1}{N} \sum_{\mathbf{r}} C(\mathbf{r}) e^{i\mathbf{k}\cdot\mathbf{r}} = \frac{1}{N} \left| \mathbf{M}(\mathbf{k}) \right|^2 \tag{4.5}$$

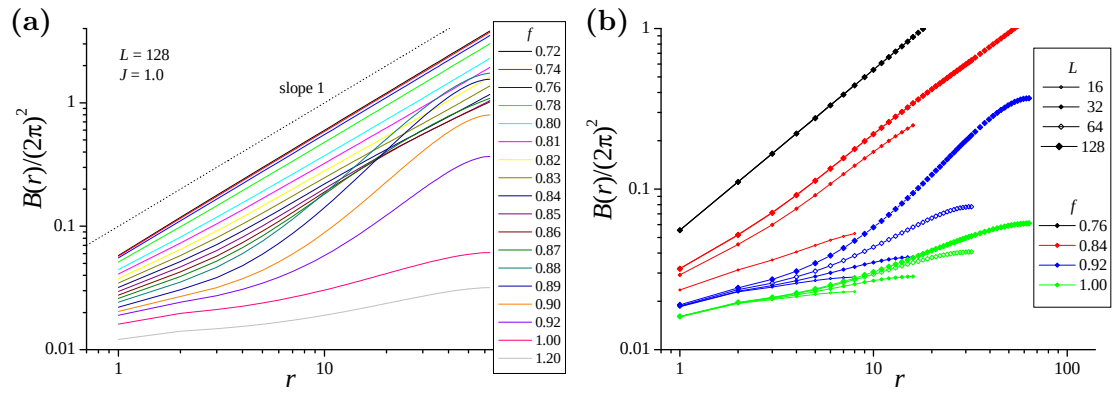

Figure 4.3: Phase displacement at distance r. (a) f dependence with small steps. (b) system size dependence for several f's.

where

$$\mathbf{M}(\mathbf{k}) = \sum_{\mathbf{r}} \mathbf{M}(\mathbf{r}) e^{i\mathbf{k}\cdot\mathbf{r}}, \quad \mathbf{M}(\mathbf{r}) = \Big(\cos\theta(\mathbf{r}), \sin\theta(\mathbf{r})\Big) \tag{4.6}$$

The usual structure factor for the density field has peaks at the reciprocal vectors when a periodic order exists and the $\mathbf{k} = 0$ component indicates the mean density. In contrast, the structure factor of $\mathbf{M}_i$ has a peak at the origin which indicate the periodicity because θ means the fluctuation measured from a certain periodic state as $e^{i(\mathbf{q}\cdot\mathbf{r}-\theta)}$.

The f dependence of the structure factor is shown in Figure 4.4(a). As f increases, the short wave length component decreases and long wave length component increases conversely. We find that $S(k)$ of a snapshot behaves as a squared Lorentzian,

$$S(k) \propto (1 + k^2\xi^2)^{-2}, \tag{4.7}$$

for small k. Here, ξ means the phase correlation length. Fitting curves are shown in Fig.4.4(b), where the data for several sample sizes are plotted in the same figure. Sample size dependence is observed little in $S(k)$. Phase correlation length ξ grows with f and get over the linear size of a simulation system. It is difficult to determine directly whether the correlation length diverges or not because we can obtain ξ's only in one decade. Instead we employ the sum rule,

$$\sum_{\mathbf{k}} S(\mathbf{k}) = L^d, \tag{4.8}$$

to argue the possibility of the divergence of correlation length at a finite f [40]. We first assume that ξ diverges in the large f regime and $S(k)$ behaves as k^{-4}. Then

$$\sum_{\mathbf{k}\neq\mathbf{0}} S(\mathbf{k}) \approx \left(\frac{2\pi}{L}\right)^d \int_{2\pi/L}^{\infty} dk k^{(d-1)-4} \propto L^4. \tag{4.9}$$

If $d < 4$, sum rule would be broken as L goes to infinity. Hence the finite short wave number cut off, $2\pi/\xi$, must exist. The present result indicates that both long range and quasi long range order do not exist even instantaneously. These behavior does not change even in the weak pinning regime, $J \gg 2.0$.

In the case of the simple exponential correlation function, the structure factor takes a Lorentzian form. The power of k decreases by 2 in the presence of the random field and it makes the lower critical dimension higher from 2 to 4. In other wards, an effective dimension decreases. This is called dimensional reduction.

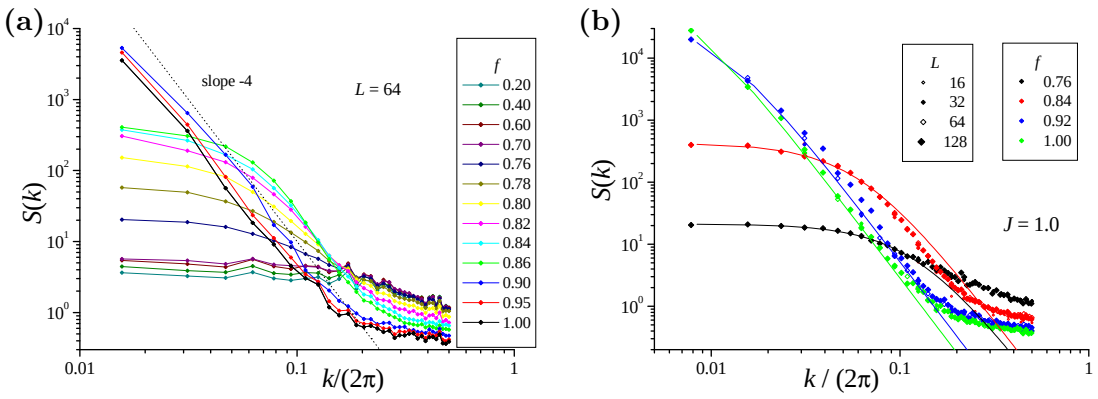

Figure 4.4: (a) The structure factors of three dimensional systems for several f's. It is averaged for time, samples and the directions, (1,0,0) and its symmetric ones. (b) $S(k)$'s for several sample sizes. Solid lines show fitting to the squared Lorentzian.

4.1.4 The Magnitude of Bragg Peak

The $\mathbf{k} = 0$ component of $S(\mathbf{k})$ is related to the magnitude of the Bragg peak of the scattering intensity. The system size dependence which is rarely seen in $S(\mathbf{k} \neq 0)$ is received by $S(0)$. In the presence of the true long range order, $S(0)$ is proportional to the system volume, then $O(N)$ while it is $O(1)$ in the state with the short range order. $S(0)$ for the quasi long range ordered phase is a power function of N whose exponent is between zero and one. Here we investigate the system size dependence of the Bragg peak.

$S(0)$'s for various L's are plotted as a function of the driving force in Figure 4.5(a). The data is less affected by the boundary condition when we use subsystems as the case of the investigation of the percolation transition in the previous chapter. $S(0)$ is closely related to the ferromagnetic order parameter r.

$$S(0) = \frac{1}{N}\left\langle \left| \sum_j e^{i\theta_j} \right|^2 \right\rangle = N\left\langle r(t)^2 \right\rangle \sim \ell^d \tag{4.10}$$

Here $\ell \sim Lr^{2/d}$ is a phase coherence length defined in eq(2.12). In the range where scaling, $\ell \sim Lr^{2/d}$, works well, $S(0)$ does not depend on L, then $O(1)$. $S(0)$ starts to grow roughly exponentially with f at $f = 0.75$, above which the number of depinned sites is $O(N)$. Moving sites are much more free from the impurity potential than pinned sites and phase coherence grows. There is, however, the stop of growth around $f = 0.84$ and even decreasing with f in the range $0.84 < f < 0.88$. Such peak is not seen in the small sample with $L < 64$.

The L dependence of $S(k)$ is shown in Figure 4.5(b). As L becomes larger, $S(0)$ saturates to a finite value below $f = 0.88$ for $L_{\max} = 128$. Then $S(0)$ is $O(1)$. In the large f regime, N linear dependence of $S(0)$ is observed. But this is considered to be a finite size effect because such behavior becomes apparent above smaller value of f for smaller $L_{\max}$. The L independent decreasing of $S(0)$ is expected to continue above $f = 0.88$ for larger $L_{\max}$.

It is strange that phase correlation decreases with f, we have considered that increasing f is related to decreasing effective temperature as mentioned in section 1.2.2. This is not due to the decreasing of the temporal fluctuation of $r(t)$ because $\langle |r(t)| \rangle_t$ also shows the same peak. We can not investigate L independent behavior above $f = 0.88$ in three dimensions due to the computational time limit.

Two dimensional system shows qualitatively same behavior and allows us to investigate higher f regime above the peak. The second increase without L dependence is observed. as shown in Figure 4.6. Same behavior is expected in three dimensions. This indicates that

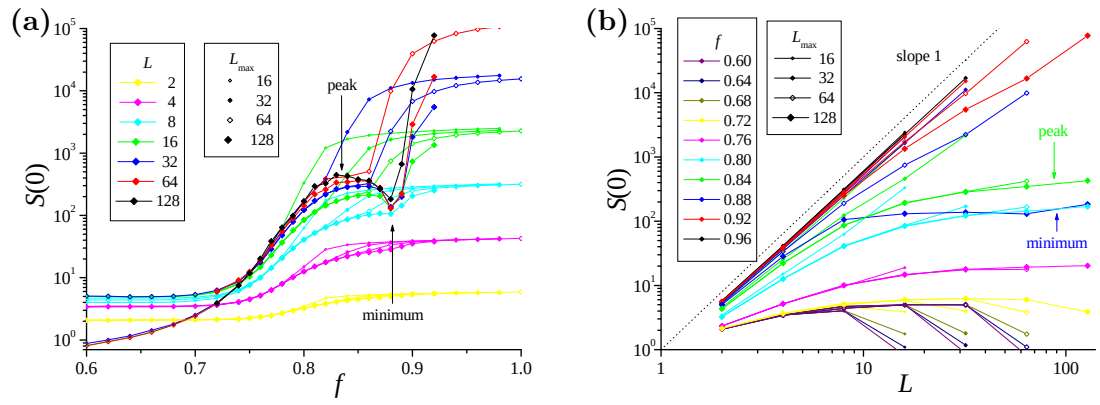

Figure 4.5: (a) The f dependence of the $k = 0$ component of the structure factor. Results for various subsystem sizes L and real sample sizes $L_{\max}$ are shown. (b) The system size dependence of $S(0)$ for several driving forces f. The value for $L = L_{\max}$ become rather small below $f = 0.72$. This is caused by the global rotational symmetry, $\langle e^{i\beta} \rangle = 0$, and zero correlation length.

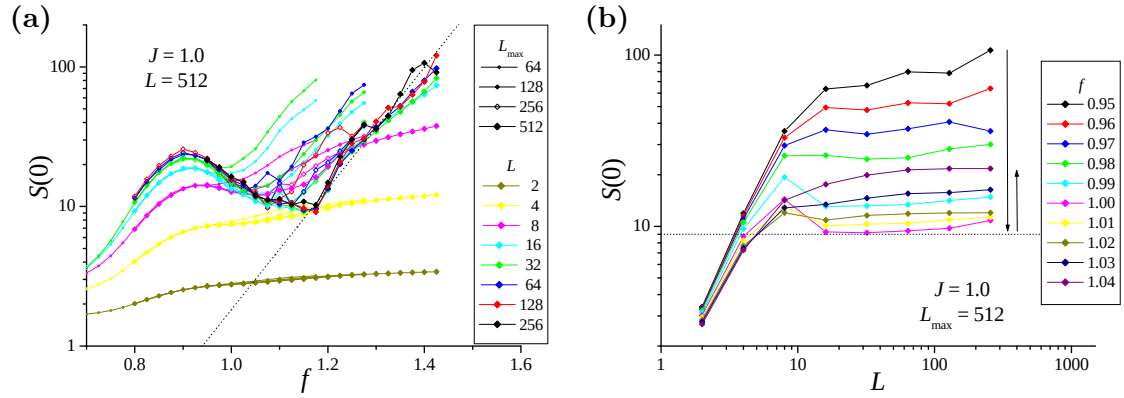

Figure 4.6: The results of the same quantity shown in Figure 4.5 for the two dimensional system. (a) The f dependence of the $S(0)$. (b) The system size dependence of $S(0)$.

the short range order of phase grows with f and the system approaches to the perfectly periodic state at $f = \infty$.

The acceleration of the growth rate for phase displacement $B(r)$ occurs in the same region of f where the peak and tentative decreasing of $S(0)$ with f is observed. We consider these have the same origin, i.e. crossover between plastic and elastic regime, as discussed in section 4.1.2. Observation of reentrant-like, non-monotonic changes is expected in the diffraction experiment.

4.1.5 Comparison with Static and Elastic Models

We also investigate the phase ordering in the absence of the driving force by changing the coupling constant J and obtain the same result that the structure factor is described with squared Lorentzian. It is shown in Figure 4.7 with the displacement function $B(r)$. We can see k^{-4} behavior more clearly up to the large k regime because temporal fluctuation in short wave length scale, which is quite large in moving state, does not exist. The simulation is started with the uniform initial condition and there are always smaller number of dislocations than for any random initial conditions. Although relaxation is sufficient, we have to pay more attention to argue whether it is the ground state or not because the

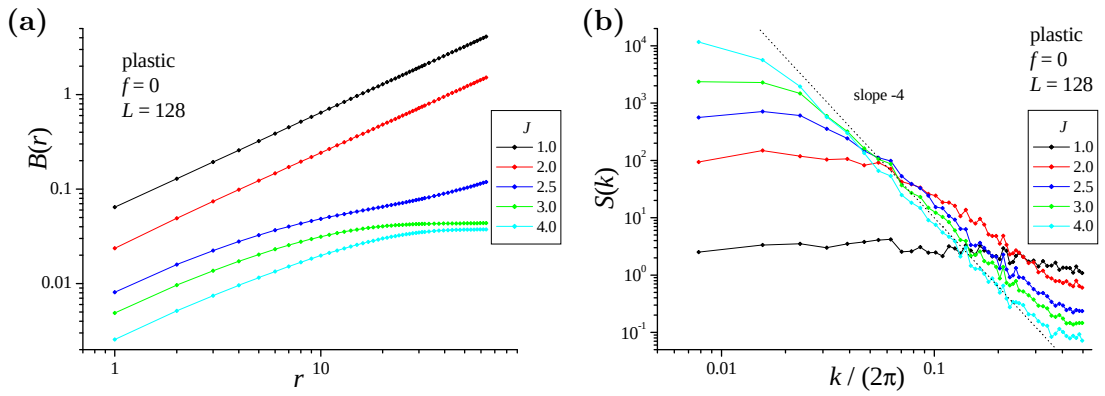

Figure 4.7: The phase displacement at distance r (a) and the structure factor (b) in the static state without drive. Each color indicates the coupling constant.

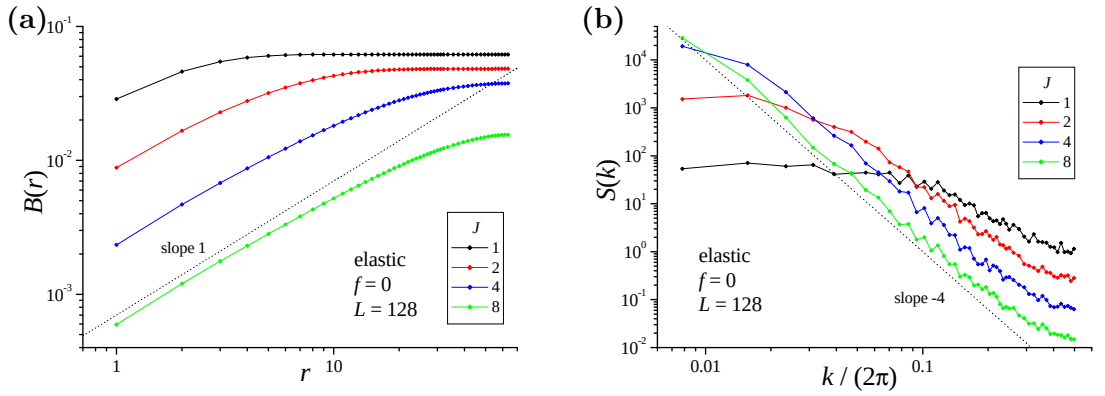

Figure 4.8: The displacement function (a) and the structure factor for the elastic manifold model without drive.

energy landscape of the disordered system is not trivial. The phase correlation grows with J and the $k = 0$ component of the structure factor becomes larger. The peak and tentative decreasing for $S(k = 0)$ as a function of J is not seen in the static regime.

Additionally we investigate the elastic model both driven and not driven cases and found that they show the same results with XY model in large J and f region as might have been expected. In these regions each phase differences are enough small and the nonlinearity of sinusoidal coupling is not relevant. The structure factor, which is the Fourier transformation of the elastic correlation function in eq.(4.3), and displacement function at $f = 0$ are shown in Figure 4.8. Almost no difference is observed between the results of elastic model and plastic model in Figure 4.7 at $J = 4$. Then all of the present results are consistent with classical Imry and Ma argument, i.e. any long range order does not exist in the system with quenched randomness and contradict the picture of Bragg glass which is widely believed. This is discussed in section 4.3.

4.1.6 Spatio-Temporal Correlation Function

So far, we found neither true nor quasi long range order even instantaneously in the random field XY model. Then the moving solid phase in finite time observation is expected to be a moving glass phase. In order to confirm this, I discuss here the glassy order, which means the temporal freezing of the disordered configuration. Such order is captured by the four

body correlation function which is expressed as

$$C(r,t) = \left\langle \cos\left[\Big(\theta_i(t') - \theta_{i+r}(t')\Big) - \Big(\theta_i(t'+t) - \theta_{i+r}(t'+t)\Big)\right]\right\rangle_{i,t'}. \tag{4.11}$$

This measure the temporal freezing of relative phase difference. This correlation function largely oscillates with t due to the washboard motion and the temporal decay, which we have interest in, hides behind it. Additionally it is technically hard to take the average for t' because it needs very large amount of the memory resource. Instead we calculate a little different type of correlation function,

$$C(r,t) = \left\langle \left| \frac{1}{t}\int_0^t dt' \exp\left[i\Big(\theta_i(t') - \theta_{i+r}(t')\Big)\right]\right|^2 \right\rangle_i. \tag{4.12}$$

$\theta_i(t)$ can be expressed as

$$\theta_i(t) = \theta_0^i(t) + \omega_p^i t + \delta\theta_i(t). \tag{4.13}$$

The first term is an intermittently changing part. It seems to be a constant for much longer time scale than $2\pi/\omega_p$ but suddenly increases or decreases like a step function when phase slip occurs between the elastic domains to which site i and j belong separately. Very slow and smooth change inside the elastic domain is also included in θ_0. The second part is a linearly increasing part. The motion of θ_i seems periodic in short time scale. The velocity ω_p^i is a little different from $\omega_{\rm DC}^i$ due to the change in the first term. (This part is essential in the transition between plastic flow and moving solid.) The third term is the fluctuating part with the frequency ω_p and $\langle\delta\theta_i(t)\rangle_t = 0$. Of course, there is not strict separation as this but it is useful to consider the mechanism of decay of the correlation function. When $\delta\theta_i(t)$ is small, the integrand in eq.(4.12) is approximated by

$$\exp\Big[i(\theta_0^i(t) - \theta_0^{i+r}(t))\Big] \exp\Big[i(\omega_p^i - \omega_p^{i+r})t\Big]. \tag{4.14}$$

There is two reasons for the temporal decay of correlation function in eq.(4.12). One is comes from the difference of the frequency ω_p on the second factor in eq.(4.14). If $\omega_p^i \neq \omega_p^{i+r}$, the temporal integral in eq.(4.12) is $O(t^0)$ for $t \gg 2\pi/(\omega_p^i - \omega_p^{i+r})$ and $C(r,t)$ decreases with t^{-2}.

Another reason is the change of constant like part, $\theta_0^i(t) - \theta_0^{i+r}(t)$. Note that if the jump of $\theta_0^i(t) - \theta_0^{i+r}(t)$ is by $\pm 2\pi$ at a single phase slip, it hardly affects on the glassy order defined here. For this reason the temporal phase order does not necessarily conflict with plastic flow. If the jump is not integral multiple of 2π and randomly changes constant-like phase, the integral is proportional to $t^{1/2}$ then $C(r,t)$ decreases with t^{-1}. Same t dependence appears when $\theta_0^i(t) - \theta_0^{i+r}(t)$ smoothly changes and loses the temporal correlation.

The spatio-temporal correlation function is shown in Figure 4.9(a). The distance r is fixed and $C(r,t)$ is plotted as a function of t. Here microscopic time scale $2\pi/\omega_p$ is about 15 in this region of f. We checked that $C(r,t)$ does not decrease any more if r becomes larger in the range of f shown in Figure 4.9. For small f, large correlation remains at $t = \infty$. This is contributed by the couple of sites which are stopping or almost stopping sites. The phase differences between them do not change. Then we should not count these constants.

The short time correlation holds for longer time as f becomes larger. $C(r,t)$ decays with a long tail for large $t > 10^3$, which is described by t^{-1} rather than t^{-2}. Then it is indicated that the decay of correlation function is governed by the change of $\theta_0^i(t) - \theta_0^{i+r}(t)$ rather than the difference of ω_p.

In Figure 4.9(b), $C(r,t)$ is plotted with a time scaled by the glass crossover time $\tau(f)$, which is calculated in the previous chapter. At the same time, the constant value $C(r, t =$

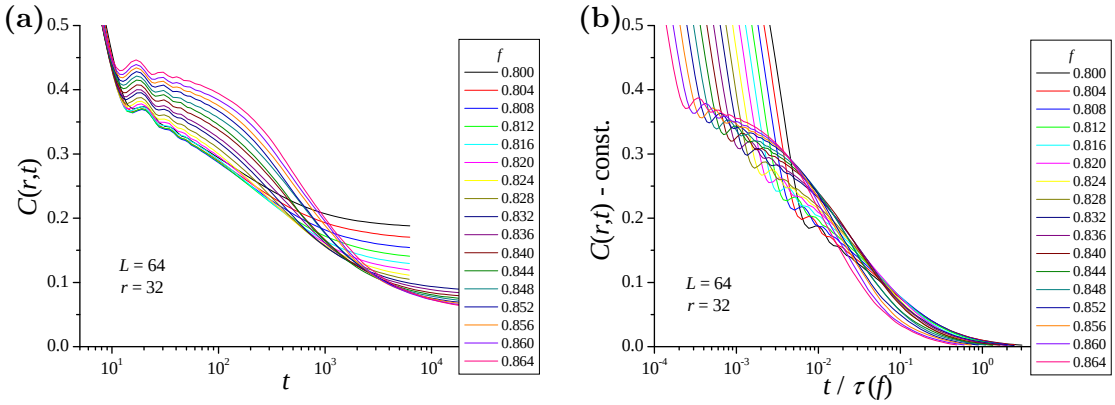

Figure 4.9: (a) Spatio temporal correlation function which measure the glassy order. The distance is fixed as $r = L/2 = 32$. (b) $C(r,t) - C(r,\infty)$ is plotted with a time scaled by glass crossover time $\tau(f)$.

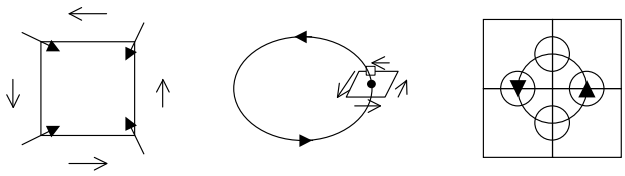

Figure 4.10: (left) A fundamental plaquette which contain a vortex. (center) A vortex loop in three dimensions. (right) The vortex loop with minimum size. The circles indicates the center of plaquettes, which is perpendicular to the paper, with a vortex.

∞), which is obtained by the fitting to t^{-1}, is subtracted from $C(r,t)$ for each f. Each curves roughly converges by such scaling. The correlation decays in the time scale of the same order with glass crossover time $\tau(f)$. It is speculated that the glassy long range order collapse with the same life time with that of the moving solid. We need more quantitative argument to conclude it.

4.2 Topological Defects

The phase ordering is strongly affected by unbounded dislocations. Its importance is remarked in the Kosterlitz-Thouless transition for the two dimensional XY model [39]. In the low temperature phase which has quasi long range order, each vortex and anti-vortex are bounded as a pair and such pairs disorder the phase only in a short range while the long range order of the system is disordered by unbounded vortices in the high temperature phase. For three dimensional disordered system, it is believed that unbounded dislocation does not exist in the Bragg glass phase and quasi long range order exists. In contrast the pure three dimensional XY model in thermal equilibrium has a low temperature phase with true long range order [41]. The present model has a middle nature between them, quenched disorder exists but it is washed out by the high velocity translation.

4.2.1 Dislocation Loops

The O(2) model, in which the present model is involved, can have topological defects i.e. vortices. In three dimensions, such dislocations form one dimensional objects, vortex loops while the vortex is a point in two dimensions. The existence of vortex is defined by the

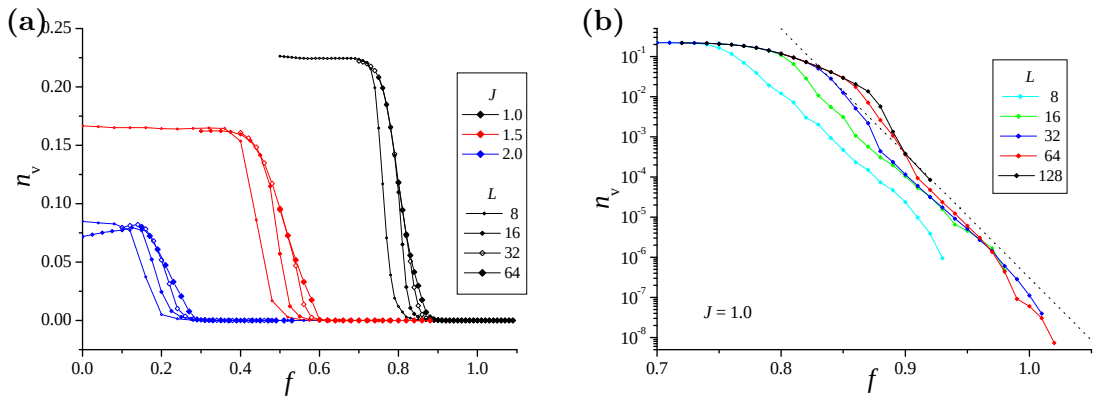

Figure 4.11: The vortex density n_v is plotted as a function of a driving force f both normal scale for several J's (a) and semi logarithmic scale for $J = 1.0$ (b). n_v is averaged value over time and samples. A dashed line in the graph indicates $n_v = e^{-(f-0.79)/0.014}$. L denotes the linear sample size.

non-zero loop integral of the phase gradient as follows.

$$\oint d\mathbf{s} \cdot \nabla\theta(\mathbf{r}, t) = 2\pi m, \quad m = \pm 1, \pm 2, \ldots \tag{4.15}$$

In the case of the lattice model, we determine that vortex runs through a fundamental plaquette if the summation of phase differences, which are restricted between $-\pi$ and π, along the anticlockwise path equals $\pm 2\pi$ (See Figure 4.10). There is three types of plaquettes in a three dimensional sample, which are parallel to xy, yz and zx-plains. The vortex density n_v is defined as a fraction of plaquettes occupied by vortices. The sign of the vortex is not taken into account here.

Here, we restricted ourselves into the case of coupling constant $J = 1.0$. Qualitative behavior does not change as far as J is less than 2.0, so-called the strong pinning regime. In this regime, Pinned state is very disordered and has a lot of vortices. As the phase coherence grows with f, the number of vortices becomes smaller.

The f dependence of the vortex density is shown in Figure 4.11. If the phases are given perfectly at random, the probability that a vortex exists in the plaquette is 1/4. In the present results, n_v is always lower than this value. n_v starts to decrease rapidly around $f = 0.75$ for $J = 1.0$ where the fraction of moving sites becomes $O(1)$. Below $f = 0.75$, n_v hardly depends on f.

In the lower row of Figure 4.12, typical vortex configurations are shown. Patterns of the local DC velocity $\omega^i_{\rm DC} = \langle\dot{\theta}_i\rangle_t$ are also plotted in the upper column for the comparison. These profiles hardly change for a much longer time than microscopic time scale $2\pi/\omega_{\rm DC}$ because they are strongly connected to the quenched random potential. There is a strong correlation between local n_v and $\omega_{\rm DC}$, a smoothly moving high velocity region is more free from vortices than a discontinuously moving slow velocity region. Although it may be difficult to notice a good correspondence between the two local quantities at a glance of only a single layer of three dimensional system in Figure 4.12, it can be seen much clearly in the case of two dimensional system.

For smaller f, plaquettes with vortices exist almost homogeneously and we can not distinguish the size of each vortex loop in the lattice model. On the other hand, each vortex loop is clearly distinguished and has very small radius for $f > 0.9$, where vortices are very rare, $n_v < 10^{-4}$. In this region, most of vortex loops consists of four plaquettes, which is the minimum size of a loop. The disorder effect of a very small vortex loop is in short range

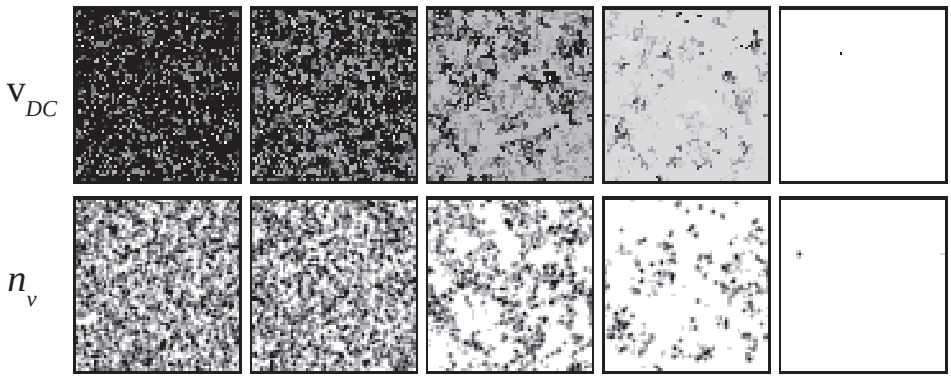

Figure 4.12: Shading plots of the vortex density and DC velocity. These show the patterns in a certain 64×64 single layer for the driving force, $f = 0.70, 0.75, 0.80, 0.85$ and 0.90 from the left to the right. n_v is averaged over time and three plaquettes in the cubic of each unit cell. The value increases from 0.0 to 0.45 between white and black for n_v and decreases from 0.50 to 0.0 for v_{DC}.

because it looks a vortex-anti-vortex pair seeing in a proper cross section. This implies that long range order but it does not exist as discussed in the previous section.

4.2.2 Effective Temperature

The number of remaining vortices decreases exponentially with f

$$n_v \propto \exp(-f/f_1) \tag{4.16}$$

for large $f(> 0.9)$ as shown in Figure 4.11(b). In the case of a pure three dimensional XY model in thermal equilibrium, vortex loops are bounded and individually excited at very low temperature. Therefore the vortex density is proportional to Boltzmann weight $e^{-\epsilon_v/k_BT}$ [42]. Here ϵ_v is the energy of an isolated vortex loop with the smallest radius. The exponential decreasing of n_v with f in the present driven dirty system can be interpreted as that the effect of random potential is represented by the effective temperature proportional to f^{-1}.

$$k_BT_{\text{eff}} = \epsilon_v(f/f_1)^{-1} \tag{4.17}$$

Indeed almost all of vortex loops have minimum size in the exponentially decreasing regime. In this regime the velocity is nearly proportional to f, so the present result agrees with the speculation by Koshelev and Vinokur, $T_{sh} \propto v^{-1}$. This is also consistent with the effective temperature which characterizes the thermal activation of moving glass state discussed in section 3.4.1.

4.2.3 Power Relaxation

When the initial condition is given as a random state, the phase order grows in order to lower the local interaction energy. Larger wave number component becomes more important as the relaxation advances up to the correlation length in the steady state. This results a relaxation described by a power function. Then n_v is expressed as

$$n_v(t) = \text{const.} \times t^{-\delta} + n_v(t = \infty). \tag{4.18}$$

$n_v(t)$ for random initial condition is shown in Figure 4.13(a). When constant value for the steady state is subtracted, the power decay is seen in the wide range of f as shown in Figure 4.13(b).

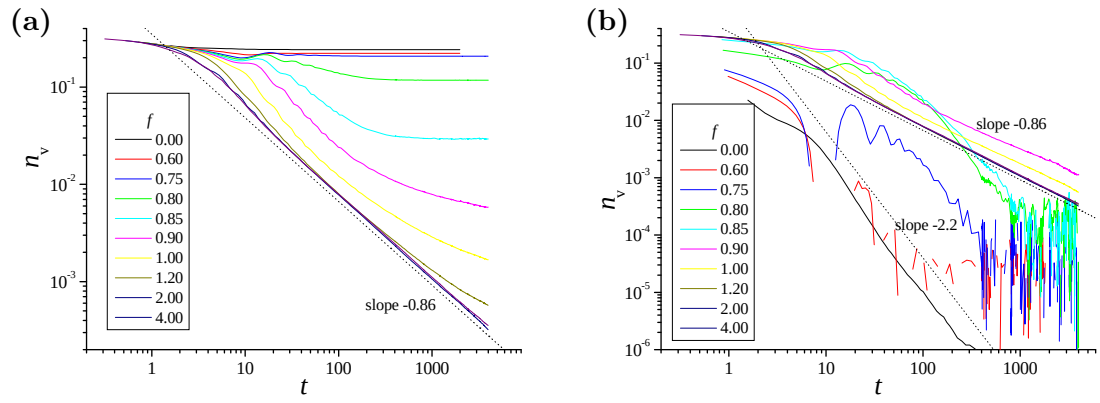

Figure 4.13: (a) The decay of vortex density with time. (b) The result after subtraction of the value at the steady state.

We find two different exponents, $\delta = 2.2$ for small f and $\delta = 0.86$ for large f. The crossover occurs around $f = 0.9$, above which n_v in the steady state decreases exponentially with f. In the former case, the random potential takes an important role. Characteristic time scale does not seen even at $f = 0$ although the coupling constant is relatively small and the phase correlation length is almost zero. In the large f regime above $f = 1.2$ where $\delta = 0.86$, the curve of $n_v(t)$ hardly changes with f even if f and microscopic time scale $2\pi/f$ changes for several decades. It is checked that this dynamics is same with that in the absence of the pinning potential.

4.3 Discussion

In this chapter, I have discussed the phase order, mainly instantaneous one. It is shown that the structure factor has k^{-4} shape in the long wave length regime, which indicates that the phase correlation length is always finite based on the sum rule of the structure factor then both true and quasi long range ordered phase do not exist.

We can not eliminate the possibility that the crossover to the quasi long range order behavior would occur in much smaller k, i.e. the structure factor changes its shape from k^{-4} to the more slowly divergent form which is related to the power decay.

Giarmarchi and Doussal, who analyze the periodic elastic model for FLL systems in detail, states that such crossover appears only when all the higher harmonic components of displacement field, that denote the localized nature of flux line, are taken into account [38]. This may be a reason why the quasi long range order is not found in the present calculation.

Although any evidence of quasi long range order is found in our simulations, we need more careful argument to conclude the absence of such ordered state. In the disordered systems, the energy landscapes are complex and the ground states are not obtained easily. Here I show several studies on three dimensional models and compare the present one with them. Although the Bragg glass phase for FLL systems is widely believed according to some analytic studies [26, 43, 44, 27], there are few numerical studies for the random field model even in static case in comparison with other random spin systems such as spin glasses [45] and vortex glasses [46, 47, 48].

Gingras and Huse performed Monte Carlo simulations based on the random field XY model [49]. The difference from the present model is only the randomness in pinning strength h which is constant in the present one. They showed that the average spacing between *static* dislocations becomes smaller with the pinning strength weakened faster than the elastic coherence length estimated by Imry and Ma [22]. Then they predict the phase

transition to the quasi long range ordered state at the finite pinning strength.

Fisch performed Monte Carlo simulations based on the Z_N ferromagnet model with random field, N is up to 12 [50]. He shows that there are paramagnetic, ferromagnetic and quasi long range ordered phases. The main basis of the phase transition between ferromagnetic and quasi long range ordered states is that the exponent of the structure factor is proportional to k^{-3} and $k^{-2.87}$ respectively. He also made some studies on modified models [51, 40].

McNamara et. al. calculate the exact ground state of an elastic manifold in the periodic random potential [52] and found that the structure factor is proportional to k^{-3}. This is obviously contradict to the present result, k^{-4}. In their simulations the random potential is given by random variables for discretized phase θ_i while the model we analyze has sinusoidal one, $\cos(\theta_i - \beta_i)$. I consider this difference may be relevant because the former potential would yield much more local minima at various θ_i's then the conflict between ferromagnetic coupling and random potential becomes weaker.

All of these works suggest the quasi long range order. It is likely that our results for static case does not capture the ground state, which is speculated to have quite different nature from other metastable states. However there are few works and certain degree of variations exists in the detail of models. Further studies are desired to conclude the presence of Bragg glass.

In the nonequilibrium case, which is our main target, we obtain macroscopically same steady states independently of the initial conditions at least. They may be related to the metastable states obtained by quenching in static case. It is very difficult problem, however, whether we can define the steady state in a dissipative system which is comparable to the ground state in the static case. I note that there is a possibility that the observation of steady state is related to that of equilibrium state rather than quenched metastable state since the system may have a "ergodicity" due to the chaotic dynamics even at zero temperature. Nevertheless this is an opened question.

In the last part of this chapter, we argued the behavior of dislocations which takes an important role on the disorder of phase. We found that vortex density exponentially decreases with the driving force then vortices are excited as if it were in the thermal equilibrium state with shaking temperature. It seems that Koshelev and Vinokur's idea of shaking temperature works well in the nonperturbative scheme where topological defects are excited.

There is a large difference, however, between disordered moving systems and pure equilibrium systems. The three dimensional XY model takes a phase transition at finite temperature between para magnetic phase and ferro magnetic phase [42]. On the contrary, we found that the driven random-field XY model does not have any long range order of phase variable at finite external field and coupling constant by analyzing structure factor. When the phase correlation length is much longer than the radius of vortex loop, however, the energy of a bounded small vortex loop in the present model should hardly differs from that in the ferromagnetic phase. We consider this is the reason why we obtain a good mapping onto the pure system in equilibrium. To clarify the difference among the ordering of three systems, i.e. a moving system with quenched disorder, an equilibrium state of pure system and an equilibrium state with quenched disorder, is a future work.

Chapter 5

Summary and Discussion

In this thesis, I discuss the dynamics of the periodic structures under the external drive based on the driven random field XY model. The most advantage of this model over the well investigated elastic model is that it allows the plastic flow state in which the local velocity is inhomogeneous and plastic deformation occurs steadily. Our goal is to clarify whether there is any moving phase with the spatio-temporal long range order or not within the range of the model. There are two kinds of view point, the DC velocity order, which distinguishes plastic flow and moving solid, and crystalline order, which distinguishes liquid, glass and crystal. The transition controlled by the driving force is particularly studied.

At first I showed that this model qualitatively reproduces various experimental results for CDWs, FLLs and so on in chapter 2. The most drastic difference from the elastic model description appears in the depinning. When plastic deformation is allowed, only a small fraction of the system moves in the vicinity of the depinning point. As the ratio of the internal coupling to the pinning strength increases, the crossover to the elastic behavior occurs and the depinning threshold shows a peak. This is considered to correspond to the peak effect which is observed in the experiment of FLL systems.

Spatially inhomogeneous plastic flow is observed above the depinning threshold. We investigate the distribution of local DC velocities, in which some power low behaviors are found. The orders both of phase and local DC velocity grows with the driving force. The uniformity of DC velocity is strongly correlated with the temporal periodicity of the dynamics. The broad band noise and narrow band noise are observed in the plastic flow and moving solid regimes respectively.

The behavior of the systems with small degrees of freedom is quite different from that of large ones. They show discontinuous transitions and hysteresis. These describe the experiments of CDW systems considerably, the most remarkable feature is delayed switching. This provides some information about the size of the domains, which can be regarded as an elastic body, in comparison with the sample size in experiments.

After we showed the validity of this model, the spatial order of DC velocity was investigated in chapter 3. We consider that the moving solid phase is represented by an infinitely large cluster in which no plastic deformation occurs, then analyze the percolation transition of the non phase slip bond, which represents the transition between plastic flow and moving solid. This is a new point of view to analyze the dynamical correlation, not of phase but of DC velocity, in the nonequilibrium steady state. In the finite time observation, the percolation transition actually occurs. The critical driving force, however, increases with the observation time and logarithmically diverges. Moving solid phase which holds for an infinitely long time does not exist in the presence of quenched disorder. The glass crossover time, i.e. the life time of moving solid phase, can be clearly defined from the analysis of the observation time dependence of the percolation transition. This time scale exponentially increases with the driving force. We found that the spatial configuration of DC velocity is

universal when one observes in this time scale.

In chapter 4 the instantaneous phase ordering is discussed. We do not find any long range order. This does not depend on whether driving force is imposed or not and whether the interaction is elastic or sinusoidal. Such disordered configuration is speculated to freeze as long as the moving solid remains according to the spatio-temporal correlation function.

We found that the excitation of dislocations are expressed exponential of the driving force as well as the glass crossover time. This indicates that the idea of shaking temperature [3], which is proportional to the inverse of the driving force, well characterize the internal state of moving systems in the high velocity regime. The phase correlation in the long scale is, however, different from that in the pure ferro coupling system at finite temperature. The effect of quenched randomness is not entirely replaced by the effective temperature however fast the system moves.

The quasi long range ordered state in three dimensions, Bragg glass, is widely believed to exist in FLL systems. The present results contradict it even if ignoring the possibility that the size of samples in our simulations is inadequate to observe it. In the static case, the most likely reason is that the ground state is not obtained. It the driven case, we obtain initial condition independent steady states. However there is a far more difficult problem whether the state related to the ground state can be defined or not in nonequilibrium steady state.

Several other reasons are considered for this contradiction. One is the lack of large wave number components in the present model as implied in Ref.[38]. If one want to treat the localized nature of flux lines properly, the density field should have higher components of reciprocal vectors while we only treat the fundamental component.

I note that there is a possibility of spatio temporal ordered phase considering another factor. Balents and Fisher studied the elastic manifold model with different type of energy dissipation, which is expressed by the term proportional to the covariant derivative of phase, $\partial_t + v\nabla$, and found the ordered phase in the high velocity regime [4]. Such term works only in the moving regime then if this term is essential to the long range order, the orderings in steadily moving state are fundamentally different from that in equilibrium state.

Although there are not a few theoretical and experimental studies which support the quasi long range order, there are just a few numerical studies even for elastic models and the existence of the Bragg glass phase is still an unsettled problem. Even if the long range order is established by introducing other factor, which is not involved in the present model, the qualitative features shown in chapter 2 are considered not to change so much, e.g. peak effect occurs in the same mechanism.

Many extended study is considered in addition to the higher harmonics and covariant derivative dissipation. One of the examples is the finite temperature effect, which is related to the creep motion in the pinned regime at the zero temperature. There are some reports of power function behavior in the current power spectrum in the presence of thermal noise [53]. Another is the multi component phase field related to high dimensional periodicity, which makes it possible to investigate anisotropic ordered states, such as smectic flow. The study of the systems with higher dimension for the space, where the phase transition is much probable, will yield the knowledge which is useful to investigate lower dimensional systems.

Acknowledgment

I would like to express my sincere gratitude to my adviser, Prof. Hiroshi Matsukawa, for valuable discussions and comments on the present thesis and all of my studies. I am also grateful to Dr. Hajime Yoshino for his helpful suggestions and collaborations. Finally I gratefully thank the stuff and students of Akai group in Osaka University for their warm supports and encouragement.

Bibliography

[1] G. Grüner. *Rev. Mod. Phys.*, 60:1129, 1988.

[2] G. Blatter, M. V. Feigel'man, V. B. Geshkenbein, A. I. Larkin, and V. M. Vinokur. *Rev. Mod. Phys.*, 66:1125, 1994.

[3] A. E. Koshelev and V. M. Vinokur. *Phys. Rev. Lett.*, 73:3580, 1994.

[4] L. Balents and M. P. A. Fisher. *Phys. Rev. Lett.*, 75:4270, 1995.

[5] H. Matsukawa. *J. Phys. Soc. Japan*, 57:3463, 1988.

[6] H. Matsukawa. *Synthetic Metals*, 29:343, 1989.

[7] S. N. Coppersmith and P. B. Littlewood. *Phys. Rev. B*, 36:311, 1987.

[8] R. E. Peierls. *Ann. Phys. Leipzig*, 1930:121, 1930.

[9] H. Frölich. *Proc. R. Soc. A*, 223:296, 1954.

[10] A. Maeda, M. Naito, and S. Tanaka. *J. Phys. Soc. Japan*, 54:1912, 1985.

[11] D. S. Fisher. *Phys. Rev. B*, 31:7233, 1985.

[12] P. Chauve, T. Giamarchi, and P. Le Doussal. *Phys. Rev. B*, 2000:6241, 2000.

[13] S. Lemerle, J. Ferré, C. Chappert, V. Mathet, T. Giamarchi, and P. Le Doussal. *Phys. Rev. Lett.*, 80:849, 1998.

[14] A. A. Abrikosov. *Sov. Phys. JETP*, 5:1174, 1957.

[15] M. J. Higgins and S. Bhattacharya. *Physica C*, 257:232, 1996.

[16] F. Pardo, F. Cruz, P. L. Gammel, E. Bucher, and D. J. Bishop. *Nature*, 396:348, 1998.

[17] A. Tonomura, H. Kasai, O. Kamimura, T. Matsuda, K. Harada, J. Shimoyama, K. Kishio, and K. Kitazawa. *Nature*, 397:308, 1999.

[18] A. B. Kolton, D. Domínguez, and N. Grønbech-Jensen. *Phys. Rev. Lett.*, 83:3061, 1999.

[19] K. i. Matsuda and S. Tanda. *Solid. State. Commun.*, 113:451, 2000.

[20] A. Zettle and G. Grüner. *Phys. Rev. B*, 26:2298, 1982.

[21] N. Ogawa and K. Miyano. *Phys. Rev. B*, 70:075111, 2004.

[22] Y. Imry and S. Ma. *Phys. Rev. Lett.*, 21:1399, 1975.

[23] A. I. Larkin. *Sov. Phys. JETP*, 31:784, 1970.

[24] H. Fukuyama and P. A. Lee. *Phys. Rev. B*, 17:535, 1978.

[25] P. A. Lee and T. M. Rice. *Phys. Rev. B*, 19:3970, 1979.

[26] T. Giamarchi and P. Le Doussal. *Phys. Rev. B*, 52:1242, 1995.

[27] P. Le Doussal and T. Giamarchi. *Phys. Rev. B*, 57:11356, 1998.

[28] P. C. Martin, E. D. Siggia, and H. A. Rose. *Phys. Rev. A*, 8:423, 1973.

[29] Y. Togawa, R. Abiru, K. Iwaya, H. Kitano, and A. Maeda. *Phys. Rev. Lett*, 17:3716, 2000.

[30] S. H. Strogatz, C. M. Marcus, R. M. Westervelt, and R. E. Mirollo. *Phys. Rev. Lett.*, 61:2380, 1988.

[31] S. H. Strogatz and R. M. Westervelt. *Phys. Rev. B*, 40:10501, 1989.

[32] D. A. Huse. *Computer Simulation Studies in Condensed Matter Physics IX, eds. D. P. Landau et al. (Springer, Berlin 1997)*, page 1964, 1997.

[33] T. Kawaguchi. *Phys. Lett. A*, 251:73, 2002.

[34] T. Kawaguchi. *Physica C*, 367:54, 2002.

[35] D. S. Fisher. *Phys. Rep.*, 301:113, 1998.

[36] J. Levy and M. S. Sherwin. *Phys. Rev. B*, 48:12223, 1993.

[37] D. Stauffer and A. Aharony. *Introduction to Percolation Theory.* Taylor & Francis Inc, 1994.

[38] T. Giamarchi and P. Le Doussal. *Phys. Rev. Lett.*, 72:1530, 1994.

[39] J. M. Kosterlitz and D. J. Thouless. *J. Phys. C*, 6:1181, 1973.

[40] R. Fisch. *Phys. Rev. B*, 62:361, 2000.

[41] T. Banks, R. Myerson, and J. Kogut. *Nuc. Phys. B*, 129:1977, 1977.

[42] A. P. Gottlob, M. Hansenbusch, and S. Meyer. *Nuc. Phys. B (Proc. Suppl.)*, 30:838, 1993.

[43] T. Garel, G. Iori, and H. Orland. *Phys. Rev. B*, 53:2941, 1996.

[44] D. S. Fisher. *Phys. Rev. Lett.*, 78:1964, 1997.

[45] K. Binder and A. P. Young. *Rev. Mod. Phys.*, 58:801, 1986.

[46] T. Olson and A. P. Young. *Phys. Rev. B*, 61:12467, 2000.

[47] H. Kawamura. *Phys. Rev. B*, 68:220502, 2003.

[48] Q. Chen and X. Hu. *Phys. Rev. Lett.*, 90:117005, 2003.

[49] M. J. P. Gingras and D. A. Huse. *Phys. Rev. B*, 53:15193, 1996.

[50] R. Fisch. *Phys. Rev. B*, 55:8211, 1997.

[51] R. Fisch. *Phys. Rev. B*, 52:12512, 2000.

[52] D. McNamara, A. A. Middleton, and C. Zeng. *Phys. Rev. Lett.*, 60:10062, 1999.

[53] T. Miyashita and H. Takayama. *J. Phys. Soc. Japan*, 87:2889, 1988.